Astroparticle Physics 2020/21

Lectures:

1. Historical introduction, basic properties of cosmic rays
2. Hadronic interactions and accelerator data
3. Cascade equations
4. Electromagnetic cascades
5. Extensive air showers
6. Detectors for extensive air showers
7. High energy cosmic rays and the knee in the energy spectrum of cosmic rays
8. Radio detection of extensive air showers
9. Acceleration, astrophysical accelerators and beam dumps
10. Extragalactic propagation of cosmic rays
11. Ultra high energy cosmic rays
12. Astrophysical gamma rays and neutrinos
13. Neutrino astronomy
14. Gamma-ray astronomy

http://particle.astro.ru.nl/goto.html?astropart2021

lecture 11
Ultra-high-energy Cosmic Rays

Cosmic rays

Solar flares

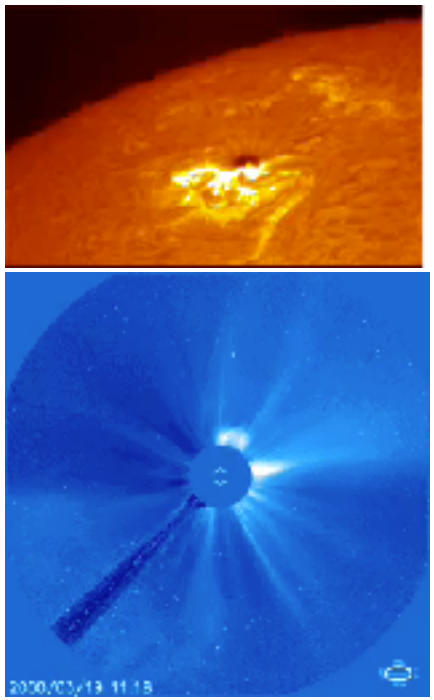

solar particles

JRH, Adv. Space Res. 41 (2008) 442

Cosmic rays

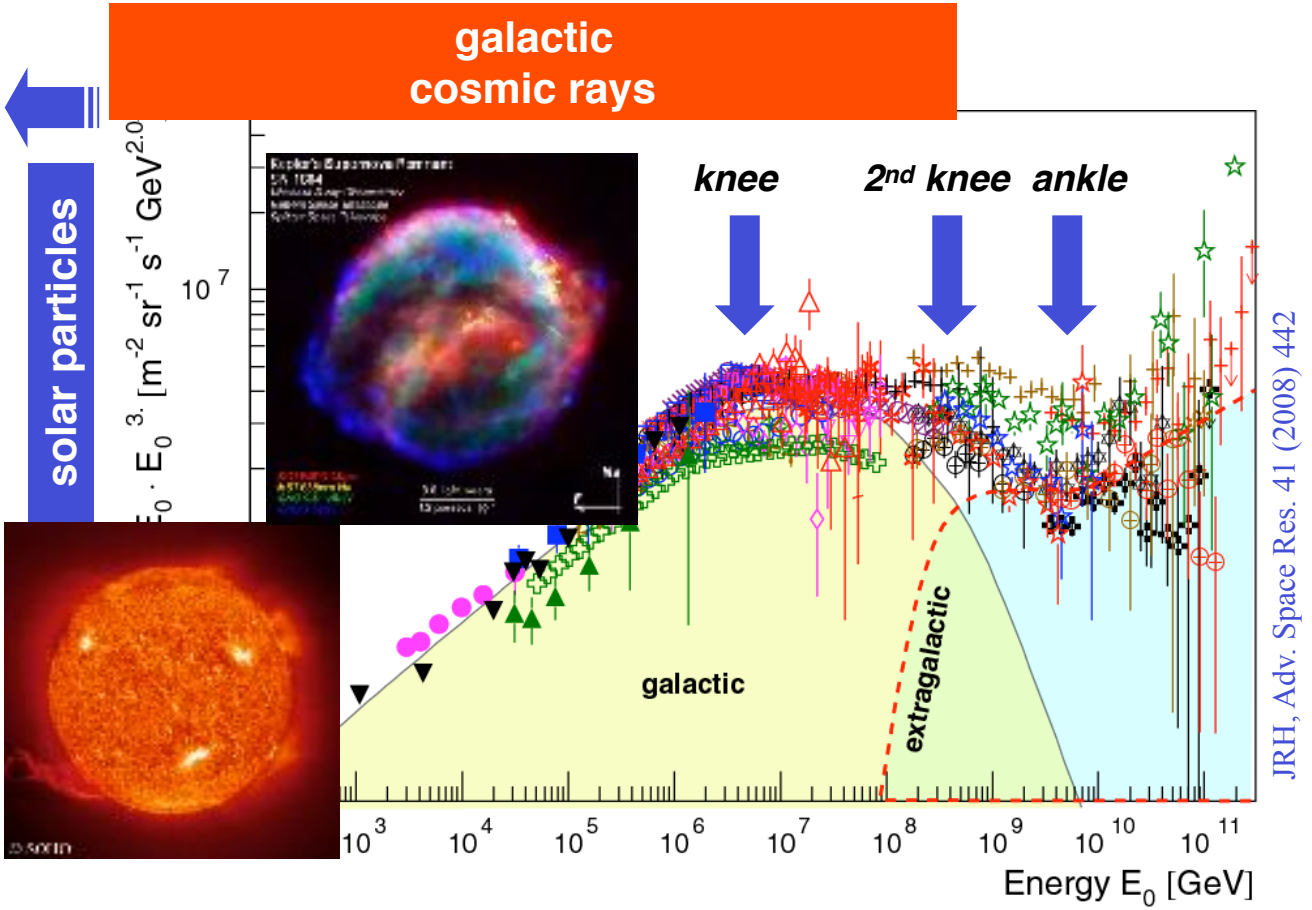
galactic
cosmic rays
solar particles
knee
2nd knee
ankle
galactic
extragalactic
Energy E0 [GeV]
JRH, Adv. Space Res. 41 (2008) 442

Cosmic rays

Radius of particle in magnetic field

$$r = \frac{p}{ZeB} \qquad r[pc] = 1.08 * \frac{E\ [PeV]}{B\ [\mu G]}$$

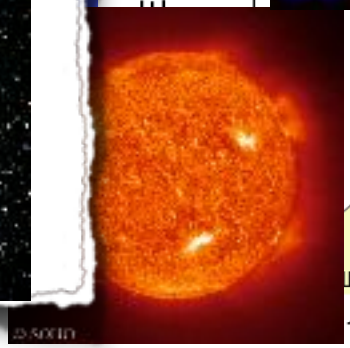

galactic cosmic rays

extragalactic cosmic rays

r= 0.04 pc 3.6 pc 360 pc 36 kpc

Cosmic rays

Energy content of extragalactic cosmic rays

$$\rho_E = \frac{4\pi}{c} \int \frac{E}{\beta} \frac{dN}{dE} dE$$

ρ_E=3.7 10^{-7} eV/cm^3

total power

P=5.5 10^{37} erg/(s Mpc^3)

→ ~2 10^{44} erg/s per active galaxy

→ ~2 10^{52} erg/s per cosmol. GRB

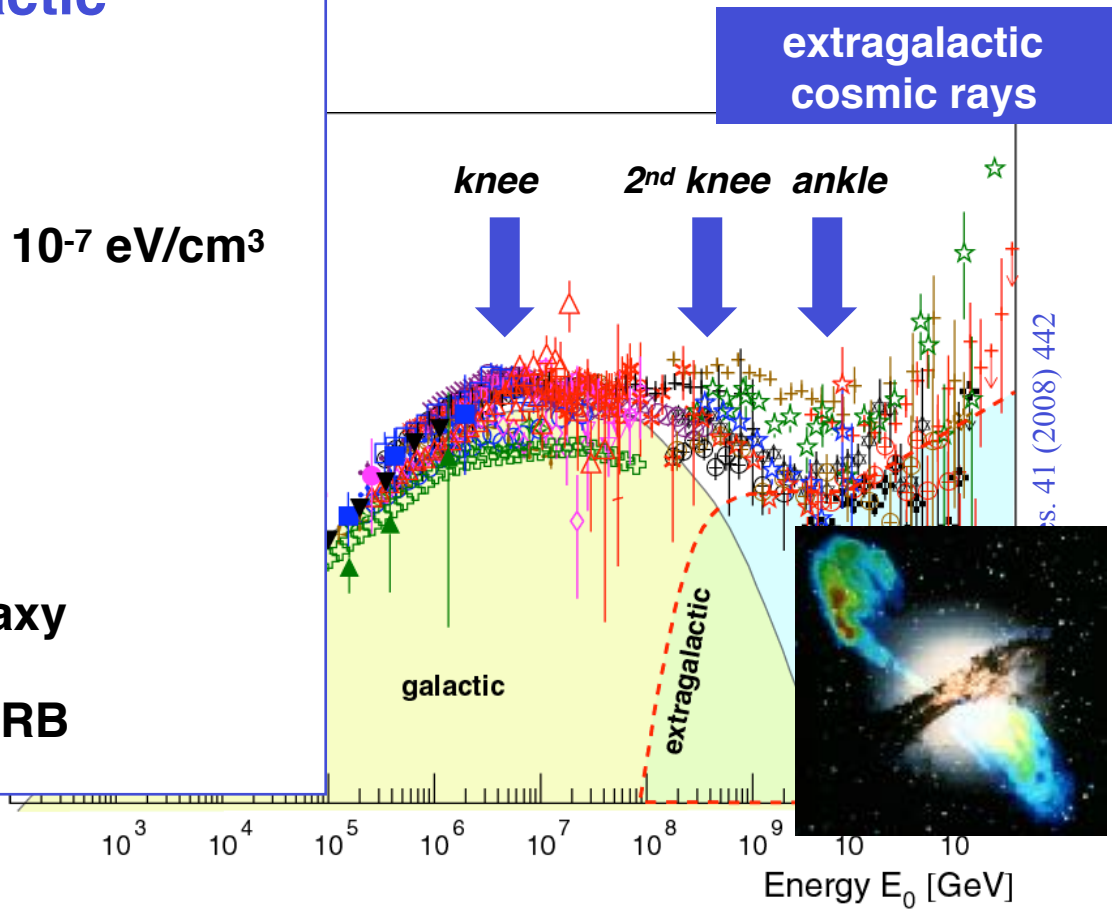

Measuring air showers with multiple techniques

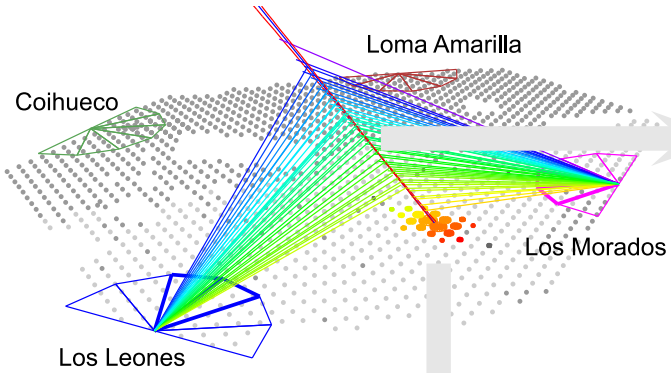

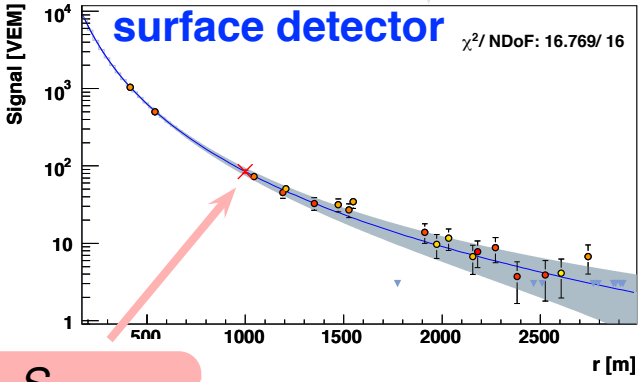

S_{1000}

$E_{\text{surface}} = f(S_{1000}, \theta)$

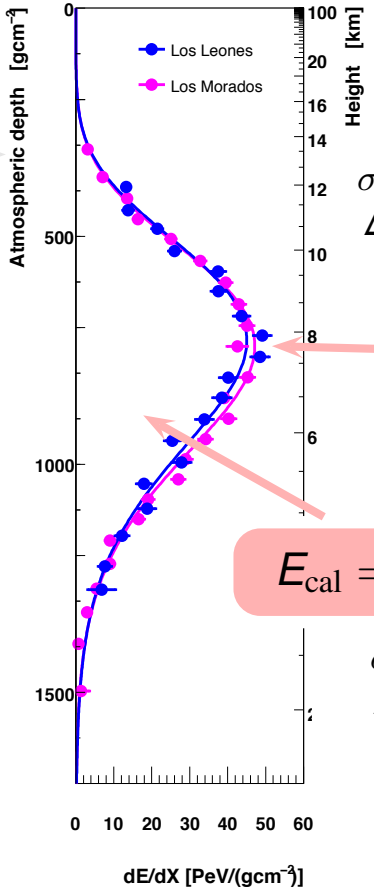

$\sigma_{X_{\text{max}}} \leq 20\,\text{g/cm}^2$
$\Delta_{\text{sys}} \leq 10\,\text{g/cm}^2$

X_{max}

$E_{\text{cal}} = \int \frac{dE}{dX}\, dX$

$\sigma_E/E \sim 8\,\%$
$\Delta_{\text{sys}} \approx 15\,\%$

fluorescence detector

radio detector

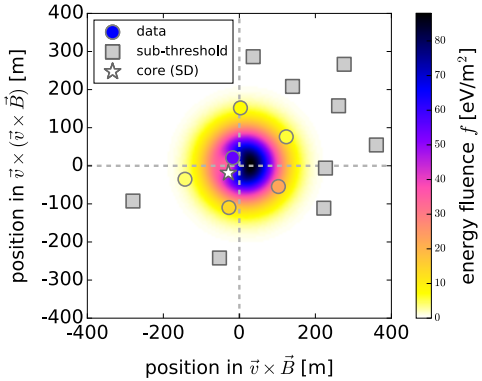

X_{max}, E_{cal}

exposure

Auger 9.0*10⁴ km² sr yr

TA 0.8*10⁴ km² sr

[6 of 30]

Energy spectrum

ENERGY SPECTRUM OVER 3 DECADES IN ENERGY

SD vertical

energy thr.
3 EeV

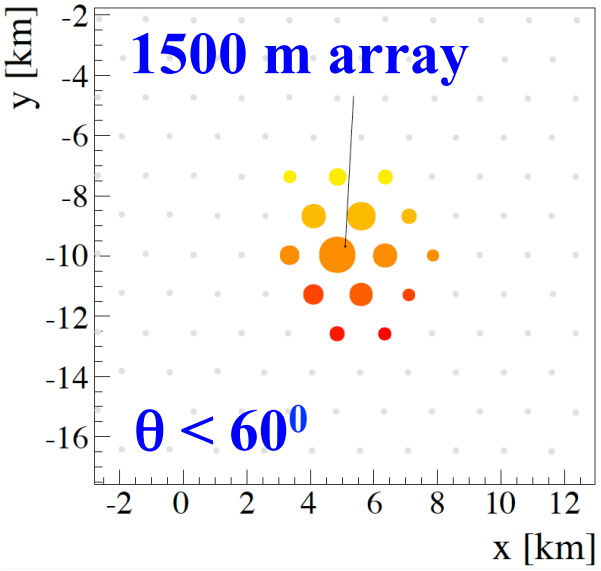

SD Inclined

energy thr.
4 EeV

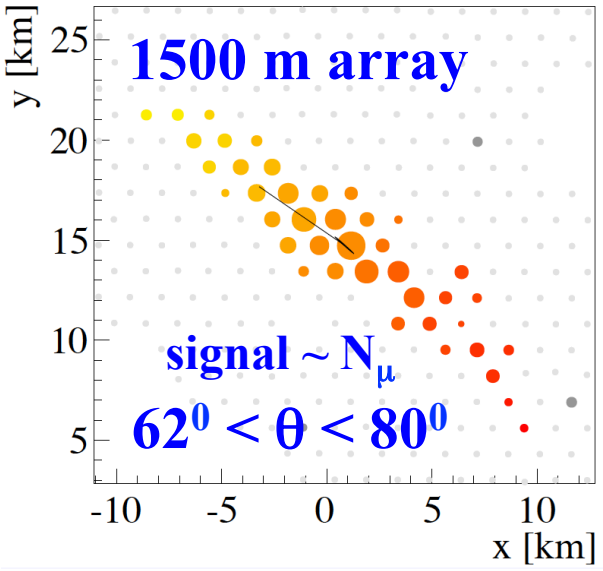

SD infill

energy thr.
0.3 EeV

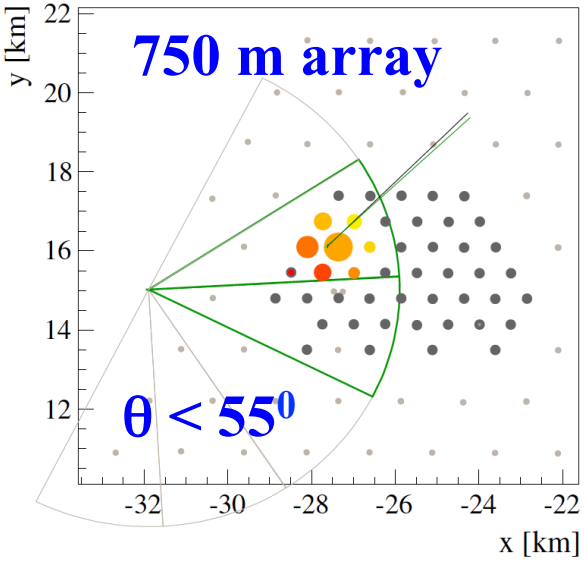

hybrid
13% duty cycle

energy thr.
1 EeV

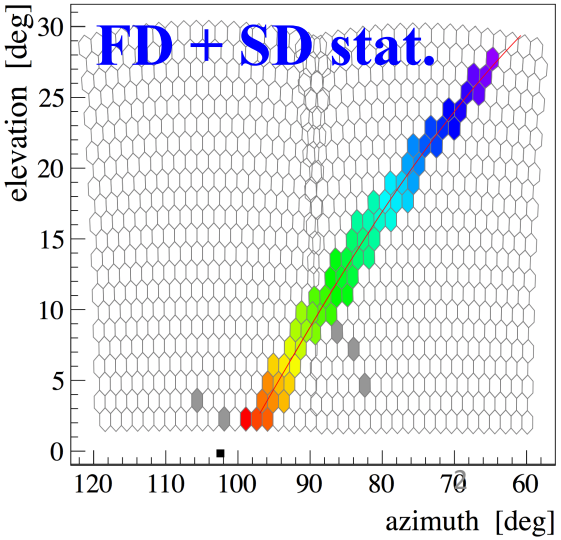

Auger (V. Verzi) UHECR2014

FD ENERGY SCALE

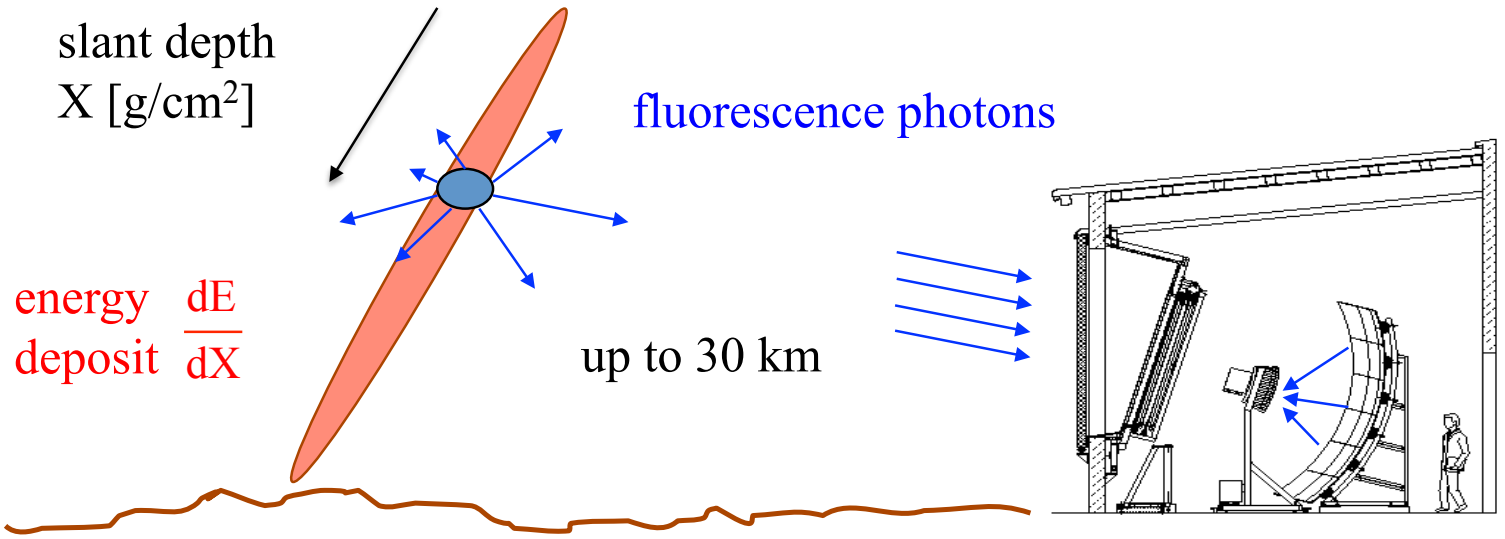

Fluorescence yield

Atmosphere

FD calibration

dE/dX reconstruction $\Rightarrow E_{cal} = \int \frac{dE}{dX} dX$

Invisible energy (ν, μ, ..) $\Rightarrow E_{inv}$

$$E = E_{cal} + E_{inv}$$

systematic uncertainties correlated and uncorrelated among different showers (crucial to correctly propagate the FD uncertainties to SD energies)

AIRFLY - FLUORESCENCE YIELD

The Airfly Collaboration: Astropart. Phys. **42** (2013) 90. Astropart. Phys. **28** (2007) 41. Nucl. Inst.. Meth. A 597 (2008) 50. M. Bohacova talk at 6th Air Fluor. Workshop

- **relative spectrum and its pressure dependence**
- **humidity and temperature dependence of collisional cross sections**
- **absolute intensity of the 337 nm line**

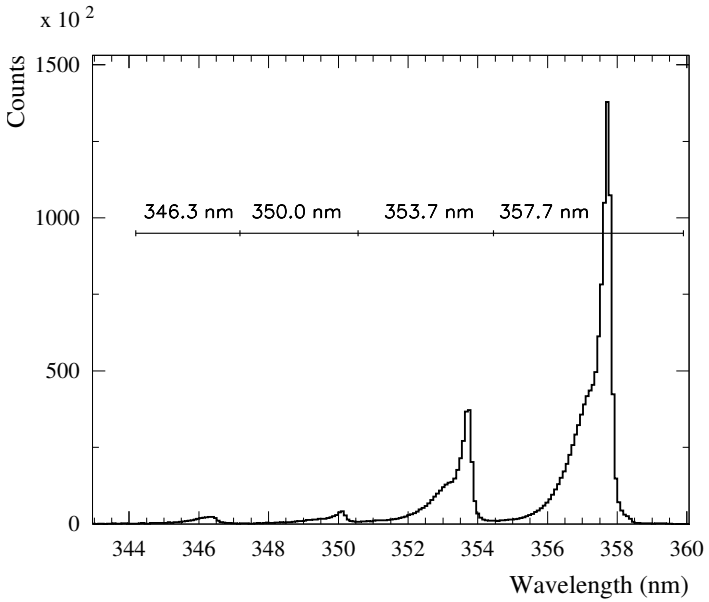

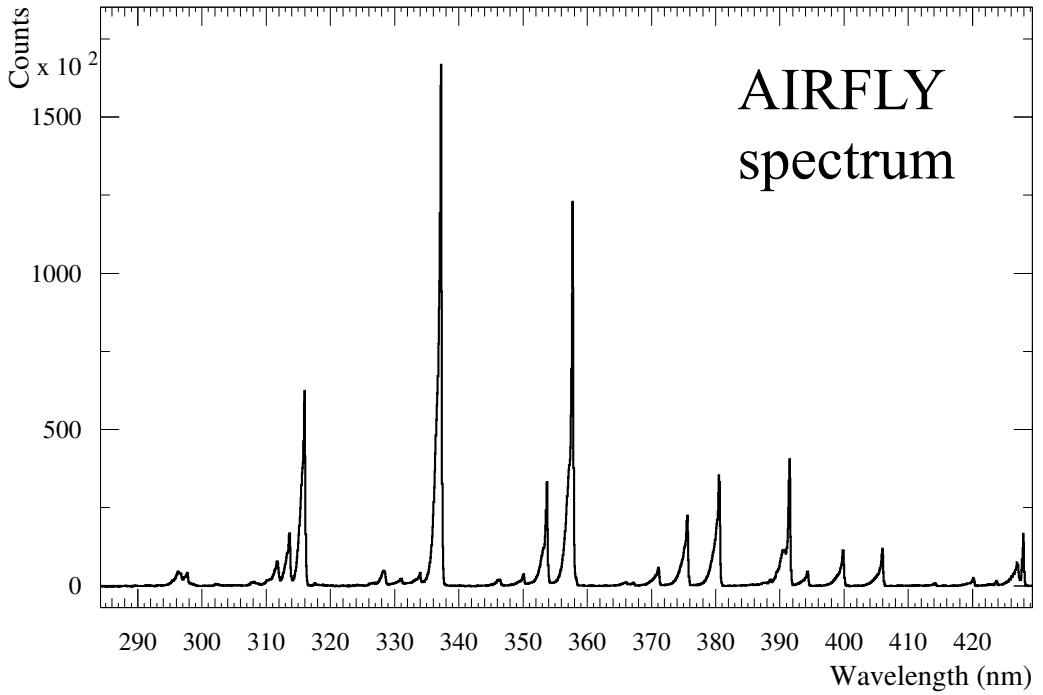

"effective" definition of the wavelength bands

- **don't care of possible contaminations between nearby bands**
- **straightforward and correct propagation of Airfly measurement uncertainties**

7

ATMOSPHERE

production and transmission of the light (aerosols and molecular scattering)

- **atmospheric profiles from Global Data Assimilation System (GDAS)**
- **hourly aerosol optical depth profiles**
- **aerosol phase function**
- **λ dependence of aerosol scattering cross sec.**
- **cloud coverage**

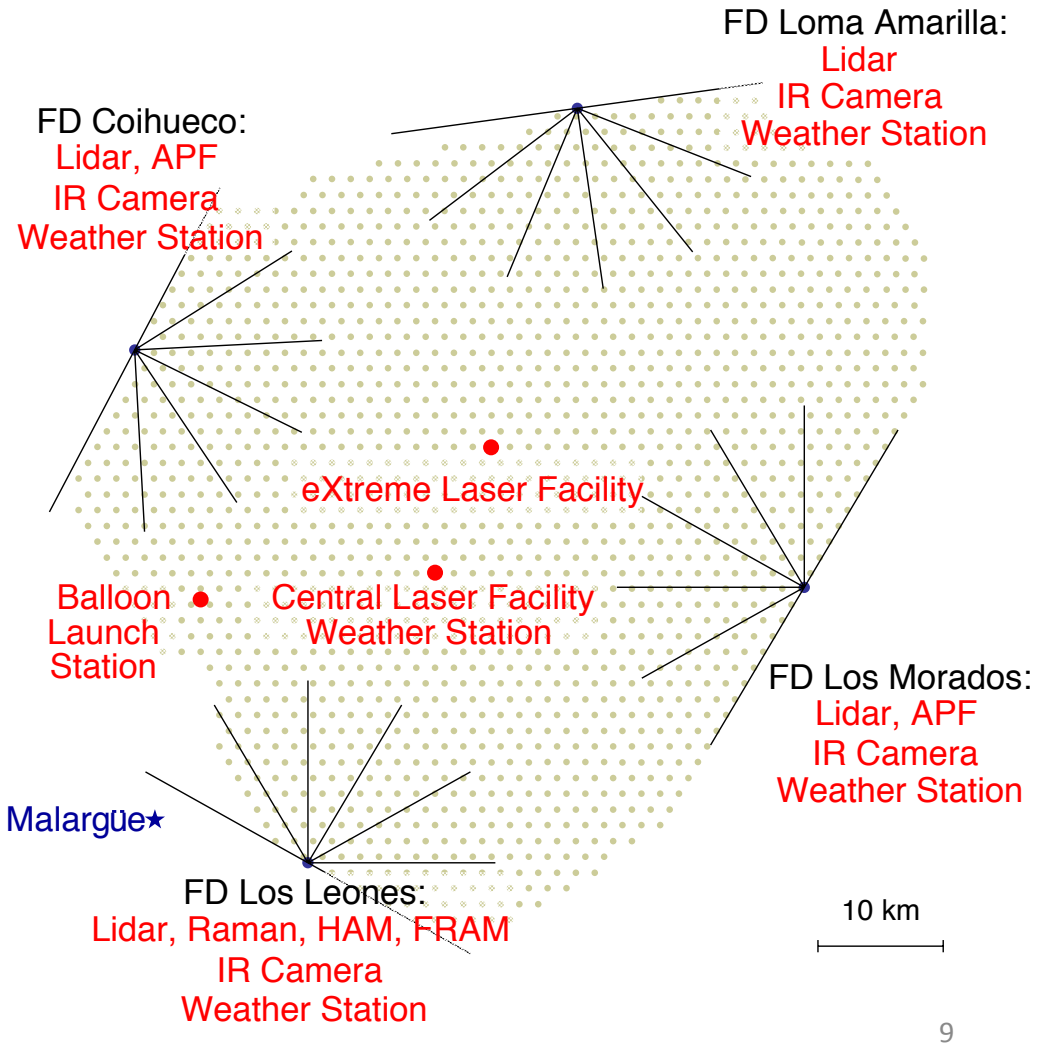

The Pierre Auger Collaboration
Astropart. Phys. **33** (2010) 108
Astropart. Phys. **35** (2012) 591
JINST **8** (2013) P04009
L. Valore ICRC 2013 #0920

SD Energy Calibration

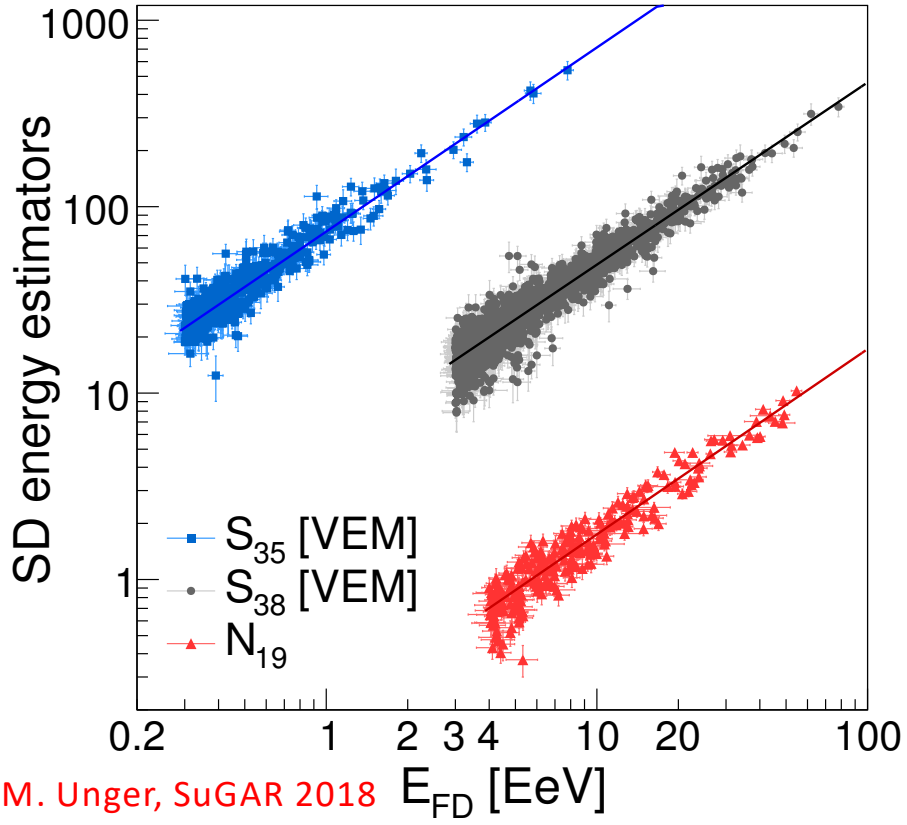

M. Unger, SuGAR 2018

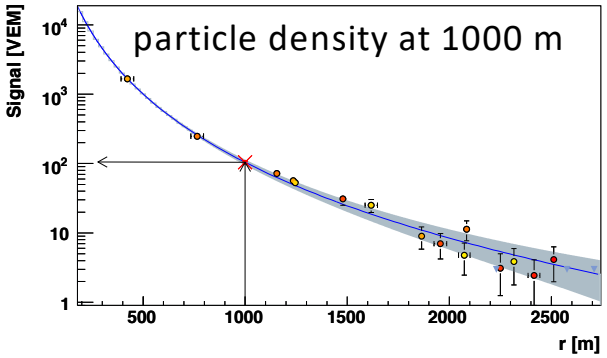

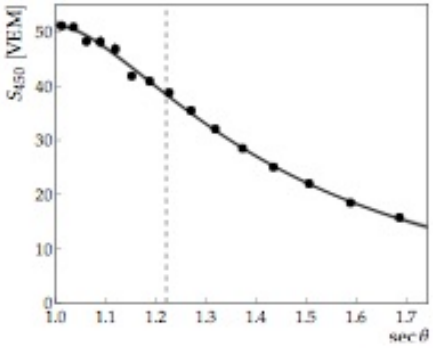

Infill: particle density at 400 m

FD longitudinal profiles

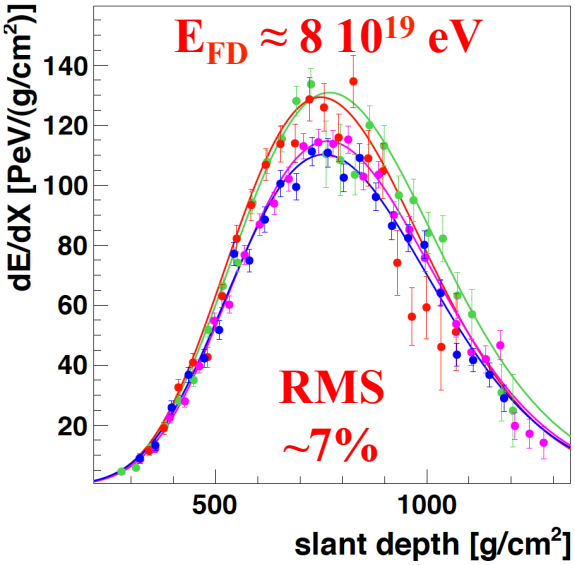

6/19/18

ENERGY SPECTRA

- SD 750 m spectrum: 29585 events above 3×10^{17} eV (08/2008 – 12/2012)
- correction for bin-to-bin migrations due to the detector resolution and steepness of spectrum (< 15%)

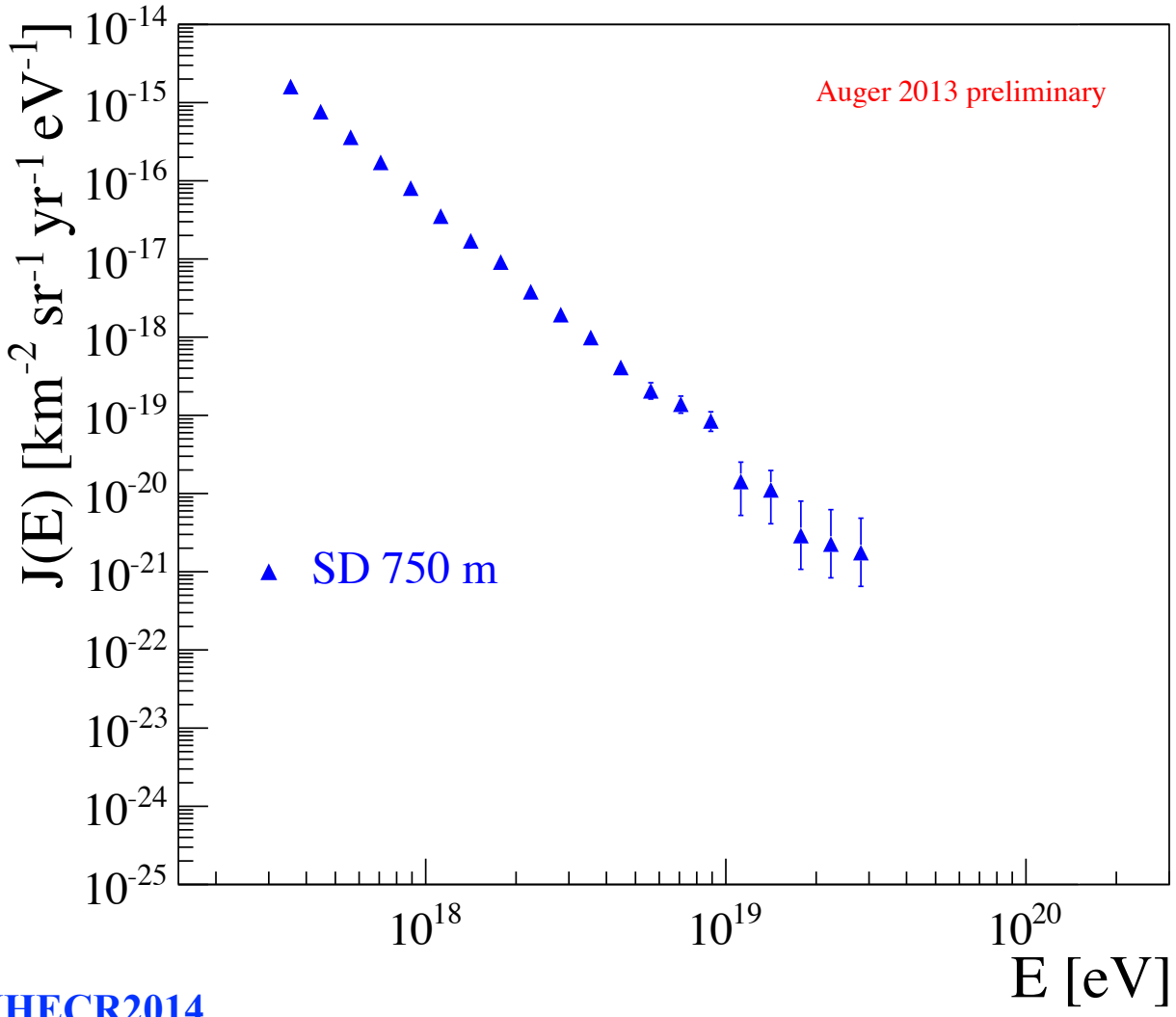

ENERGY SPECTRA

- hybrid spectrum: 11155 events above 10^{18} eV (11/2005 – 12/2012)
- correction for bin-to-bin migrations due to the detector resolution and steepness of spectrum (< 3%)

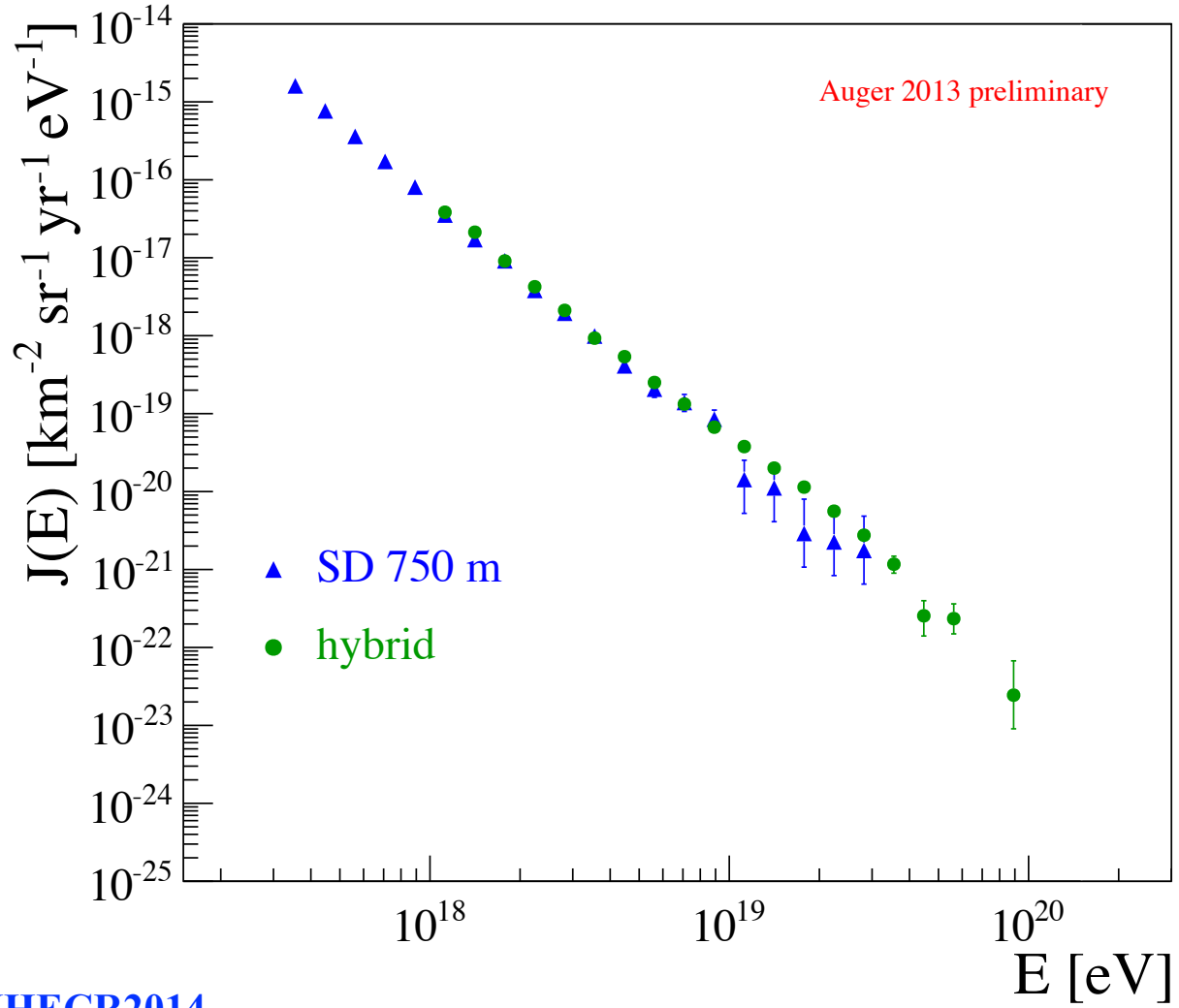

ENERGY SPECTRA

- SD inclined: 11074 events above 4×10^{18} eV (01/2004 – 12/2012)
- correction for bin-to-bin migrations due to the detector resolution and steepness of spectrum (< 12%)

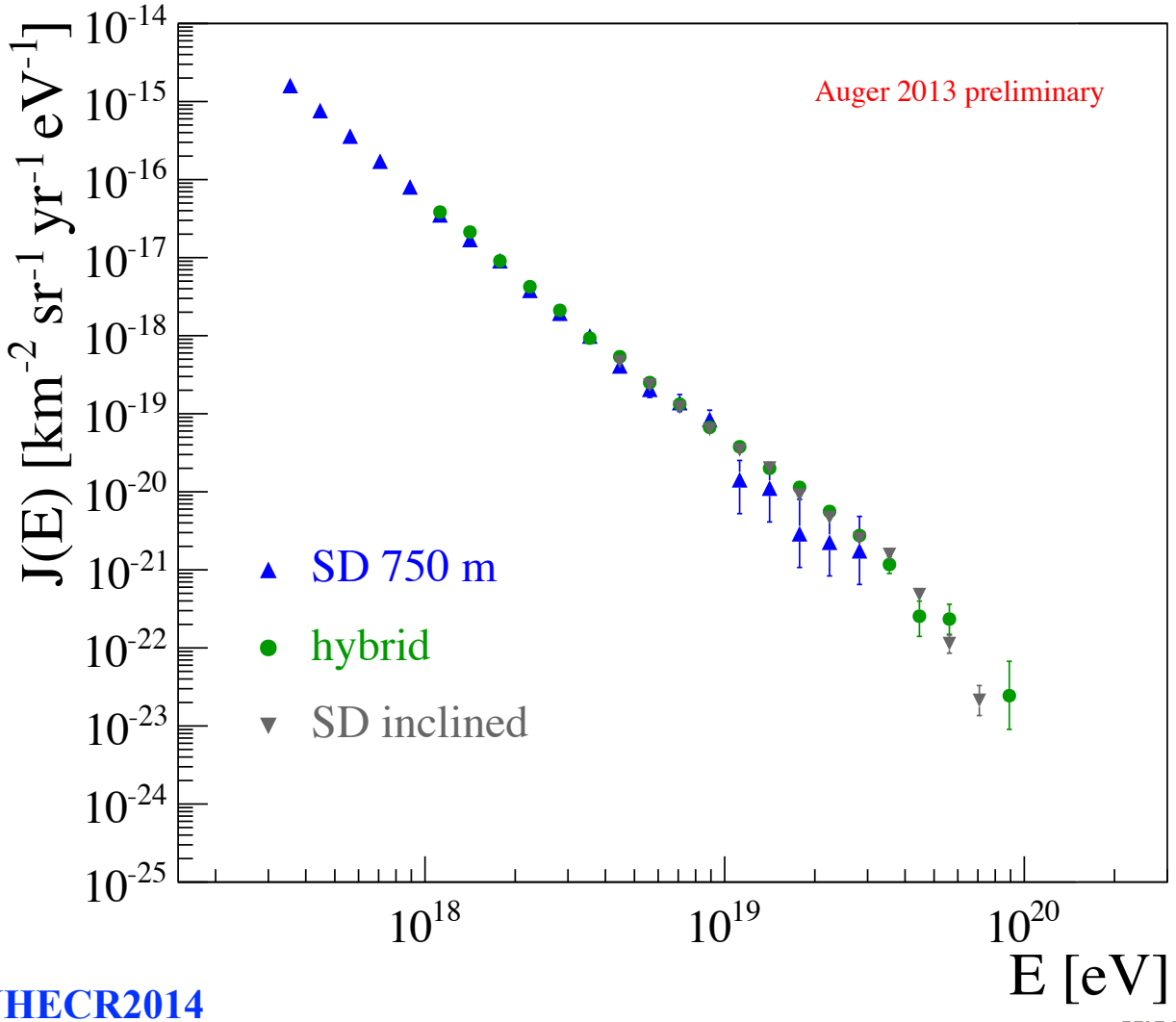

ENERGY SPECTRA

- SD inclined: 82318 events above 3×10^{18} eV (01/2004 – 12/2012)
- correction for bin-to-bin migrations due to the detector resolution and steepness of spectrum (< 17%)

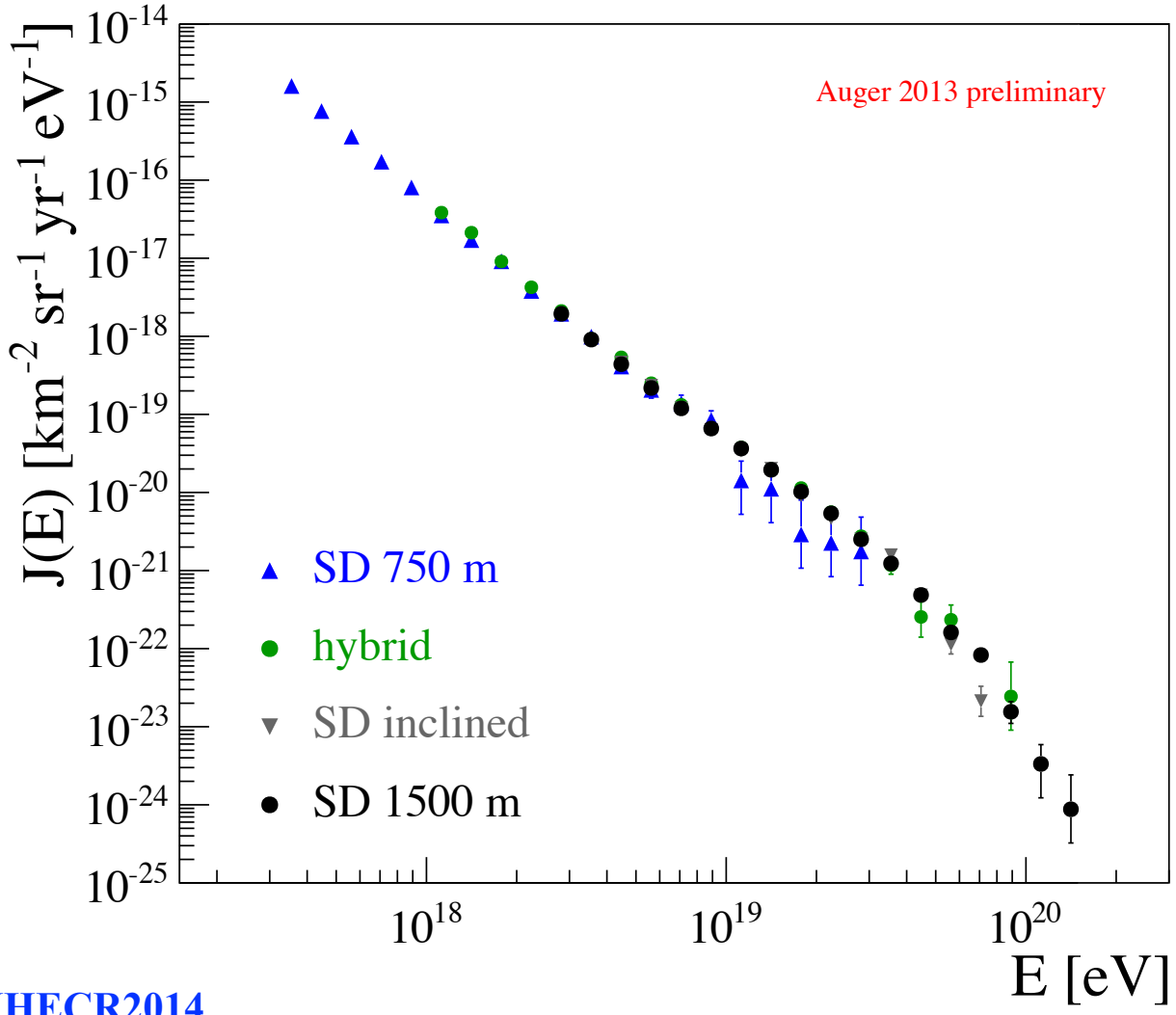

COMBINED ENERGY SPECTRA

- combination after few % correction to the normalizations

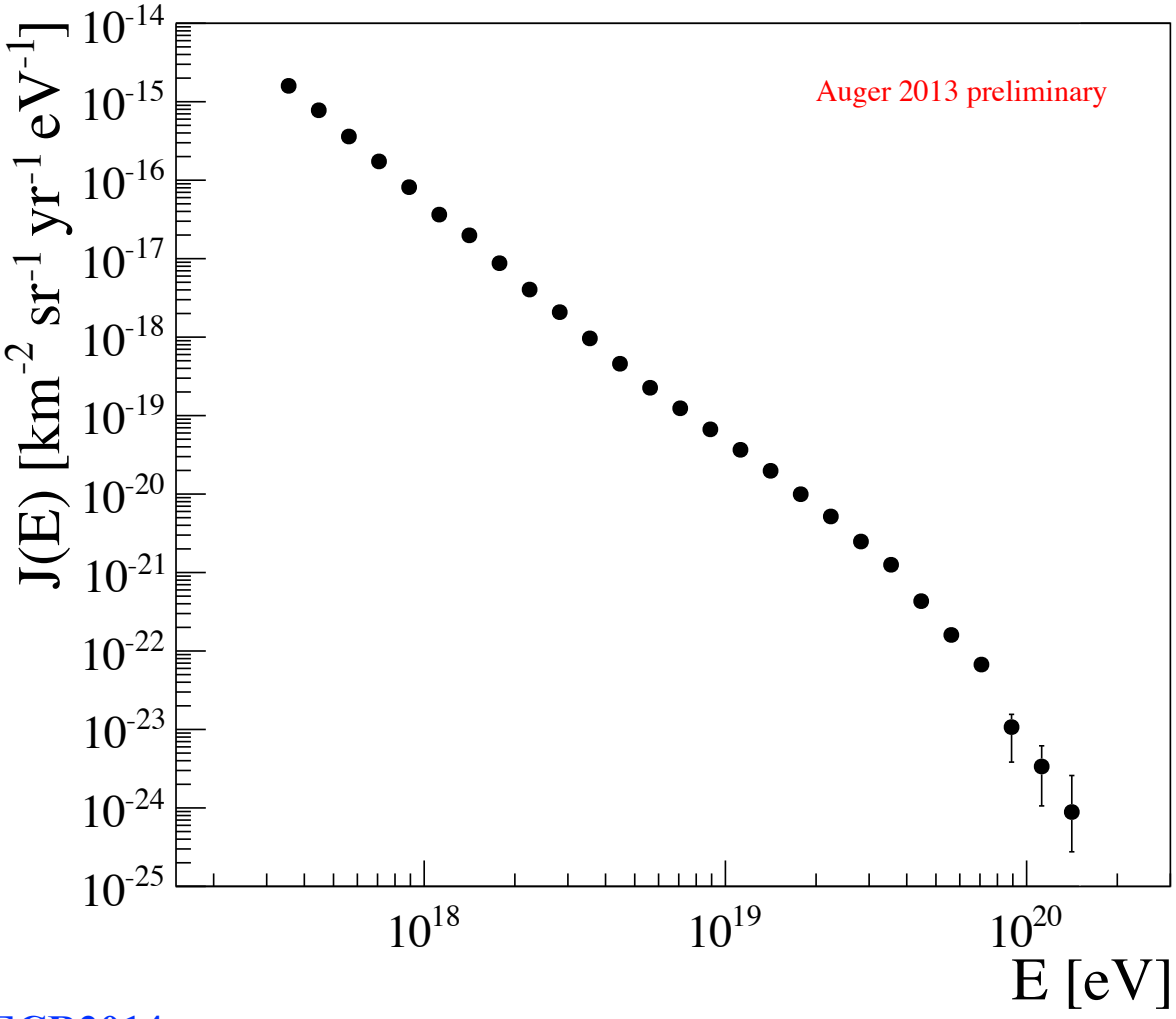

Auger (V. Verzi) UHECR2014

COMBINED ENERGY SPECTRA

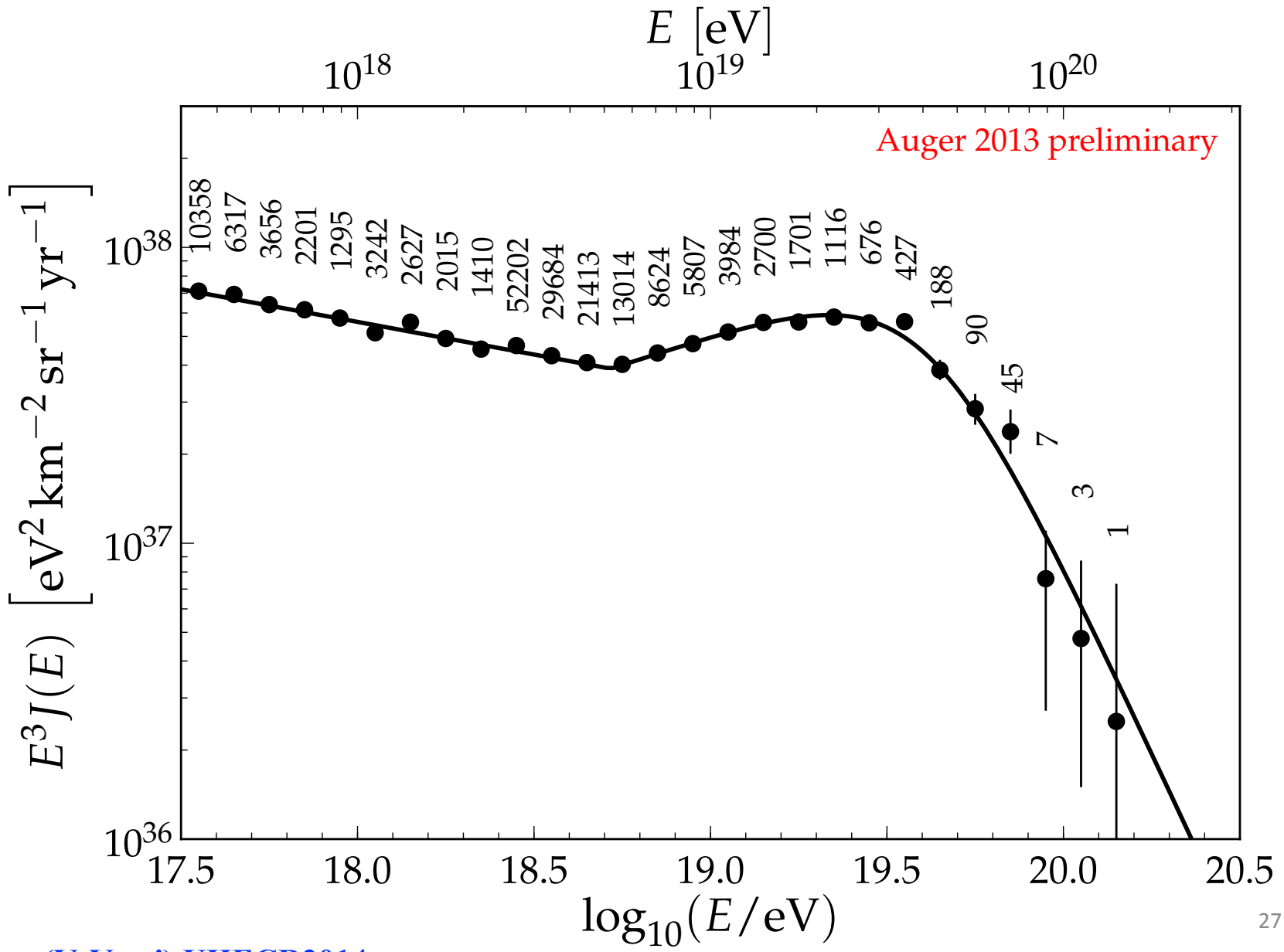

Auger (V. Verzi) UHECR2014

PIERRE AUGER OBSERVATORY

The Cosmic Ray Spectrum

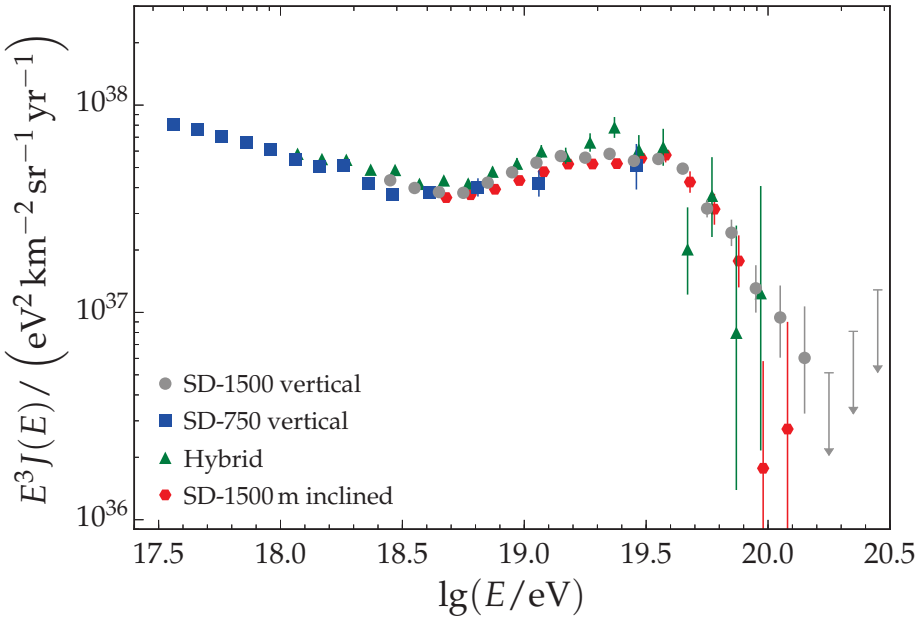

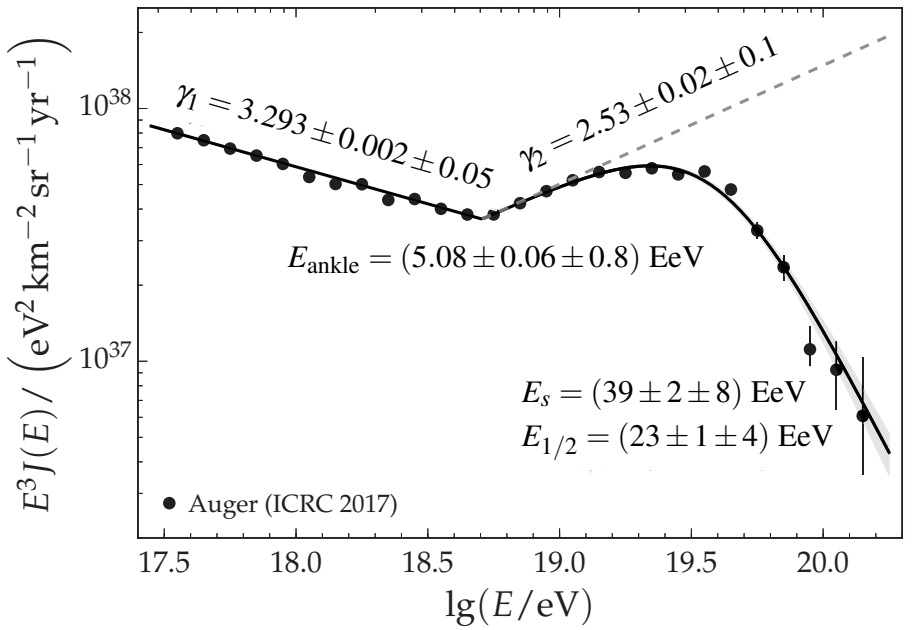

F. Fenu, ICRC 2017

reason for fall-off at highest energies?

- **maximum rigidity of accelerators?**
- **interactions with CMB?**

TA & PAO

Energy spectrum

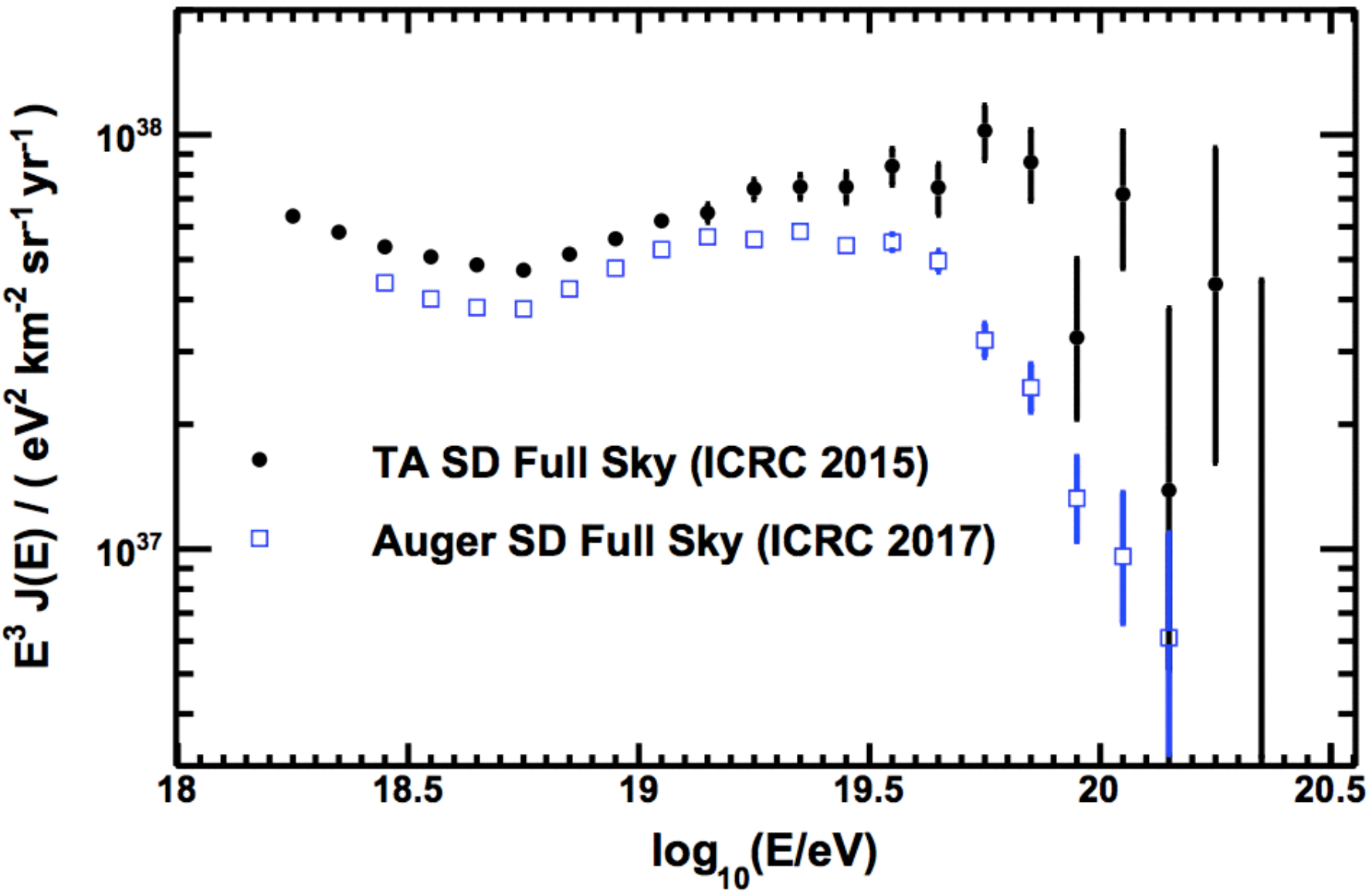

TA & PAO

Fluorescence yield

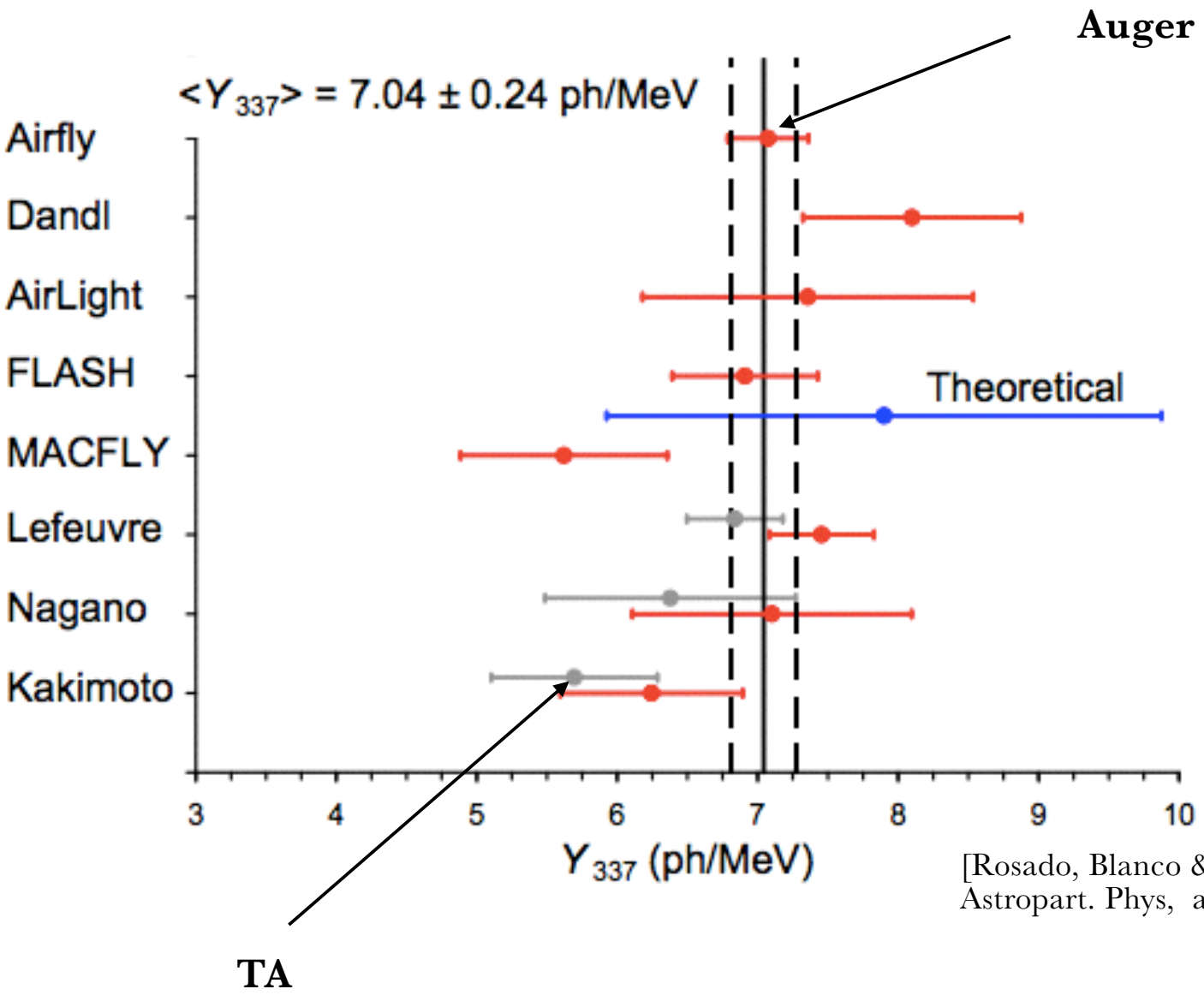

[Rosado, Blanco & Arqueros, Astropart. Phys, arXiv:1401.4310]

Invisible energy

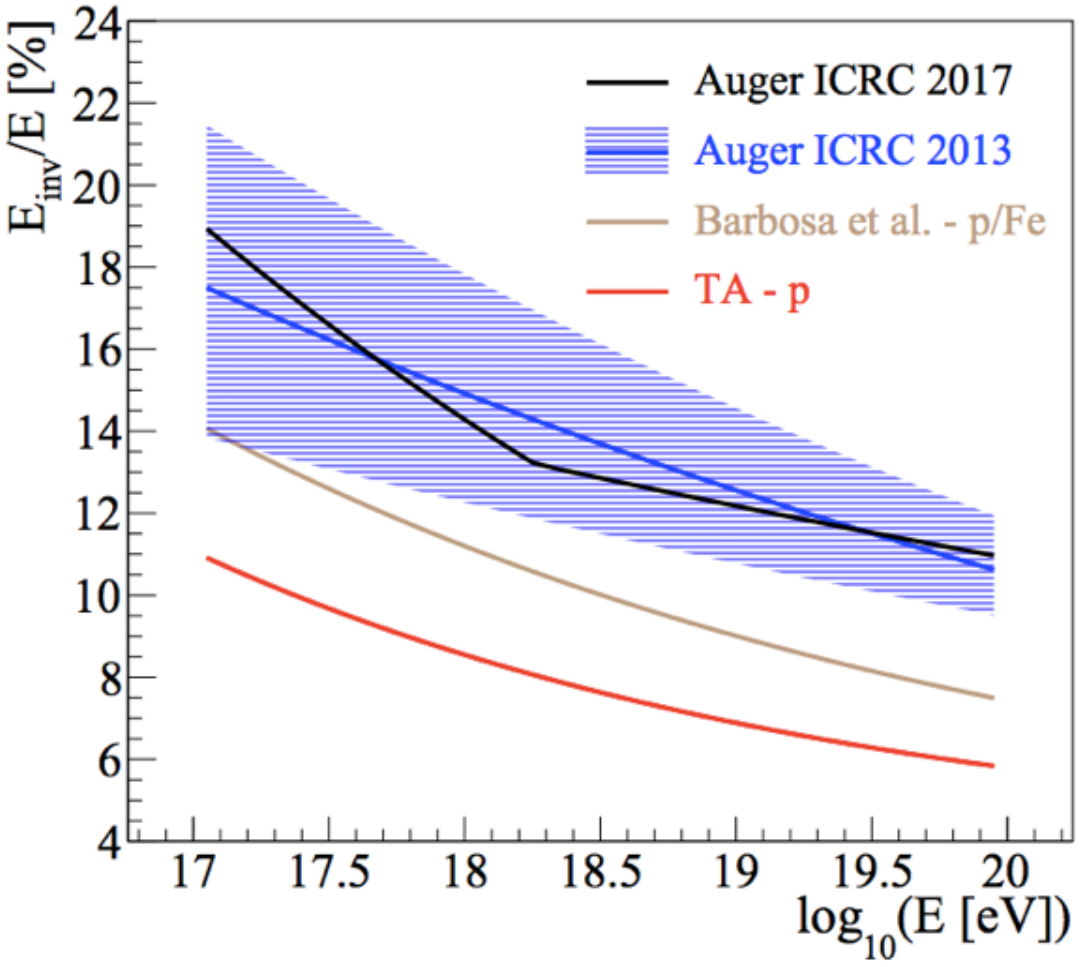

➡ **Good rationale to understand the global difference and so to apply a global rescaling**

TA & PAO

Rescaled energy spectrum

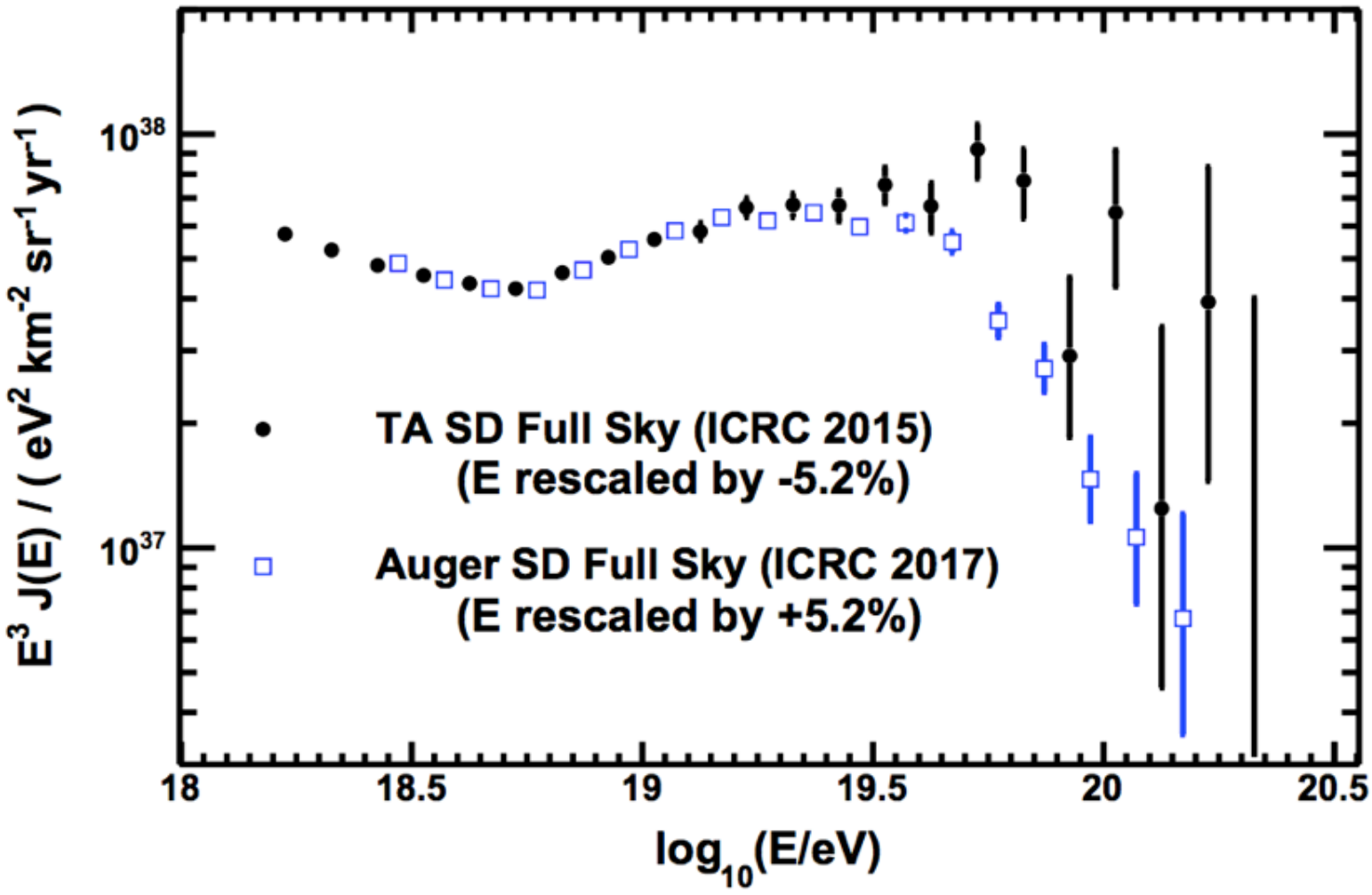

➡ Astrophysical effect or systematic uncertainties?

TA & PAO

Focus on the common field of view

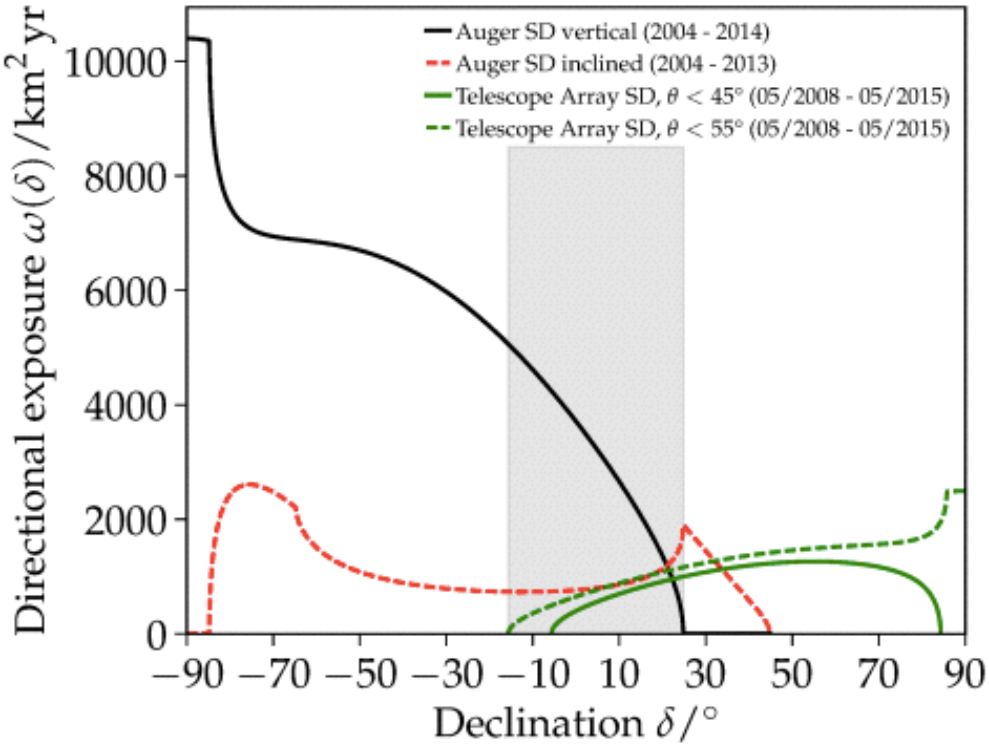

- Possibly, different intensities in different regions of the sky >10 EeV
- *But* same intensity in the common field of view
- If anisotropies, possible distortions by the directional exposure functions

➡ Remove distortions induced from different directional exposures in case of anisotropies:

$$J_{1/\omega}(E) = \frac{1}{\Delta\Omega\Delta E}\sum_{i=1}^{N}\frac{1}{\omega(\delta_i)}$$

TA & PAO

Results in the common sky—shifted energies

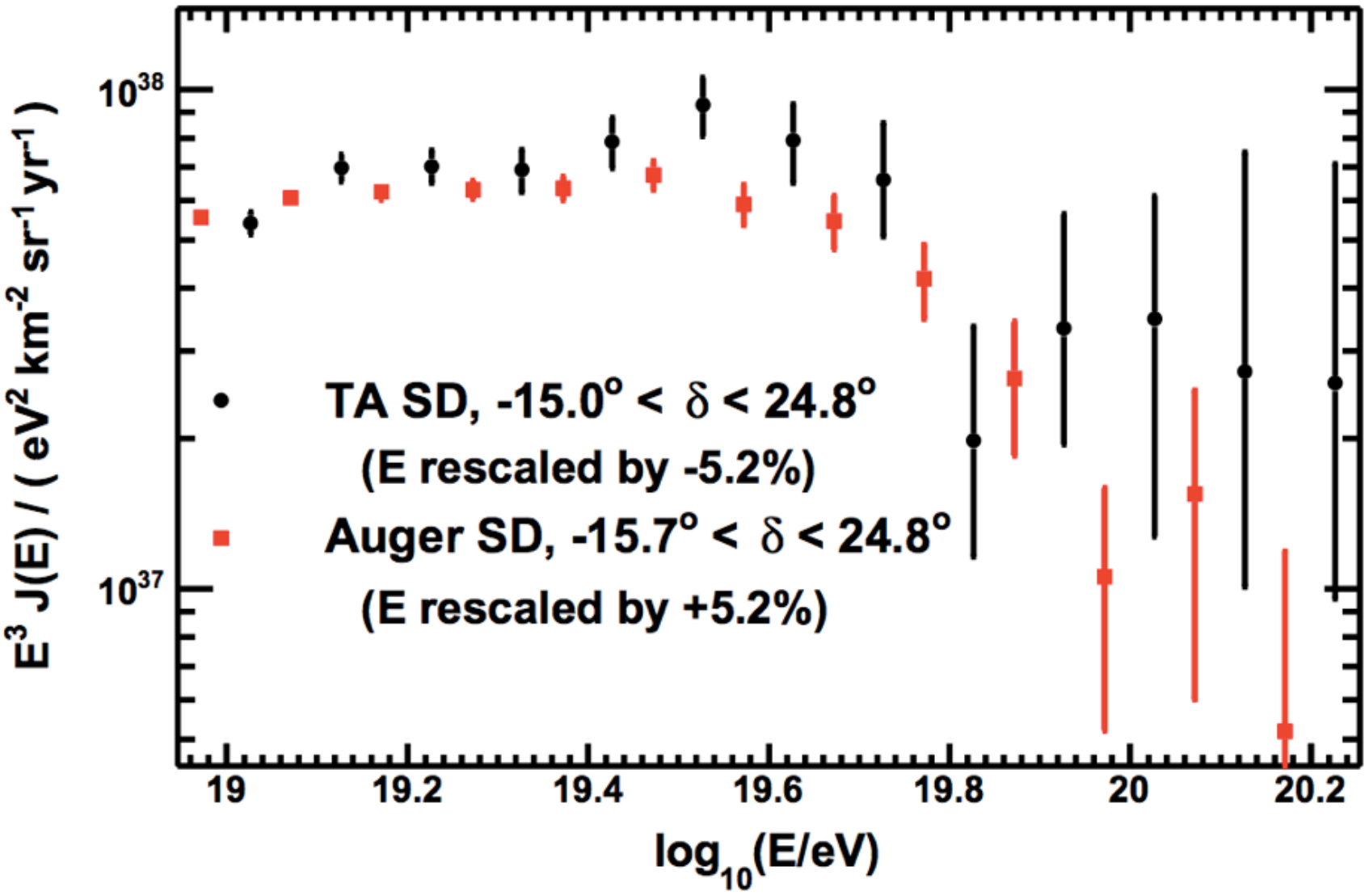

Mass composition

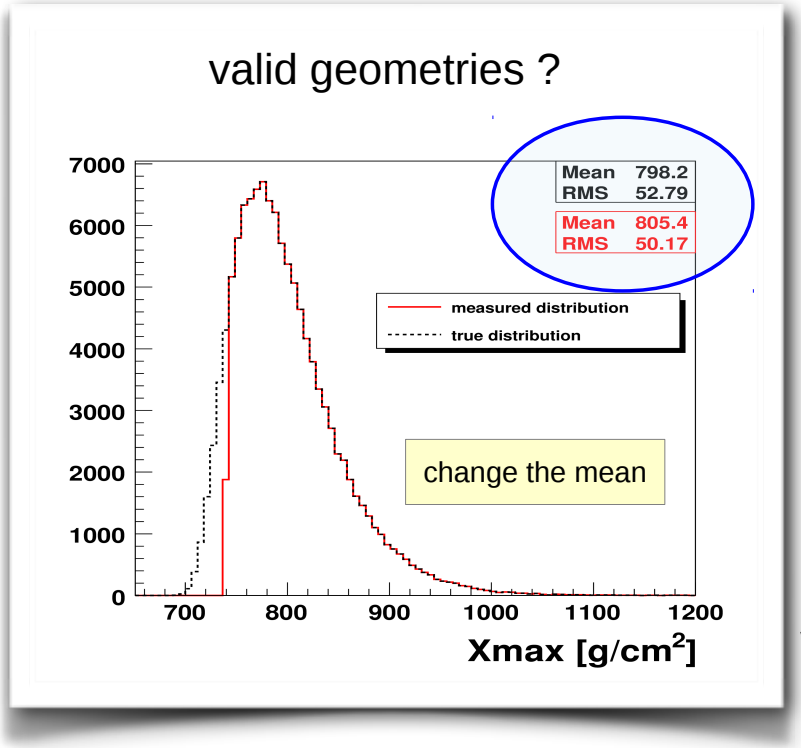

PIERRE AUGER OBSERVATORY

fiducial field of view

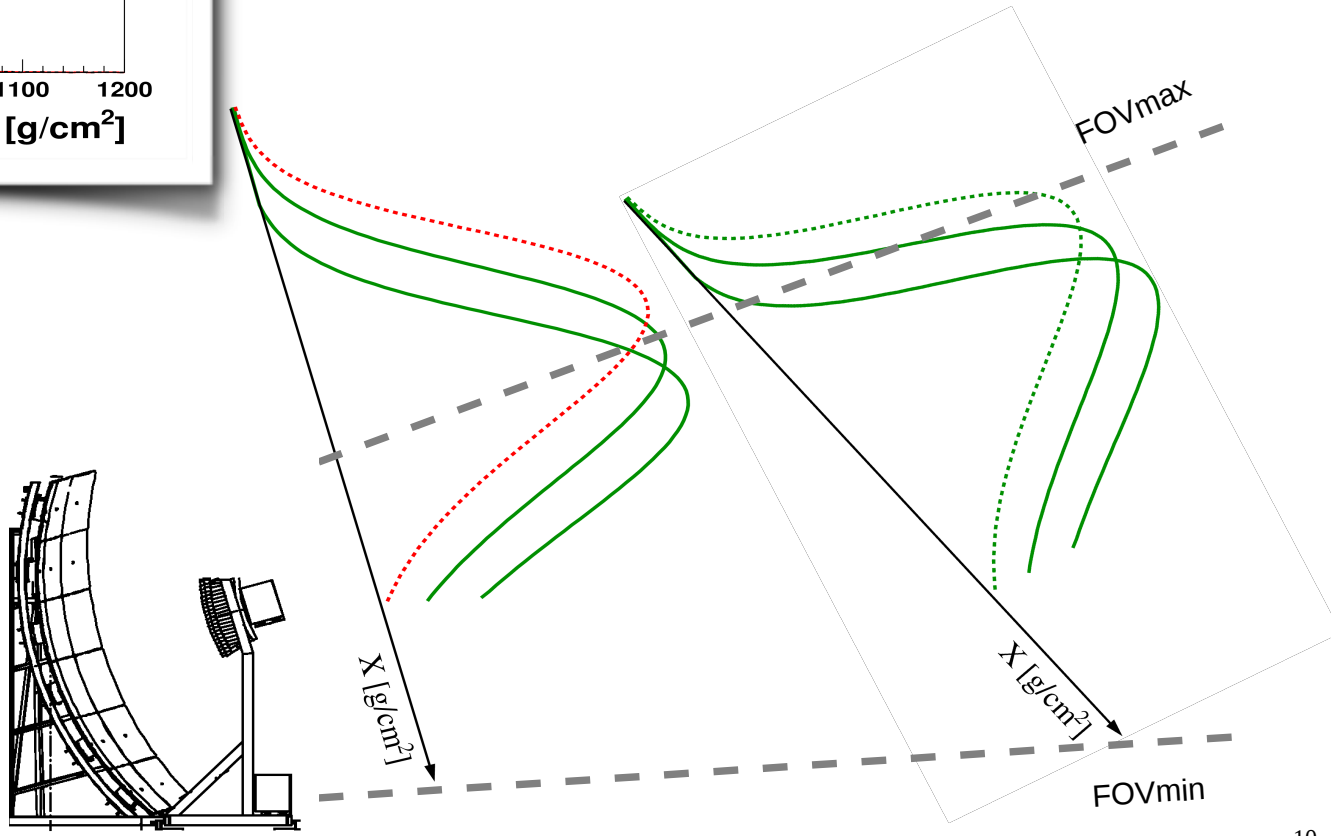

valid geometries ?

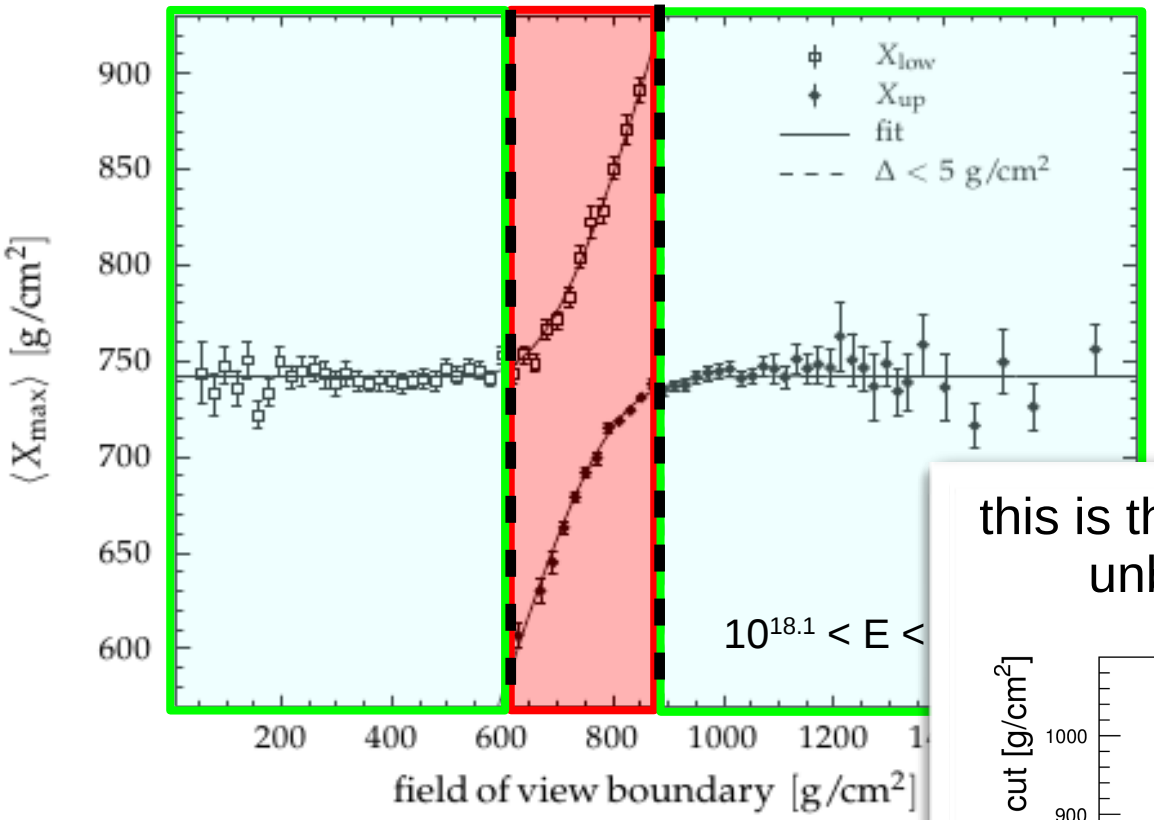

this is the valid geometry that assures unbiased Xmax distributions

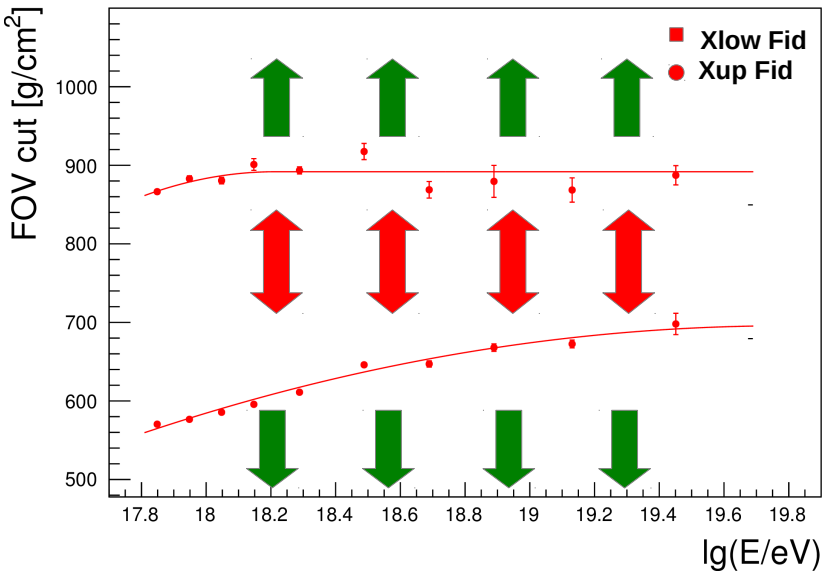

Composition: The elongation rate

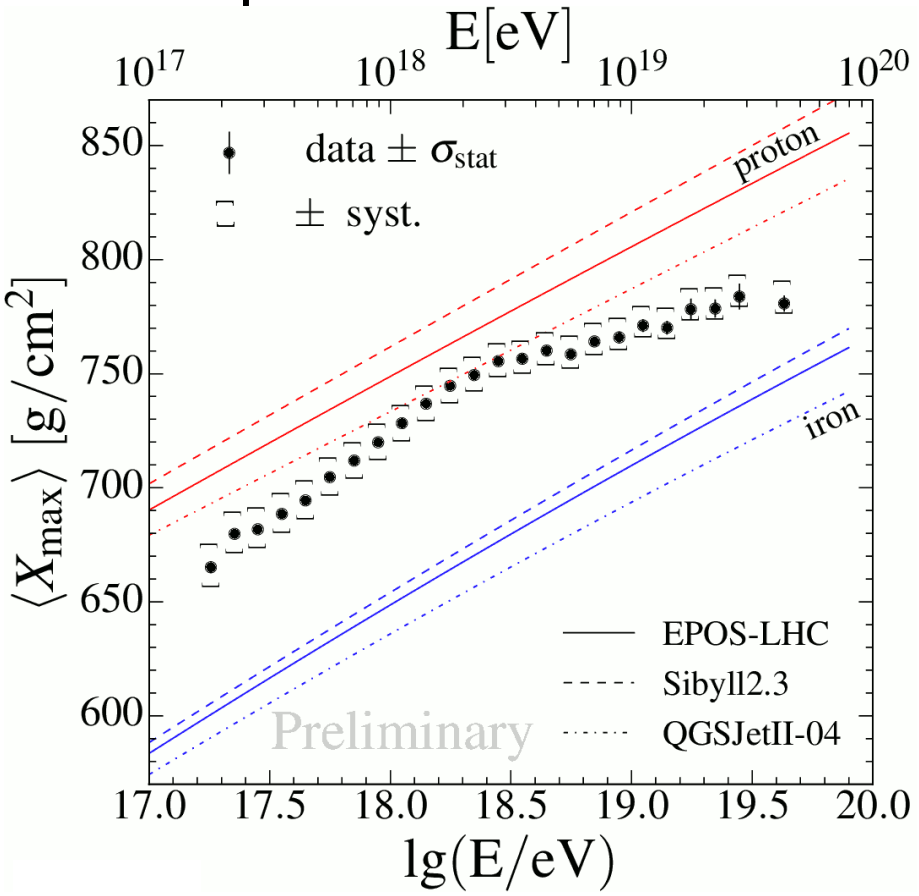

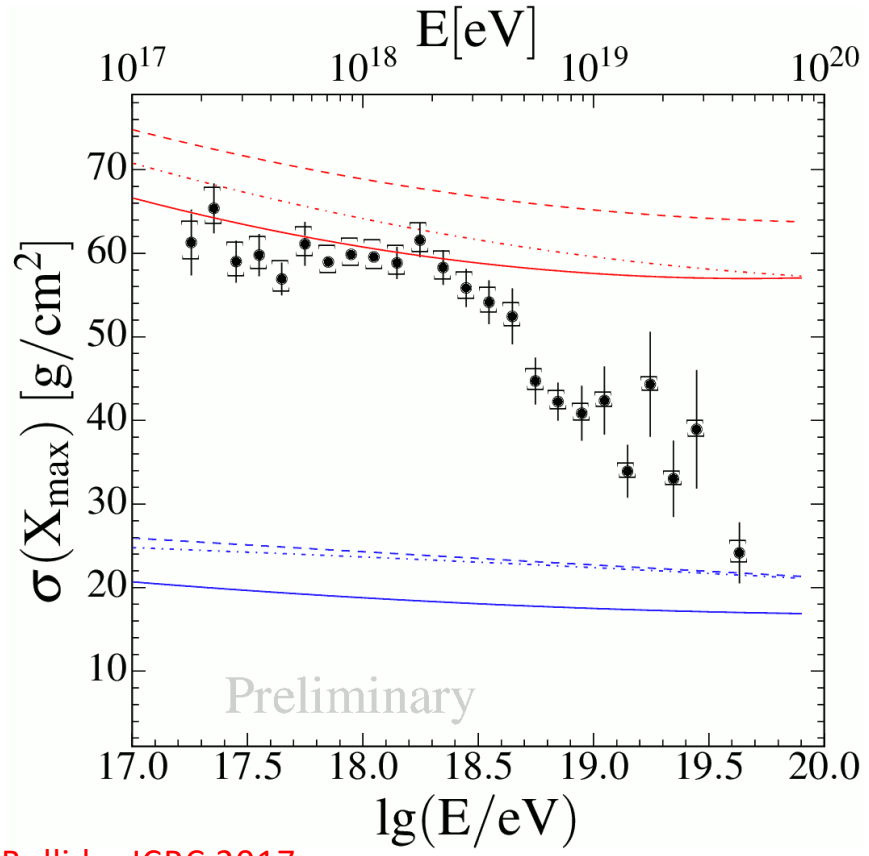

J. Bellido, ICRC 2017

$$\langle \ln A \rangle \equiv \sum_i r_i \ln A_i, \qquad \langle \ln A \rangle = \frac{X_{max}^{meas} - X_{max}^{p}}{X_{max}^{Fe} - X_{max}^{p}} \cdot \ln A_{Fe}.$$

Mean logarithmic mass

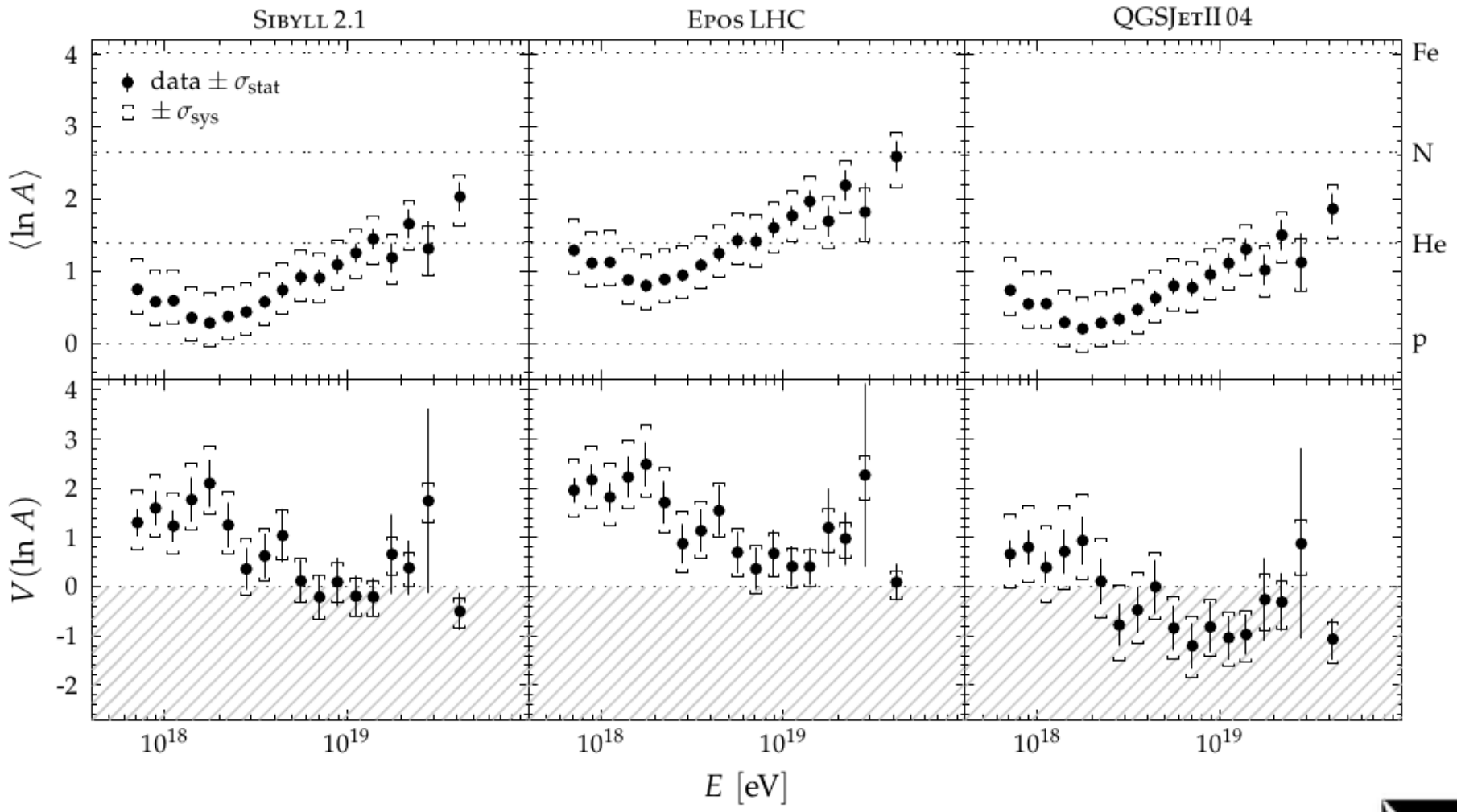

V (ln A) measures the purity of the sample:

- pure Pr or pure Fe or pure anything → *V(ln A)* = 0
- 50:50 Pr:Fe → *V(ln A)* ≈ 4

J. Lisley, ICRC 1985

PIERRE AUGER OBSERVATORY

fitting abundances

simulated air shower including the detector response

2×10^4 showers per energy bin

Proton
Helium
Nitrogen
Iron

s

Pr + Fe

Pr + N + Fe

Pr + He + N + Fe

In each bin of energy
Log Likelihood fit

$$L = \prod_j \left[\frac{e^{-C_j} C_j^{n_j}}{n_j!} \right]$$

fraction of each species

$$C_j = \frac{N_{data}}{N} \sum_s f_s X^{\mathrm{m}}_{s,j}$$

j = index of Xmax bin n_j = measured number of shower C_j = Simulation prediction

42

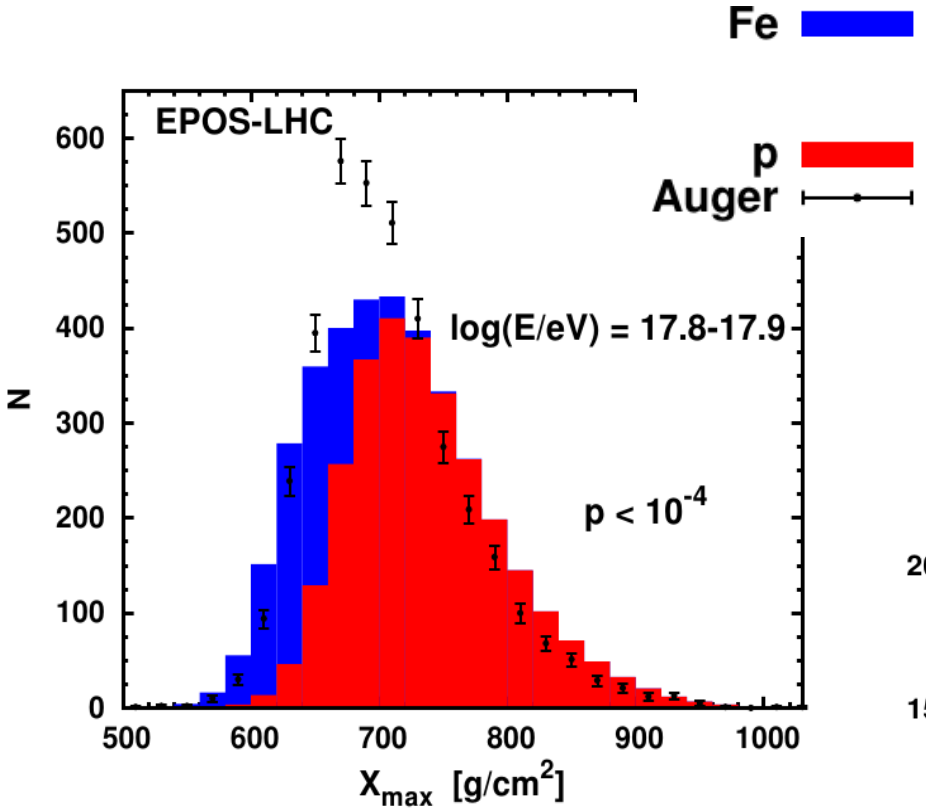

proton + iron

Similar picture for all hadronic interaction models

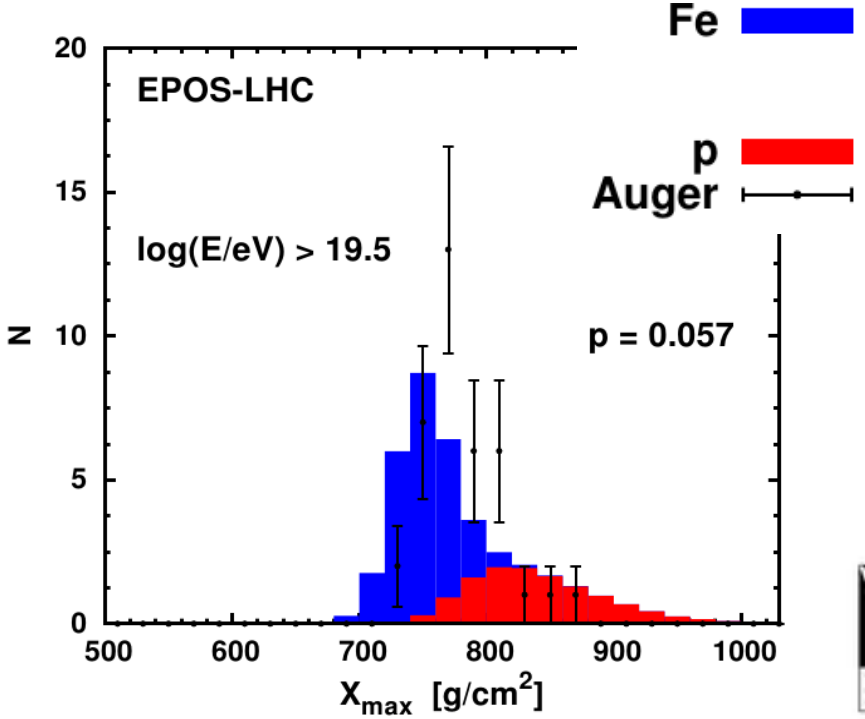

Very poor agreement with the data for most energy bins

proton + nitrogen + iron

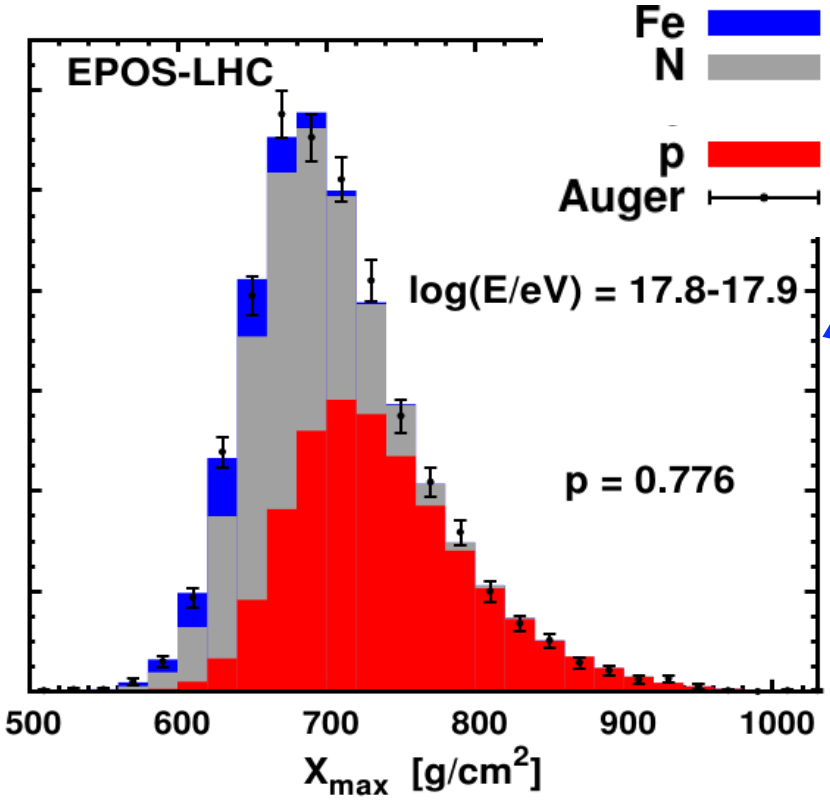

EPOS-LHC describes the data best

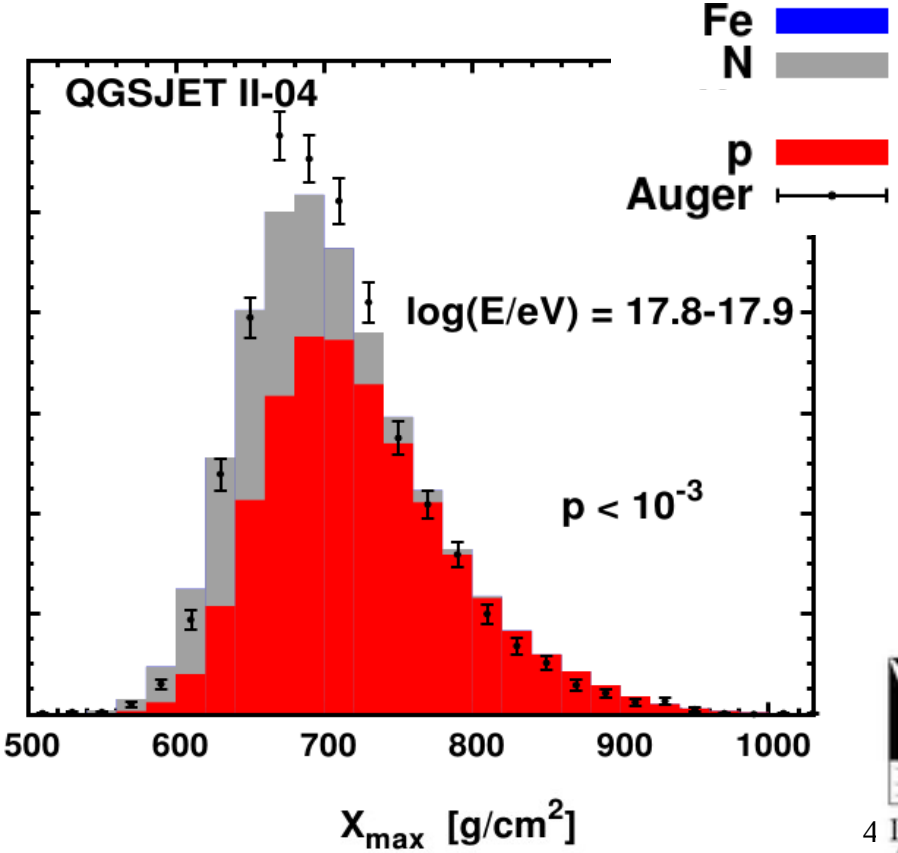

acceptable/poor agreement with the data

proton + helium + nitrogen + iron

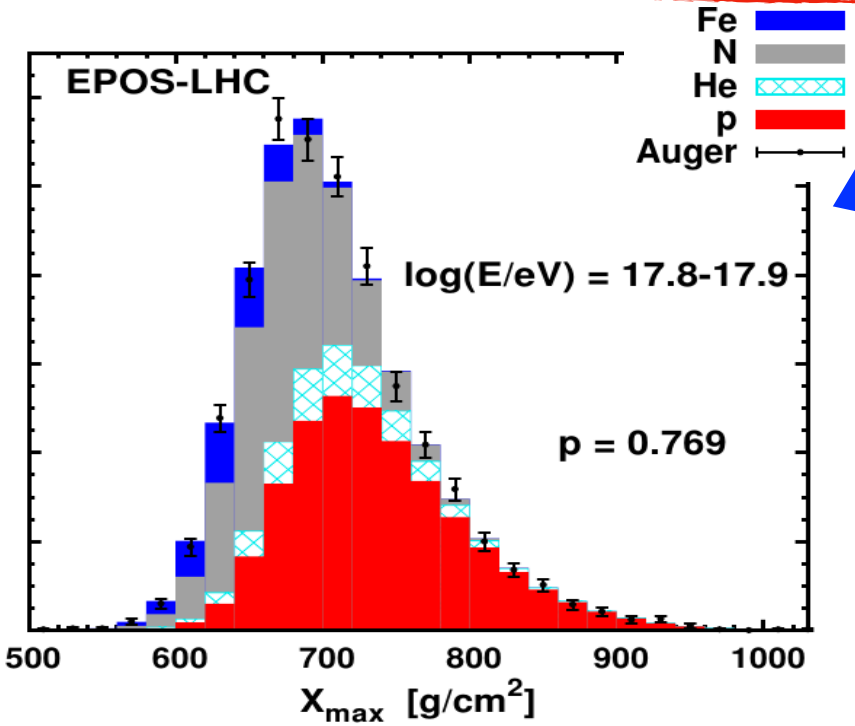

EPOS-LHC describes the data best

QGSJet II-04 describes the data worst

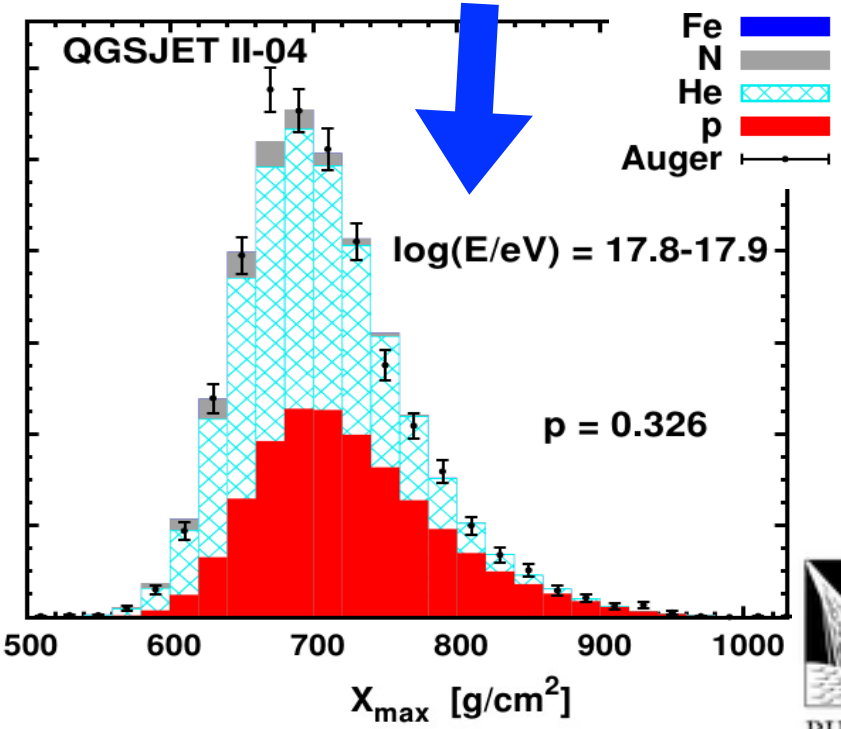

acceptable/good agreement with the data

PIERRE AUGER OBSERVATORY

proton + helium + nitrogen + iron

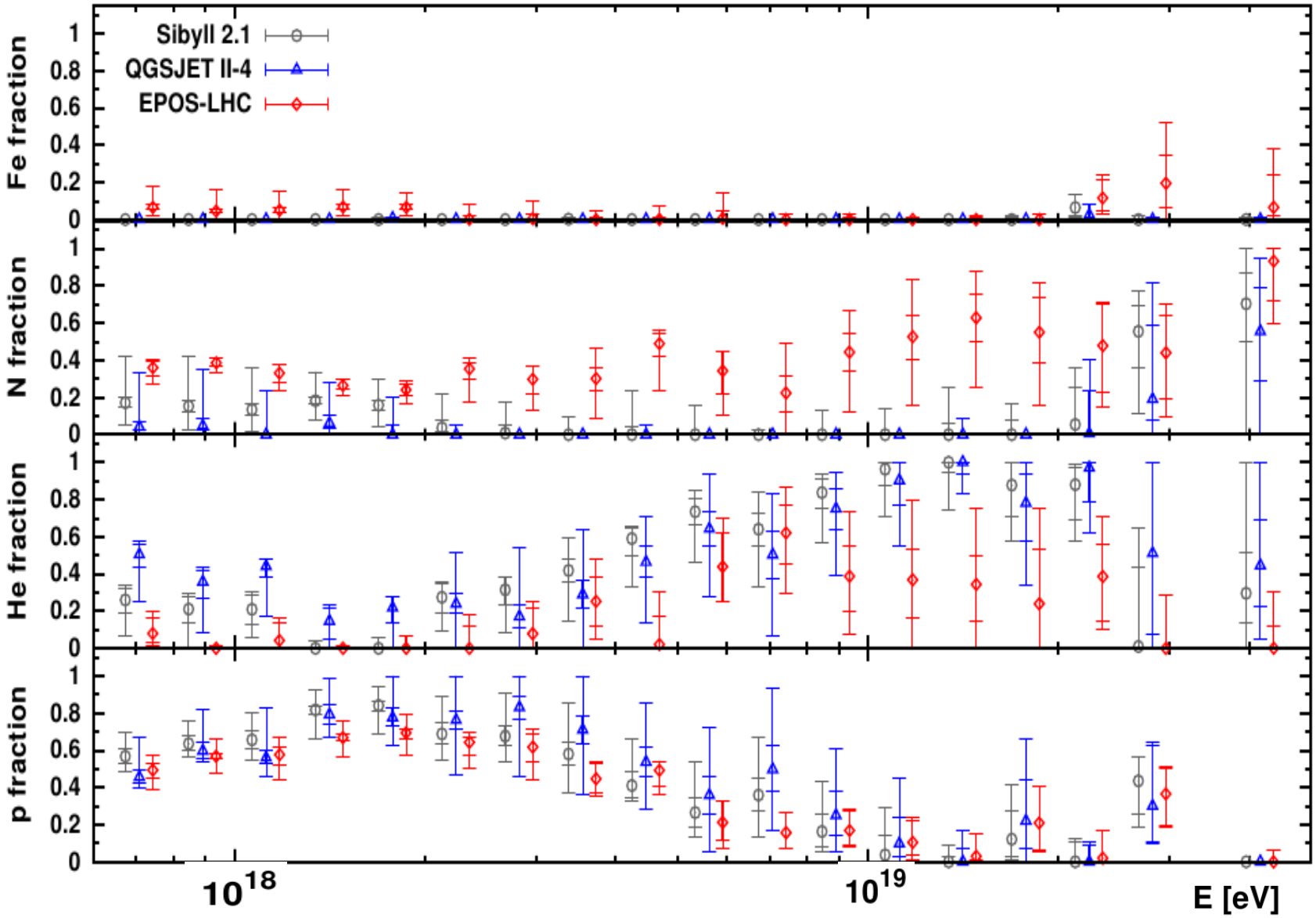

48

Auger (V. de Souza) UHECR2014

Journal of Cosmology and Astroparticle Physics
An IOP and SISSA journal

Combined fit of spectrum and composition data as measured by the Pierre Auger Observatory

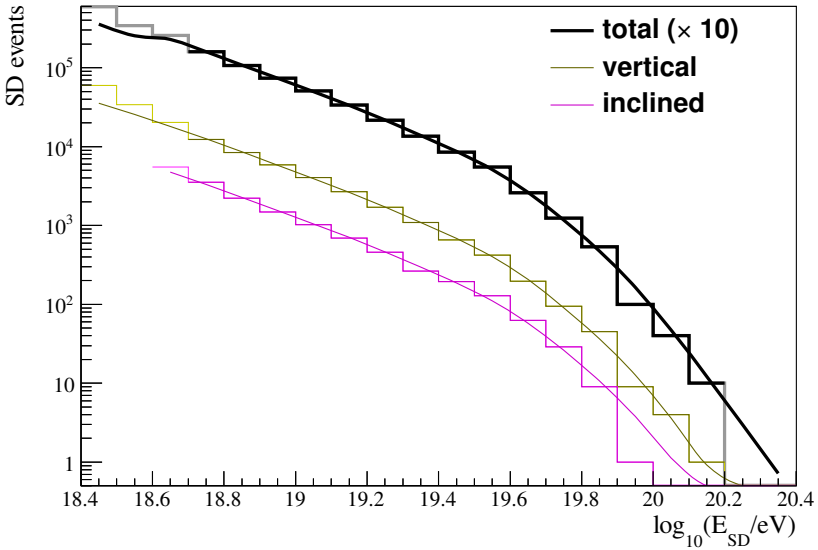

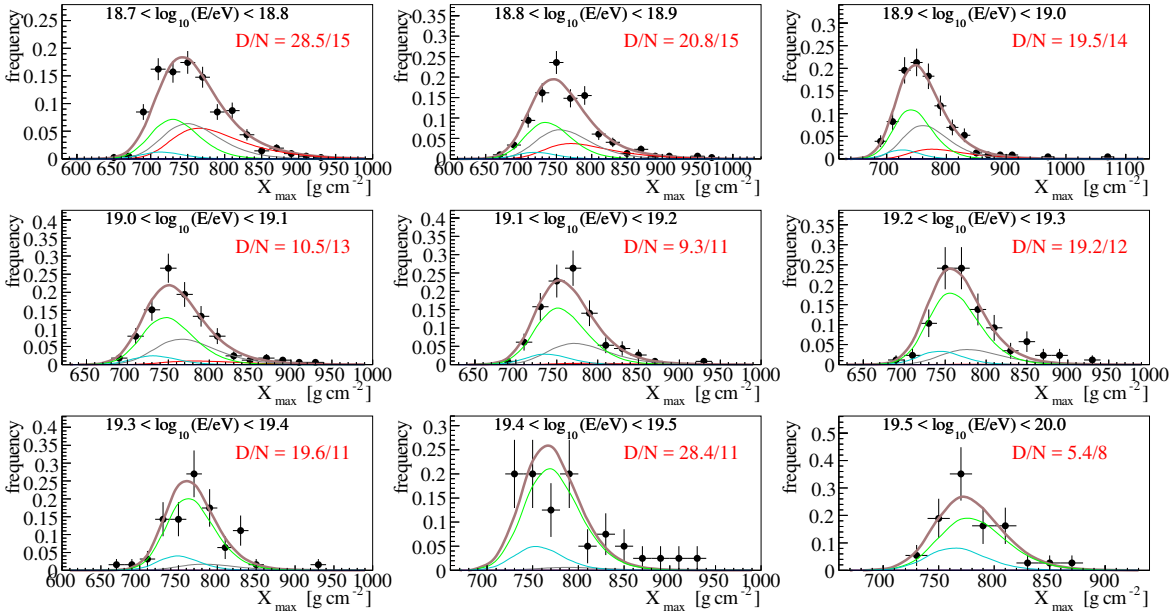

Figure 2. Top: fitted spectra, as function of *reconstructed* energy, compared to experimental coun The sum of horizontal and vertical counts has been multiplied by 10 for clarity. Bottom: the dist butions of $X_{\max}$ in the fitted energy bins, best fit minimum, SPG propagation model, EPOS-LI UHECR-air interactions. Partial distributions are grouped according to the mass number as follo $A = 1$ (red), $2 \leq A \leq 4$ (grey), $5 \leq A \leq 22$ (green), $23 \leq A \leq 38$ (cyan), total (brown).

JCAP04(2017)038

Combined fit of spectrum and composition data as measured by the Pierre Auger Observatory

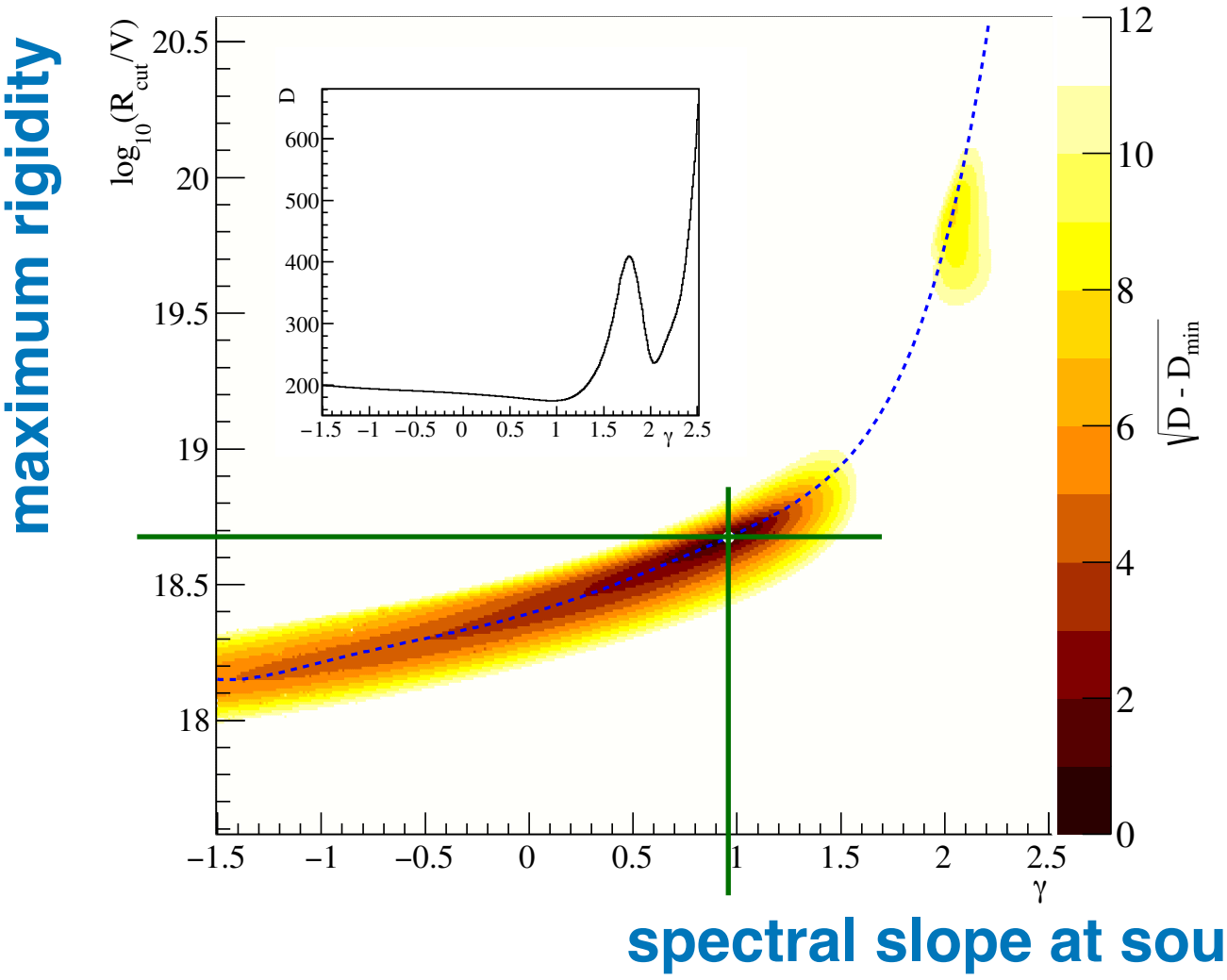

Figure 1. Deviance $\sqrt{D - D_{\rm min}}$, as function of γ and $\log_{10}(R_{\rm cut}/{\rm V})$. The dot indicates the position of the best minimum, while the dashed line connects the relative minima of D (valley line). In the inset, the distribution of $D_{\rm min}$ in function of γ along this line.

JCAP04(2017)038

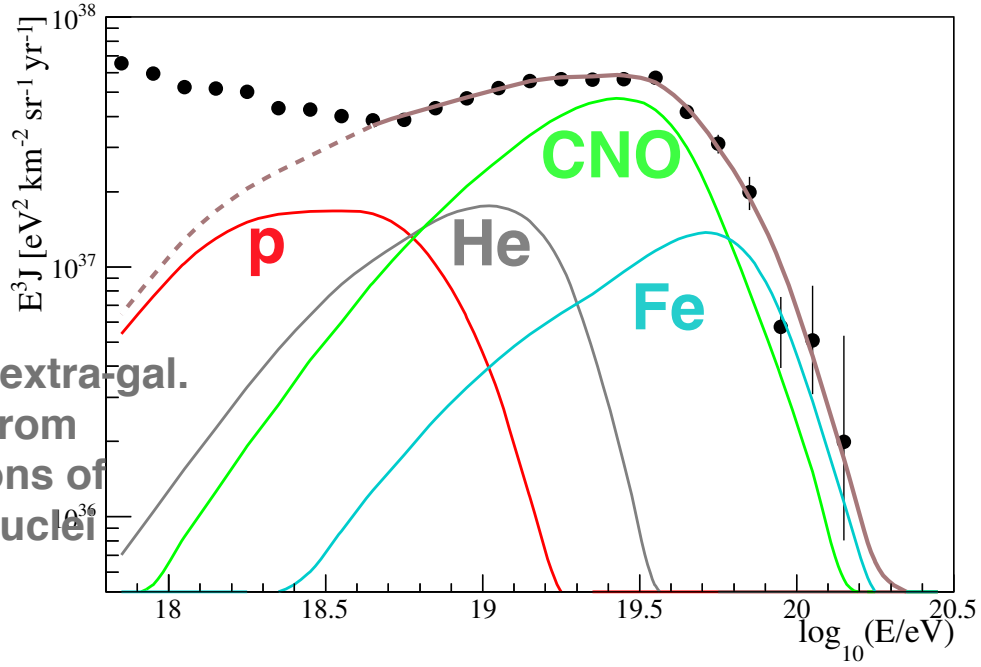

Combined fit of spectrum and composition data as measured by the Pierre Auger Observatory

Sub-EeV extra-gal. protons from interactions of heavier nuclei

p	$A = 1$
He	$2 \leq A \leq 4$
CNO	$5 \leq A \leq 22$
Fe	$27 \leq A \leq 56$

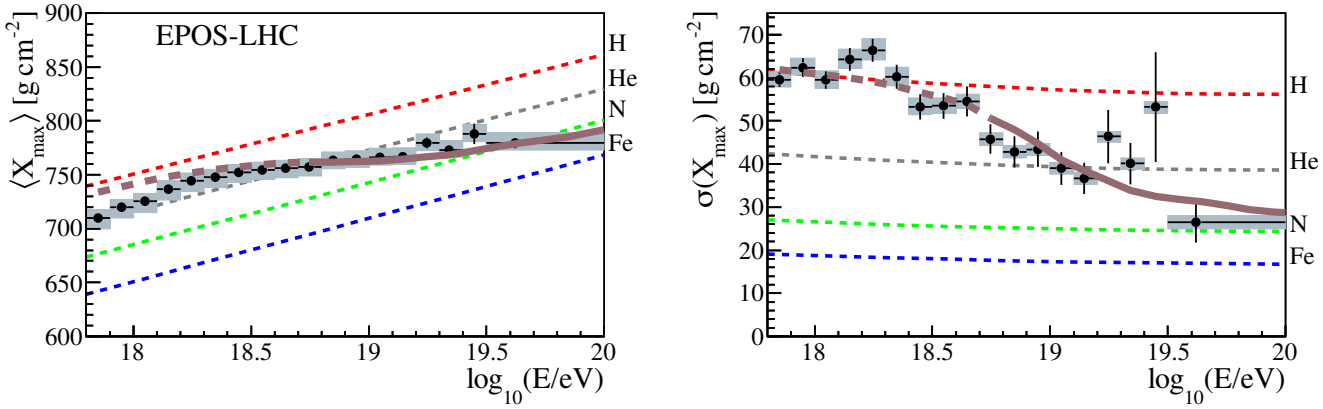

Figure 3. Top: simulated energy spectrum of UHECRs (multiplied by E^3) at the top of the Earth's atmosphere, obtained with the best-fit parameters for the reference model using the procedure described in section 3. Partial spectra are grouped as in figure 2. For comparison the fitted spectrum is reported together with the spectrum in [4] (filled circles). Bottom: average and standard deviation of the $X_{\rm max}$ distribution as predicted (assuming EPOS-LHC UHECR-air interactions) for the model (brown) versus pure ^{1}H (red), ^{4}He (grey), ^{14}N (green) and ^{56}Fe (blue), dashed lines. Only the energy range where the brown lines are solid is included in the fit.

JCAP04(2017)038

Combined fit of spectrum and composition data as measured by the Pierre Auger Observatory

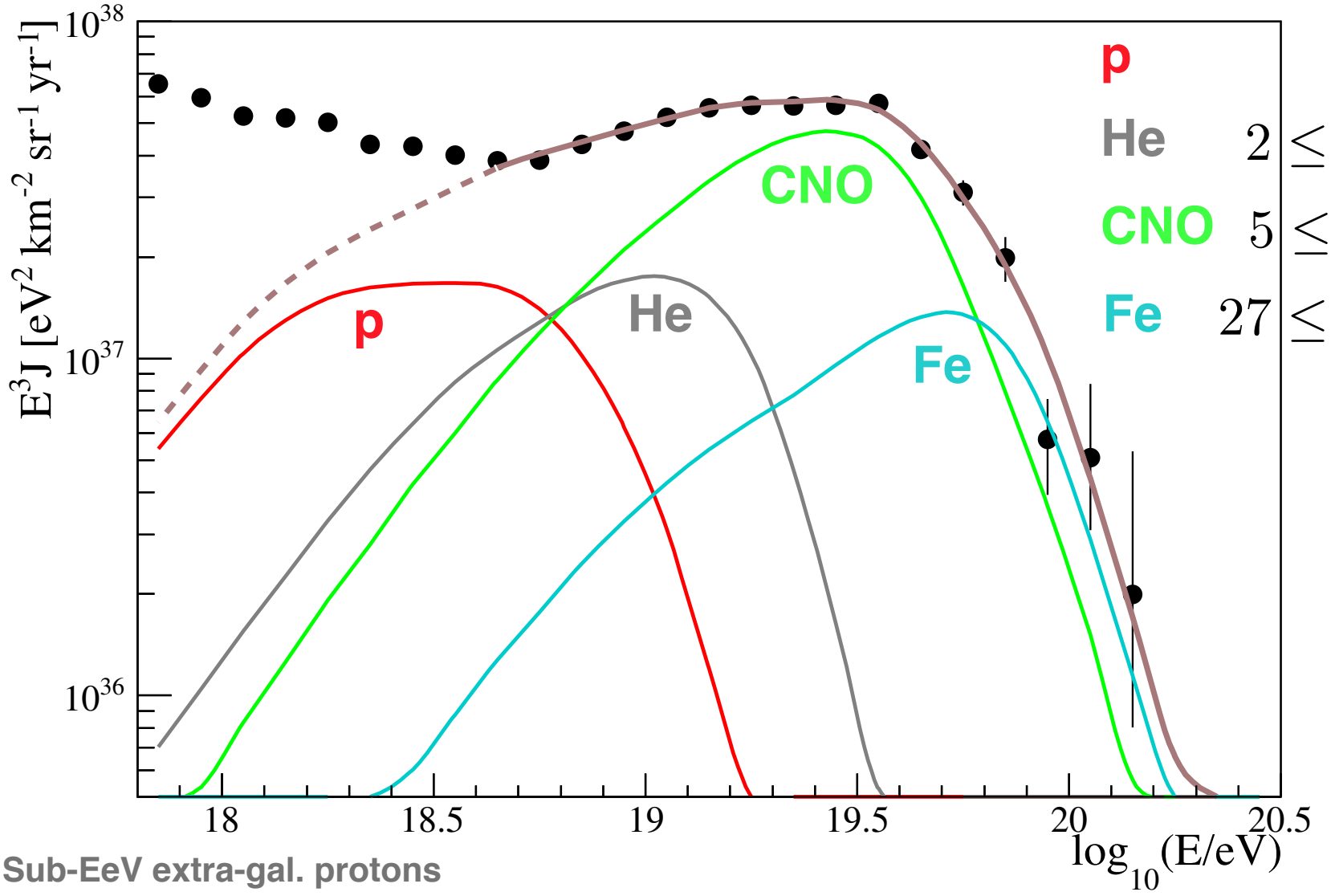

Sub-EeV extra-gal. protons from interactions of heavier nuclei

PIERRE AUGER OBSERVATORY

JCAP04(2017)038

Mean logarithmic mass

$$\ln A = \sum k_i \ln A_i$$

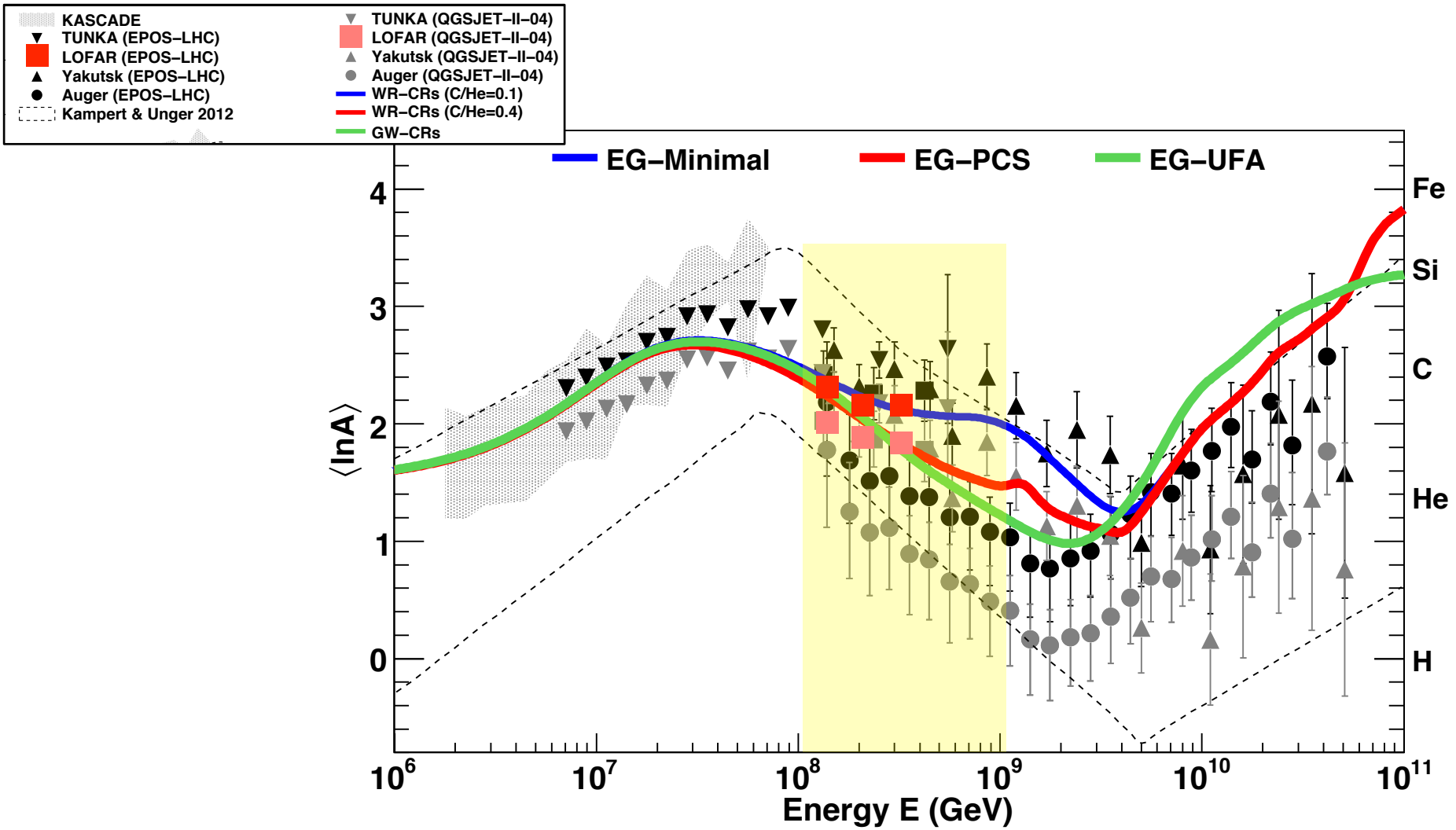

S. Thoudam et al., A&A 595 (2016) A33

Arrival direction

COSMIC RAYS

Observation of a large-scale anisotropy in the arrival directions of cosmic rays above 8×10^{18} eV

The Pierre Auger Collaboration*†

Anisotropy detected at >5.2 sigma
dipole amplitude 6.5%

physicsworld TOP 10 BREAKTHROUGH 2017

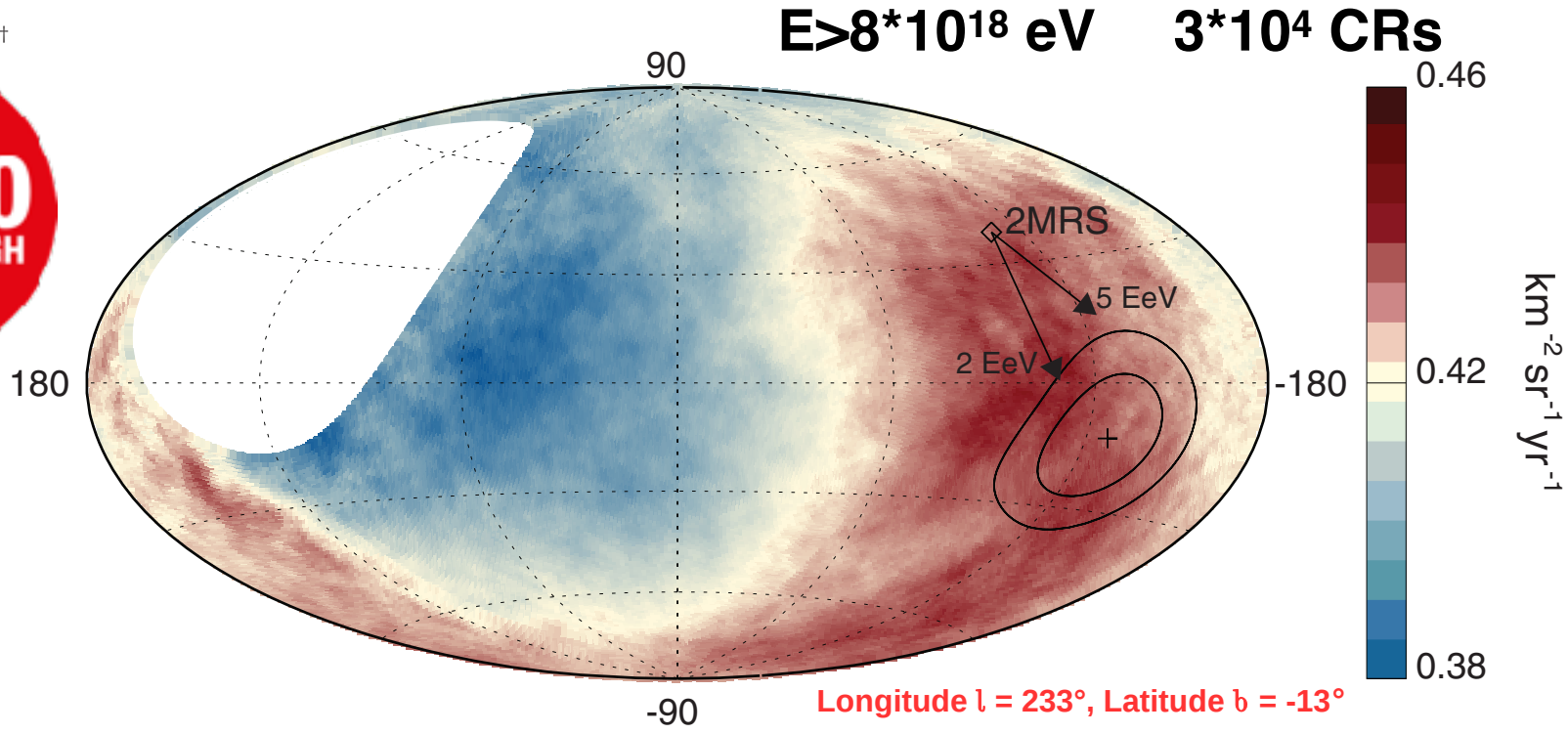

Fig. 3. Map showing the fluxes of particles in galactic coordinates. Sky map in galactic coordinates showing the cosmic-ray flux for $E \geq 8$ EeV smoothed with a 45° top-hat function. The galactic center is at the origin. The cross indicates the measured dipole direction; the contours denote the 68% and 95% confidence level regions. The dipole in the 2MRS galaxy distribution is indicated. Arrows show the deflections expected for a particular model of the galactic magnetic field (*8*) on particles with E/Z = 5 or 2 EeV.

A. Aab et al., Science 357 (2017) 1266

Extragalactic tested population

Starburst galaxies

M82

Intense star formation + winds

23 objects from *Fermi-LAT* observations within **250 Mpc** with a radio flux at **1.4GHz > 0.3 Jy**

Nearby galaxies

e.g.: NGC253, M82, NGC4945, NGC1068

Active Galactic Nuclei

Centaurus A

Jets and radiolobes

17 objects from 2FHL catalog within **250 Mpc**
(*Fermi*-LAT, > 50 GeV)

More distant galaxies

e.g.: Centaurus A, Mkn421, Mkn501

Indication of anisotropy in arrival directions of ultra-heigh-energy cosmic rays through comparison to the flux pattern of extragalactic gamma-ray sources

Active Galactic Nuclei

- 2FHL AGNs
- flux proxy: $\Phi(> 50\,\mathrm{GeV})$
- 17 objects within 250 Mpc

Star-forming of Starburst Galaxies

- Fermi-LAT search list (Ackermann+2016)
- $\Phi(> 1.54, \mathrm{GHz}) > 0.3$ Jy
- flux proxy: $\Phi(> 1.54, \mathrm{GHz})$
- 23 objects within 250 Mpc

Likelihood ratio analysis

- smearing angle ψ
- H_0: isotropy
- H_1: $(1-f)\times$ isotropy + $f\times$ fluxMap(ψ)
- $\mathrm{TS} = 2\log(H_1/H_0)$

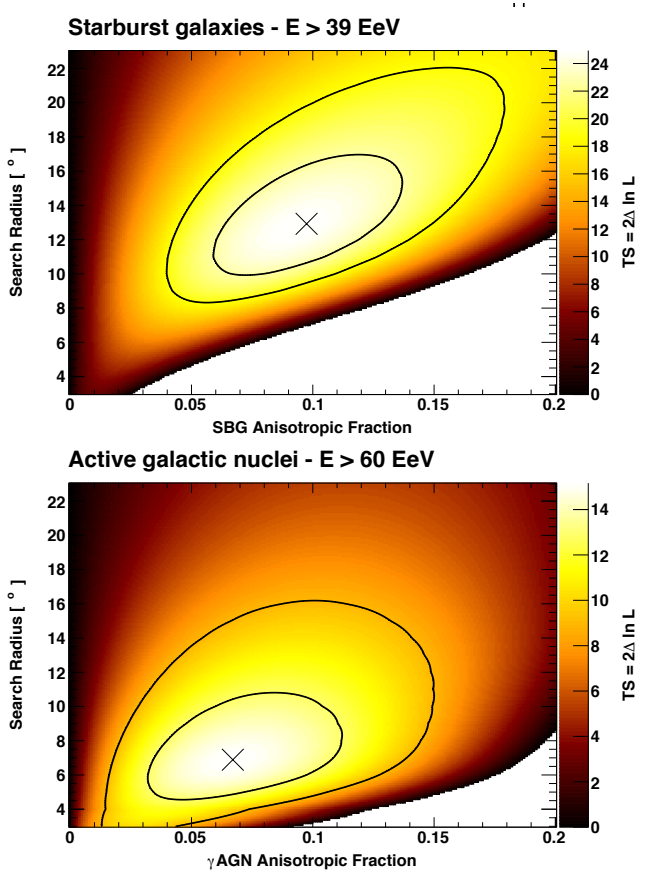

[20 of 30]

A. Aab et al. ApJ 835 (2018) L29

Indication of anisotropy in arrival directions of ultra-heigh-energy cosmic rays through comparison to the flux pattern of extragalactic gamma-ray sources

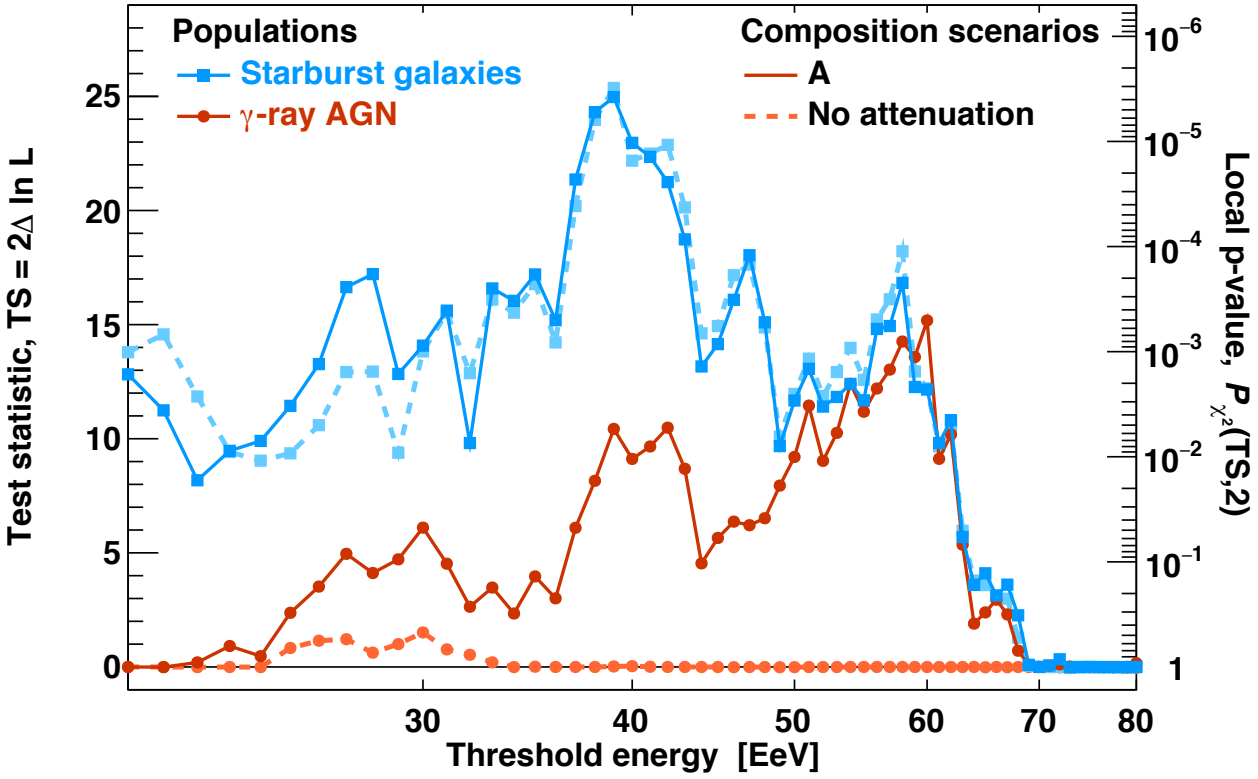

E>39 EeV

starburst

SBG fraction: 9.7%
search radius: 12.9°
pre-trail p-value: 3.8×10^{-6}
post-trial p-value: 3.6×10^{-5}
post-trial significance: 4.0 sigma

AGN

search radius: 6.9°
pre-trail p-value: 5.1×10^{-4}
post-trial p-value: 3.1×10^{-3}
post-trial significance: 2.7 sigma

A. Aab et al. ApJ 835 (2018) L29

Indication of anisotropy in arrival directions of ultra-heigh-energy cosmic rays through comparison to the flux pattern of extragalactic gamma-ray sources

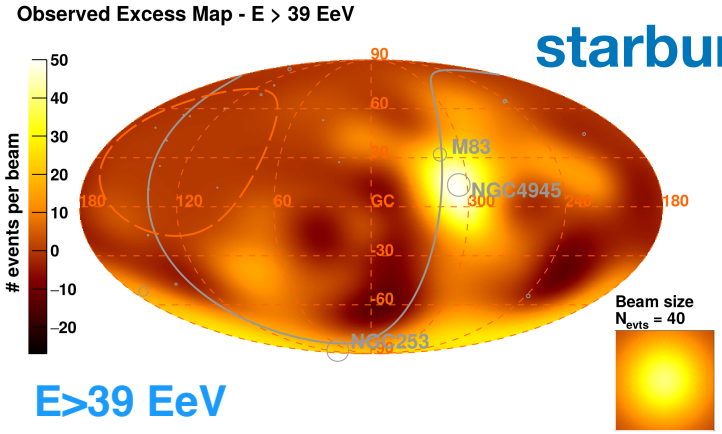

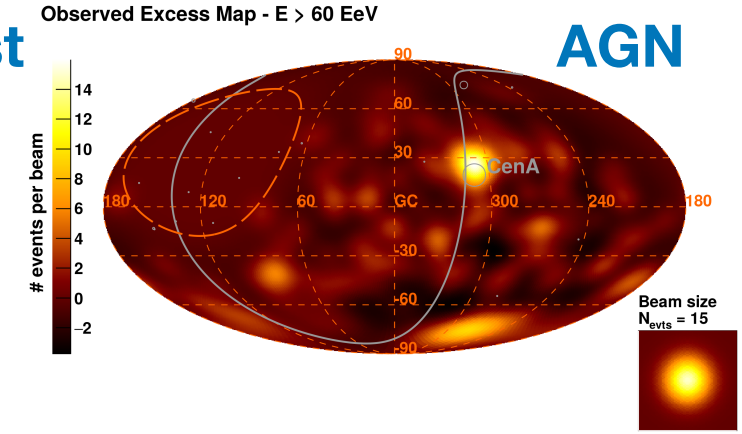

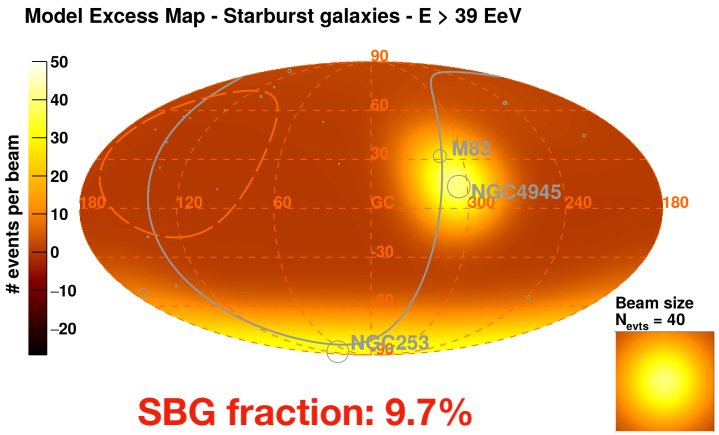

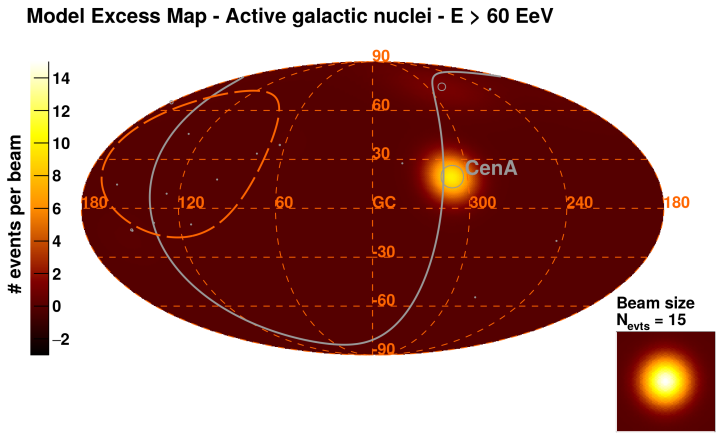

SBG fraction: 9.7%
search radius: 12.9°
pre-trail p-value: 3.8×10^{-6}
post-trial p-value: 3.6×10^{-5}
post-trial significance: 4.0 sigma

search radius: 6.9°
pre-trail p-value: 5.1×10^{-4}
post-trial p-value: 3.1×10^{-3}
post-trial significance: 2.7 sigma

A. Aab et al. ApJ 835 (2018) L29

Origin of cosmic rays
multi messenger technique

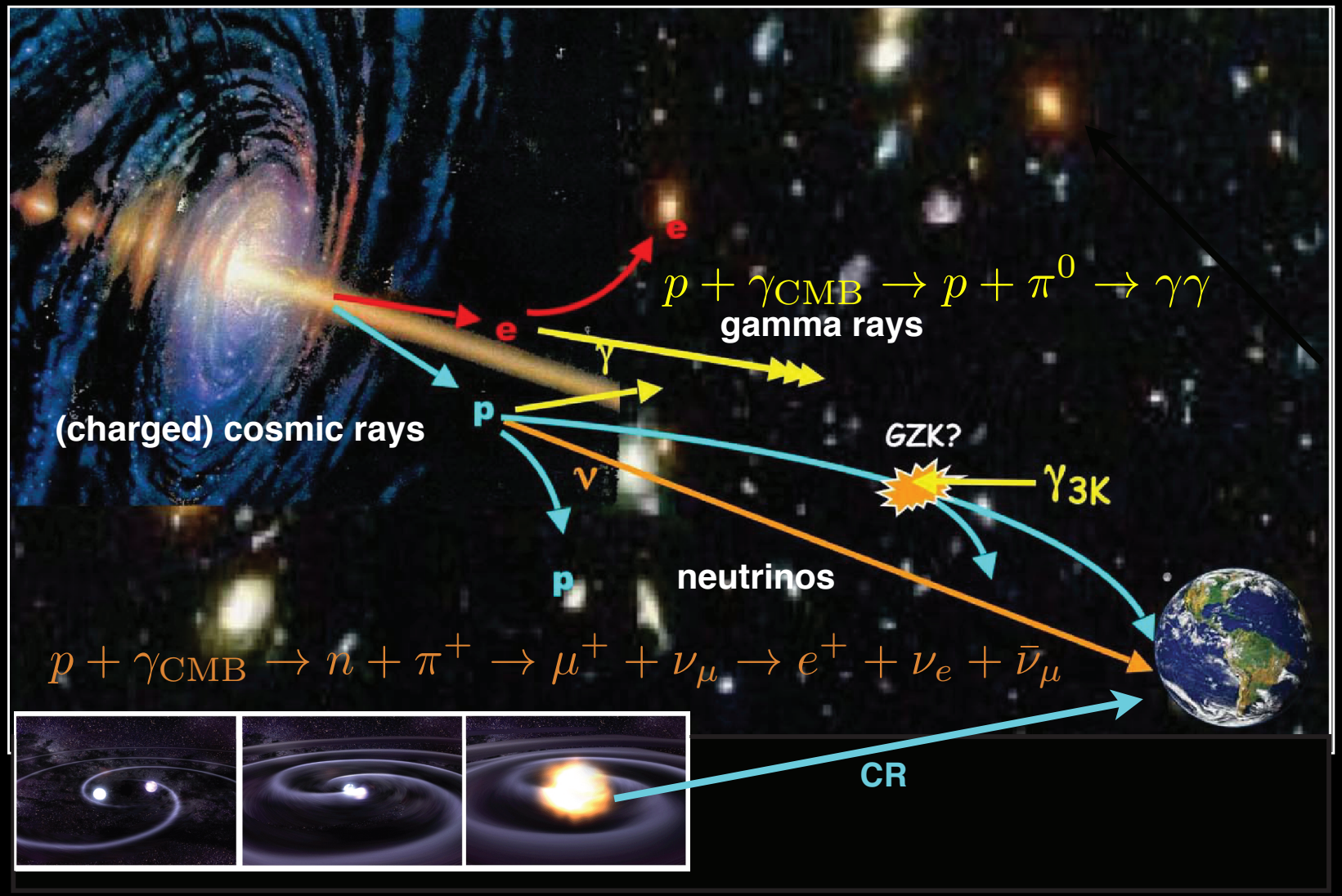

Photons

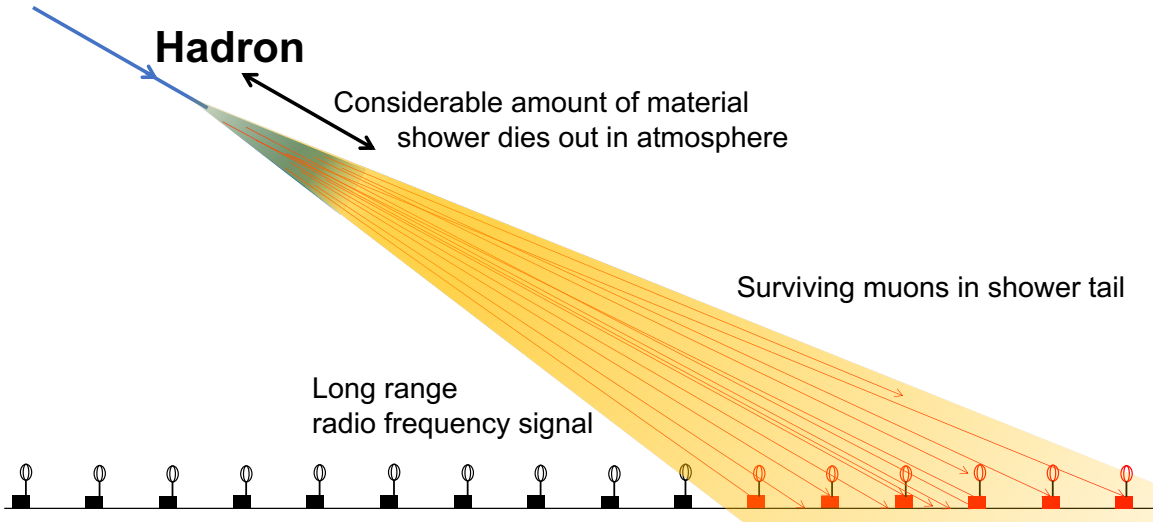

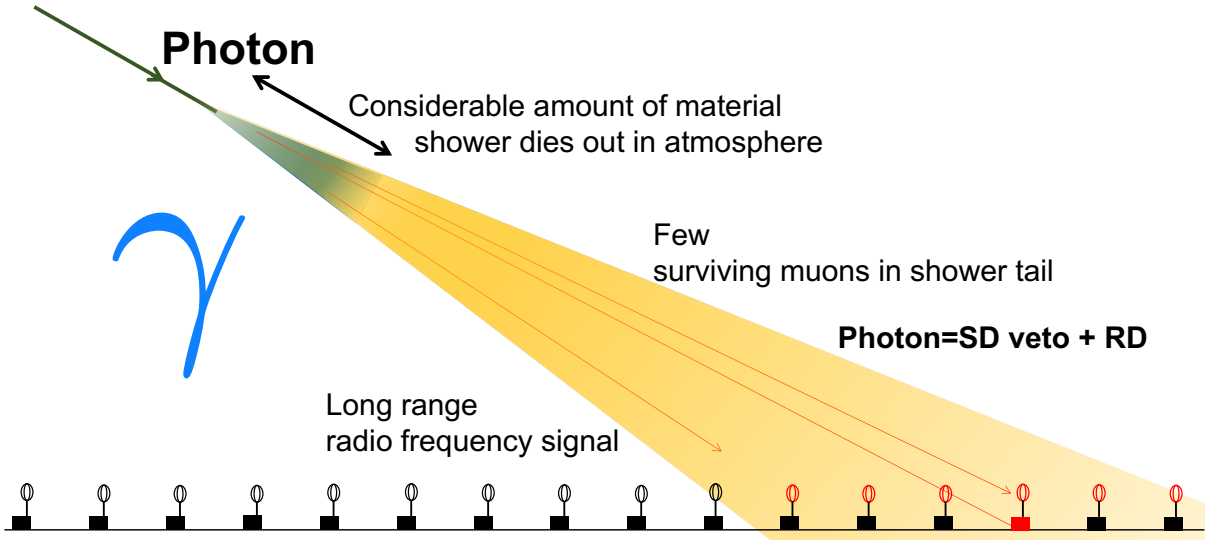

photons:
deep showers, small footprint, few WCD stations

The new RDs at each SD will also help to increase our sensitivity to neutrinos and photons.

Journal of Cosmology and Astroparticle Physics
An IOP and SISSA journal

Search for photons with energies above 10^{18} eV using the hybrid detector of the Pierre Auger Observatory

multivariate analysis

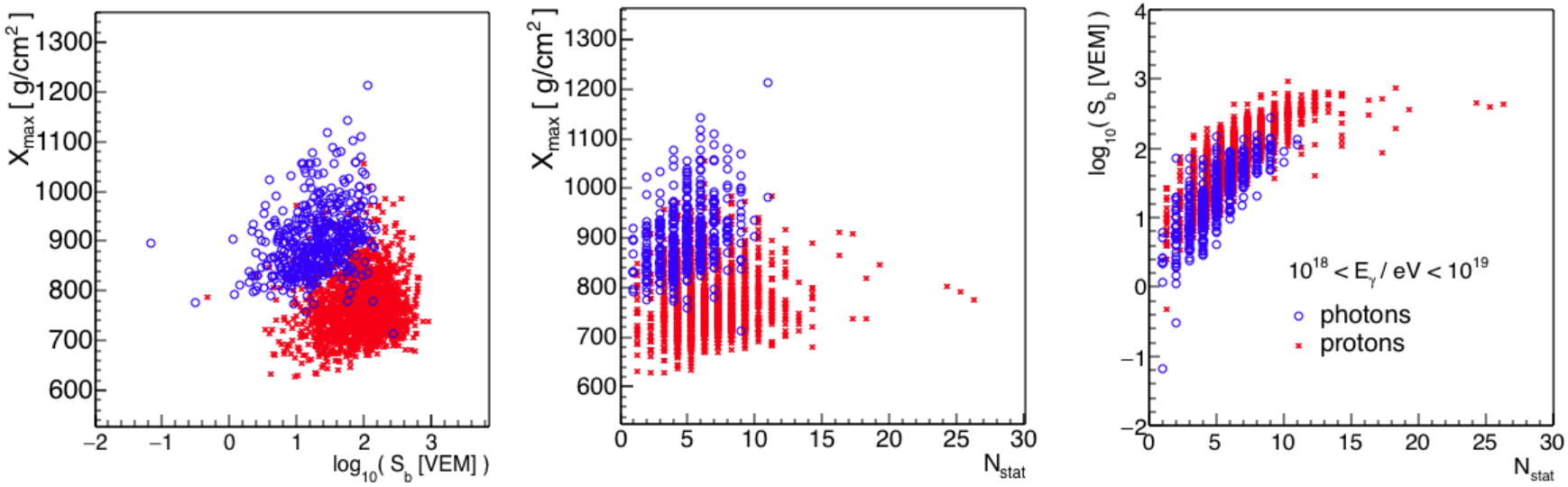

Figure 2. Correlation between the discriminating observables used in the multivariate analysis for the energy range $10^{18} < E_\gamma < 10^{19}$ eV: the red stars and the blue circles are the proton and photon simulated events, respectively. Events are selected applying the criteria in section 4. For a better visibility of the plot only 5% of events are plotted and a shift of 0.25 is applied to $N_{\rm stat}$ for proton events.

JCAP04(2017)009

Journal of Cosmology and Astroparticle Physics
An IOP and SISSA journal

Search for photons with energies above 10^{18} eV using the hybrid detector of the Pierre Auger Observatory

multivariate analysis

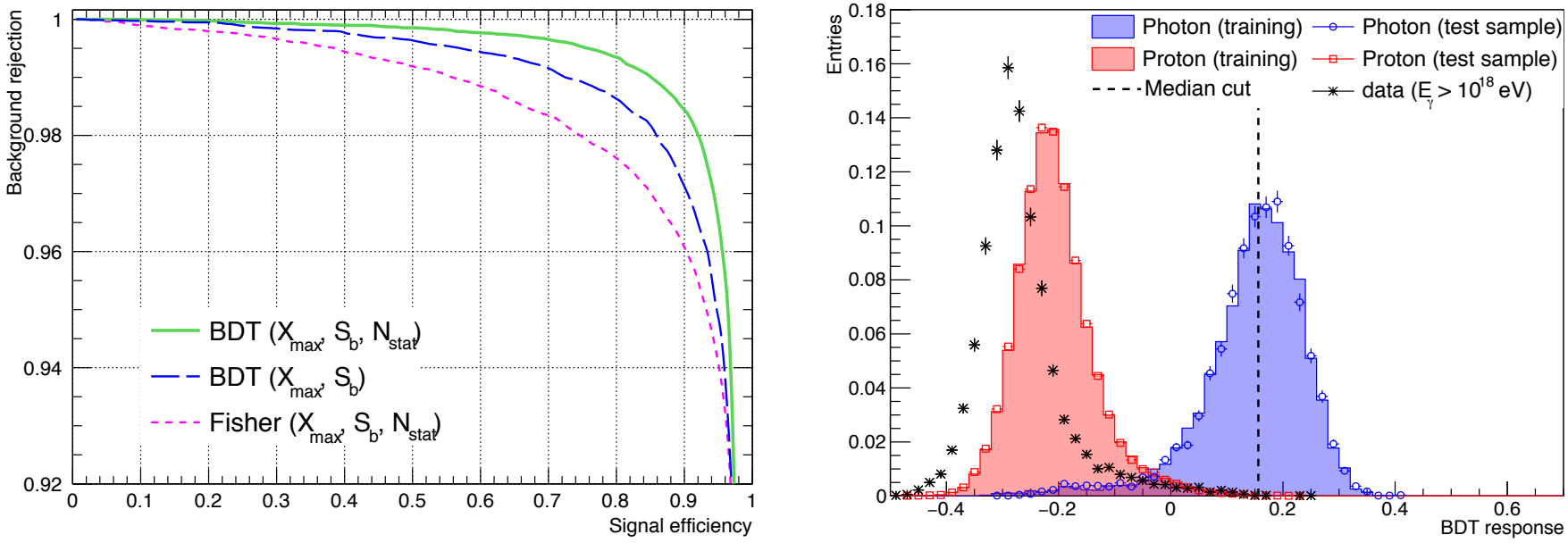

Figure 3. Left: curve of the background rejection efficiency against the signal efficiency for different algorithms and observables. Right: distribution of the Boosted Decision Tree observables for signal (photon, blue), background (proton, red) and data (black). For simulations both the training and the test samples are shown. The cut at the median of the photon distribution is indicated by the dashed line. QGSJET-II-04 used as high-energy hadronic interaction model.

JCAP04(2017)009

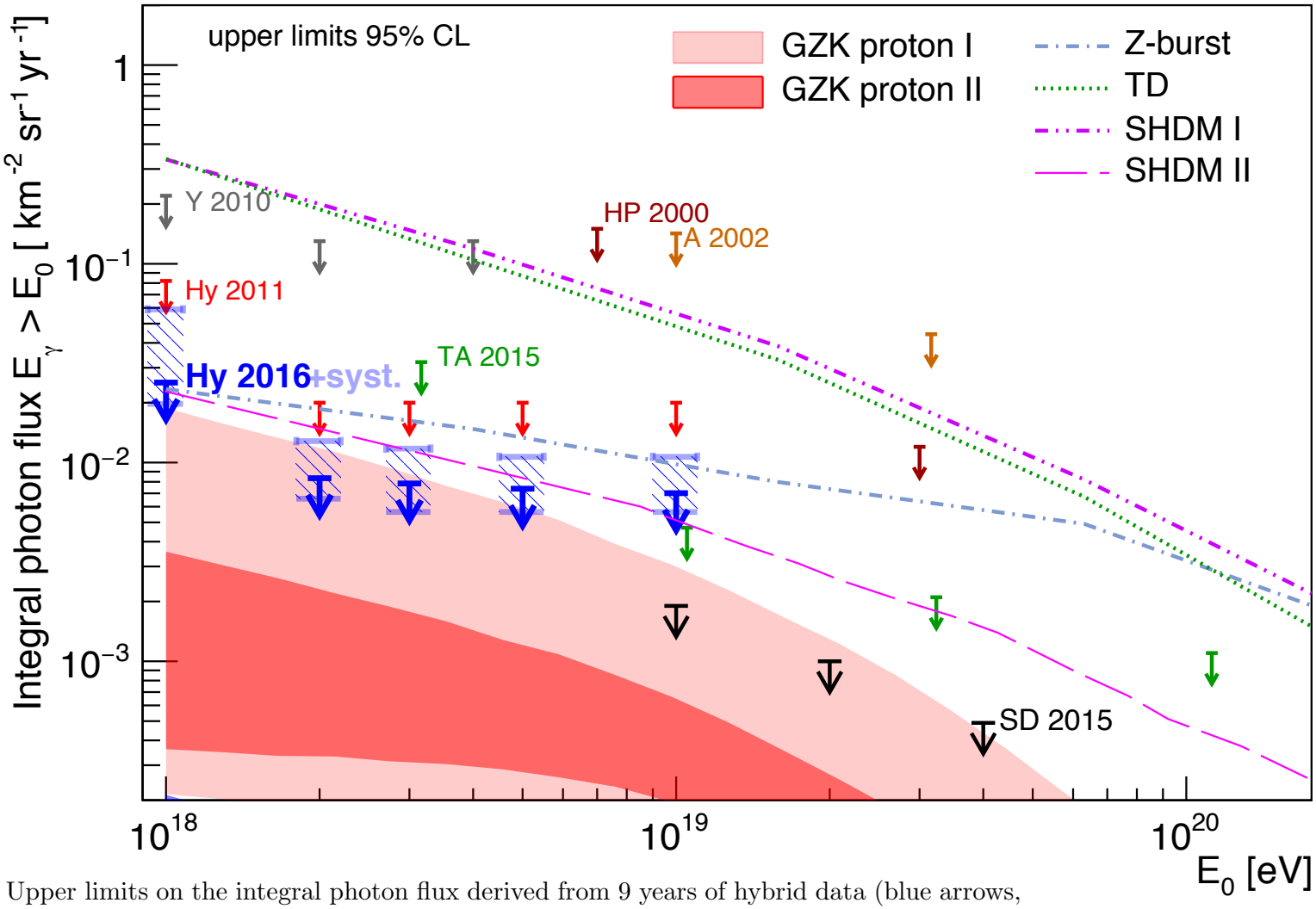

Figure 6. Upper limits on the integral photon flux derived from 9 years of hybrid data (blue arrows, Hy 2016) for a photon flux E^{-2} and no background subtraction. The limits obtained when the detector systematic uncertainties are taken into account are shown as horizontal segments (light blue) delimiting a dashed-filled box at each energy threshold. Previous limits from Auger: (SD [20] and Hybrid 2011 [19]), for Telescope Array (TA) [59], AGASA (A) [60], Yakutsk (Y) [61] and Haverah Park (HP) [62] are shown for comparison. None of them includes systematic uncertainties. The shaded regions and the lines give the predictions for the GZK photon flux [14, 16] and for top-down models (TD, Z-Burst, SHDM I [63] and SHDM II [21]).

The Astrophysical Journal Letters, 837:L25 (7pp), 2017 March 10 https://doi.org/10.3847/2041-8213/aa61a5

A Targeted Search for Point Sources of EeV Photons with the Pierre Auger Observatory

Table 1
Combined Unweighted Probabilities $\mathcal{P}$ and Weighted Probabilities $\mathcal{P}_w$ for the 12 Target Sets

Class	No.	$\mathcal{P}_w$	$\mathcal{P}$	R.A. (°)	Decl. (°)	Obs	Exp	Exposure (km^2 yr)	Flux UL (km^{-2} yr^{-1})	E-flux UL (eV cm^{-2} s^{-1})	p	p^*
msec PSRs	67	0.57	0.14	286.4	4.0	5 (7, 9*)	1.433	236.1	0.043	0.077	0.010	0.476
γ-ray PSRs	75	0.97	0.98	312.8	−8.5	6 (8, 10*)	1.857	248.1	0.045	0.080	0.007	0.431
LMXB	87	0.13	0.74	258.1	−40.8	6 (8, 11*)	2.144	233.9	0.046	0.083	0.014	0.718
HMXB	48	0.33	0.84	285.9	−3.2	4 (7, 9*)	1.460	235.2	0.036	0.066	0.040	0.856
H.E.S.S. PWN	17	0.92	0.90	266.8	−28.2	4 (8, 10*)	2.045	211.4	0.038	0.068	0.104	0.845
H.E.S.S. other	16	0.12	0.52	258.3	−39.8	5 (8, 10*)	2.103	233.3	0.040	0.072	0.042	0.493
H.E.S.S. UNID	20	0.79	0.45	257.1	−41.1	6 (8, 10*)	2.142	239.2	0.045	0.081	0.014	0.251
Microquasars	13	0.29	0.48	267.0	−28.1	5 (8, 10*)	2.044	211.4	0.045	0.080	0.037	0.391
Magnetars	16	0.30	0.89	257.2	−40.1	4 (8, 10*)	2.122	253.8	0.031	0.056	0.115	0.858
Gal. Center	1	0.59	0.59	266.4	−29.0	2 (8, 8*)	2.048	218.9	0.024	0.044	0.471	0.471
LMC	3	0.52	0.62	84.4	−69.2	2 (8, 9*)	2.015	180.3	0.030	0.053	0.463	0.845
Cen A	1	0.31	0.31	201.4	−43.0	3 (8, 8*)	1.948	214.1	0.031	0.056	0.221	0.221

Note. In addition, information on the most significant target from each target set is given. The number of observed (Obs) and expected (Exp) events and the corresponding exposure are shown. The numbers in brackets in the observed number of events column indicate the numbers of events needed for a 3σ observation unpenalized and penalized (*). Upper limits (UL) are computed at the 95% confidence level. The last two columns indicate the p-value unpenalized (p) and penalized (p^*). Due to the discrete distribution of p-values arising in isotropic simulations, $\mathcal{P}$ can differ from p in the sets that contain only a single target.

HESS: Acceleration of Petaelectronvolt protons in the Galactic Centre

Nature 531, 476 (2016)

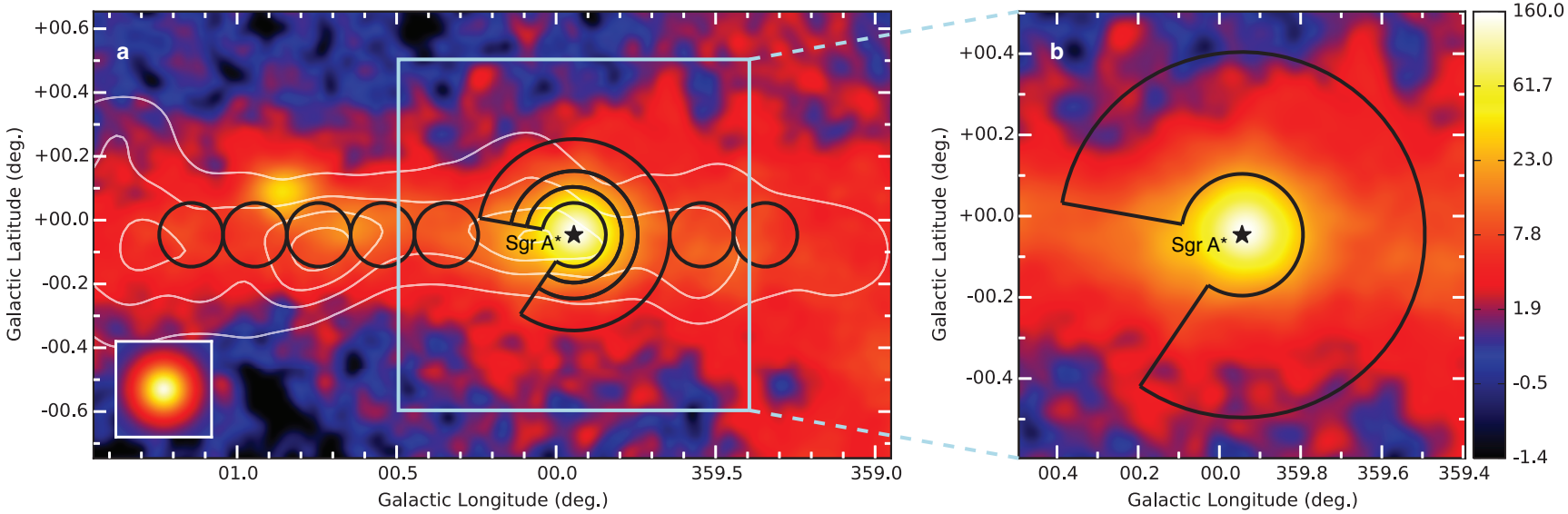

Figure 1: **VHE γ-ray image of the Galactic Centre region.** The colour scale indicates counts per $0.02^\circ \times 0.02^\circ$ pixel. *Left panel:* The black lines outline the regions used to calculate the CR energy density throughout the central molecular zone. A section of 66° is excluded from the annuli (see Methods). White contour lines indicate the density distribution of molecular gas, as traced by its CS line emission[30]. The inset shows the simulation of a point-like source. *Right panel:* Zoomed view of the inner $\sim$ 70 pc and the contour of the region used to extract the spectrum of the diffuse emission.

HESS: Acceleration of Petaelectronvolt protons in the Galactic Centre

Nature 531, 476 (2016)

Here we report deep gamma-ray observations with arcminute angular resolution of the Galactic Centre regions, which show the expected tracer of the presence of PeV particles within the central 10 parsec of the Galaxy. We argue that the supermassive black hole Sagittarius A* is linked to this PeVatron. Sagittarius A* went through active phases in the past, as demonstrated by X-ray outbursts and an outflow from the Galactic Center. Although its current rate of particle acceleration is not sufficient to provide a substantial contribution to Galactic cosmic rays, Sagittarius A* could have plau- sibly been more active over the last ~ 10^{6-7} years, and therefore should be considered as a viable alternative to supernova remnants as a source of PeV Galactic cosmic rays.

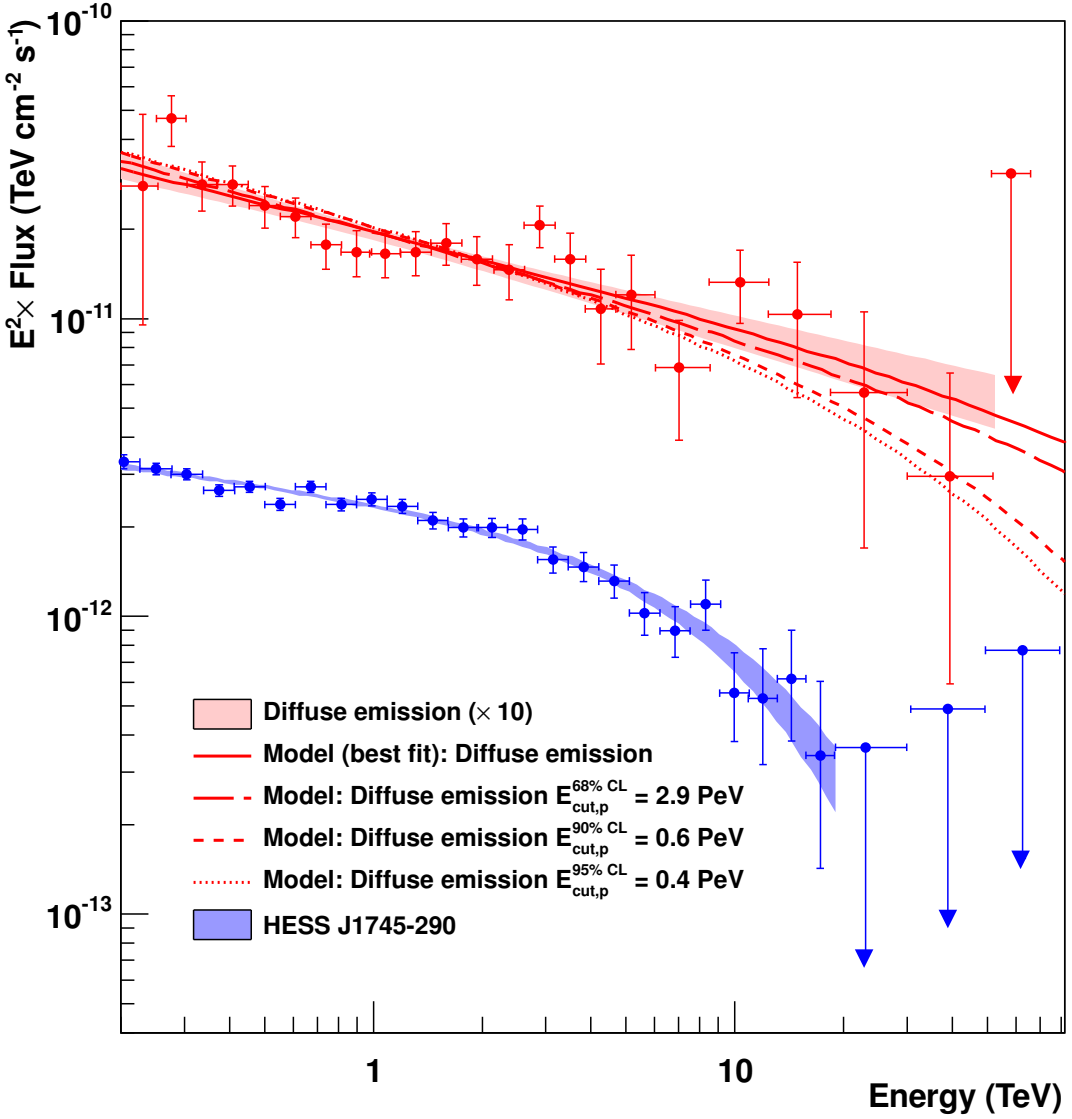

HESS: Acceleration of Petaelectronvolt protons in the Galactic Centre
Nature 531, 476 (2016)

?

Figure 3: **VHE γ-ray spectra of the diffuse emission and HESS J1745-290.** The Y axis shows fluxes multiplied by a factor E^2, where E is the energy on the X axis, in units of TeVcm^{-2}s^{-1}. The vertical and horizontal error bars show the 1σ statistical error and bin size, respectively. Arrows represent 2σ flux upper limits. The 1σ confidence bands of the best-fit spectra of the diffuse and HESS J1745-290 are shown in red and blue shaded areas, respectively. Spectral parameters are given in Methods. The red lines show the numerical computations assuming that γ-rays result from the decay of neutral pions produced by proton-proton interactions. The fluxes of the diffuse emission spectrum and models are multiplied by 10.

The Astrophysical Journal Letters, 837:L25 (7pp), 2017 March 10 https://doi.org/10.3847/2041-8213/aa61a5

A Targeted Search for Point Sources of EeV Photons with the Pierre Auger Observatory

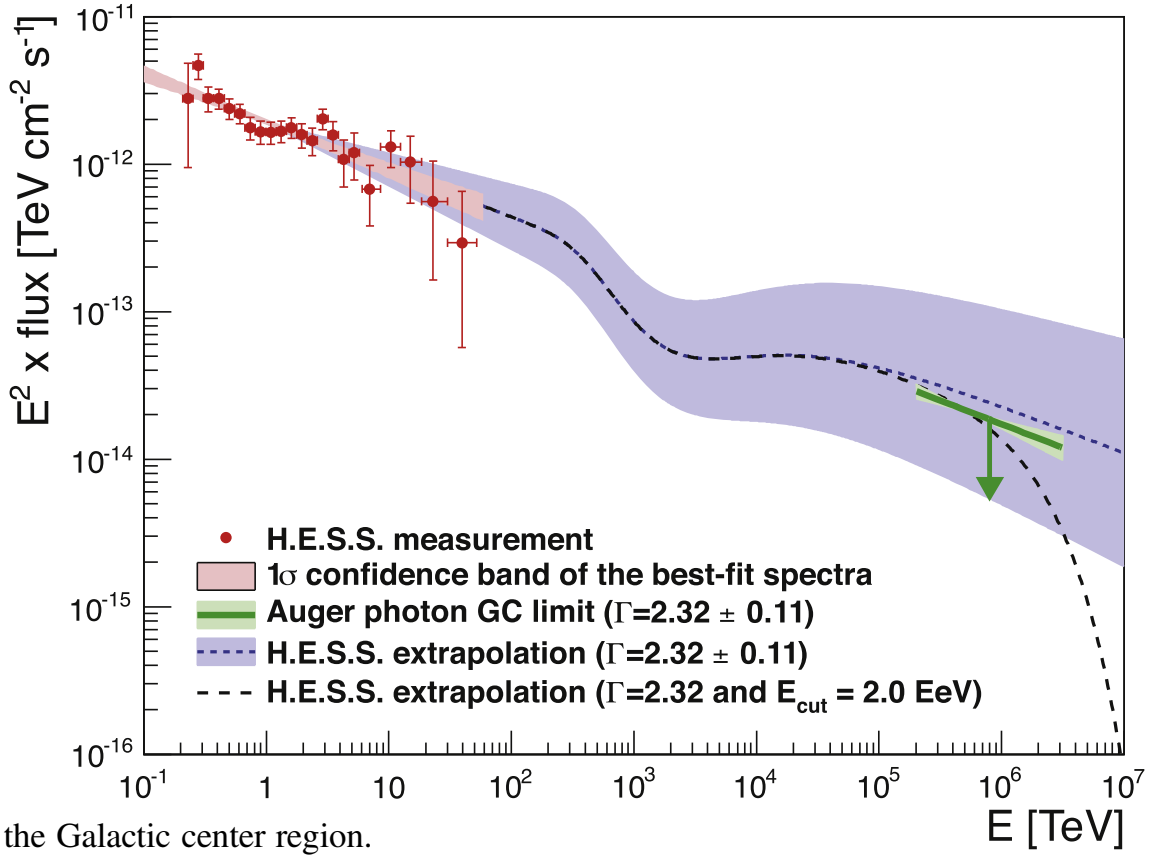

Figure 2. Photon flux as a function of energy from the Galactic center region. Measured data by H.E.S.S. are indicated, as well as the extrapolated photon flux at Earth in the EeV range, given the quoted spectral indices (Abramowski et al. 2016; conservatively the extrapolation does not take into account the increase of the p–p cross-section toward higher energies). The Auger limit is indicated by a green line. A variation of the assumed spectral index by ± 0.11 according to systematics of the H.E.S.S. measurement is denoted by the light green and blue band. A spectral index with cutoff energy $E_{\rm cut} = 2.0 \cdot 10^6$ TeV is indicated as well.

Multi-messenger astronomy

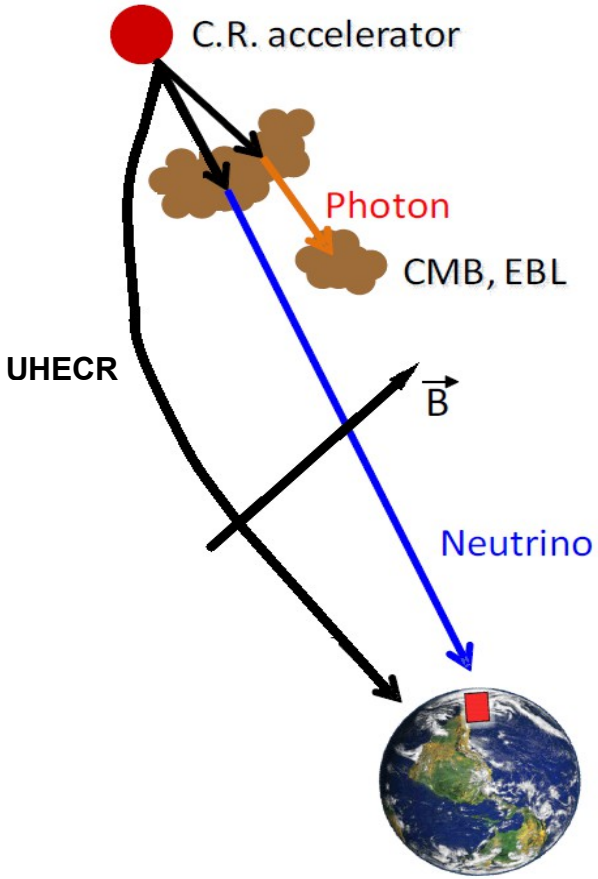

$$p + \gamma \xrightarrow[\text{or p...}]{} \pi^0 + p$$
$$\rightarrow \gamma + \gamma + p$$
$$\rightarrow \pi^+ + n$$
$$\rightarrow \mu^+ + \nu_\mu + n$$
$$\rightarrow e^+ + \bar{\nu}_\mu + \nu_e + \nu_\mu + n$$

Neutrinos

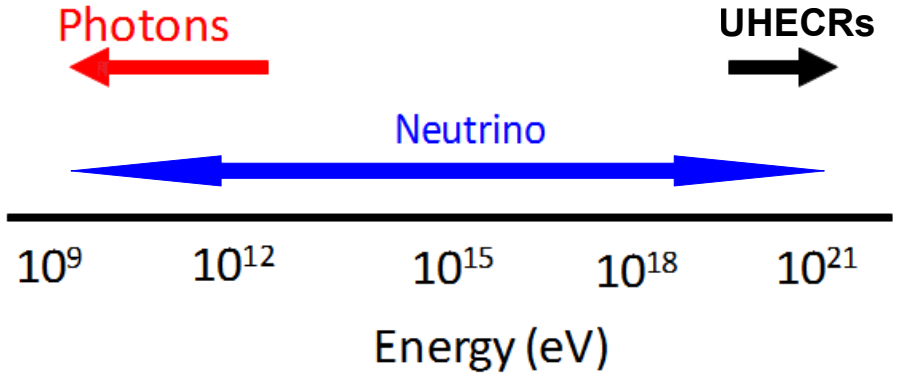

Journal of Cosmology and Astroparticle Physics
An IOP and SISSA journal

Search for correlations between the arrival directions of IceCube neutrino events and ultrahigh-energy cosmic rays detected by the Pierre Auger Observatory and the Telescope Array

JCAP01(2016)037

IceCube

TA

PAO

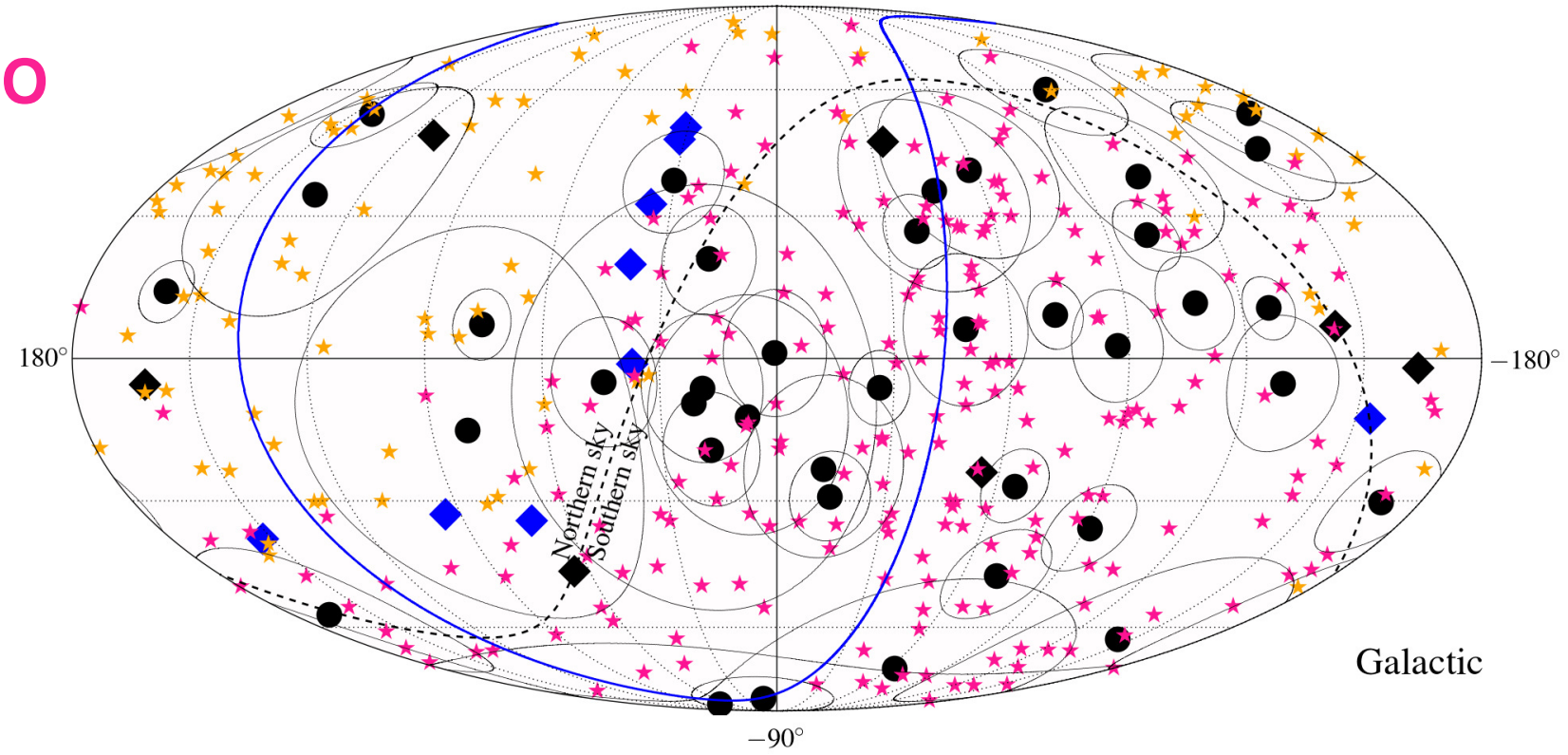

Figure 7. Maps in Equatorial and Galactic coordinates showing the arrival directions of the IceCube cascades (black dots) and tracks (diamonds), as well as those of the UHECRs detected by the Pierre Auger Observatory (magenta stars) and Telescope Array (orange stars). The circles around the showers indicate angular errors. The black diamonds are the HESE tracks while the blue diamonds stand for the tracks from the through-going muon sample. The blue curve indicates the Super-Galactic plane.

Neutrino detection with the Pierre Auger SD

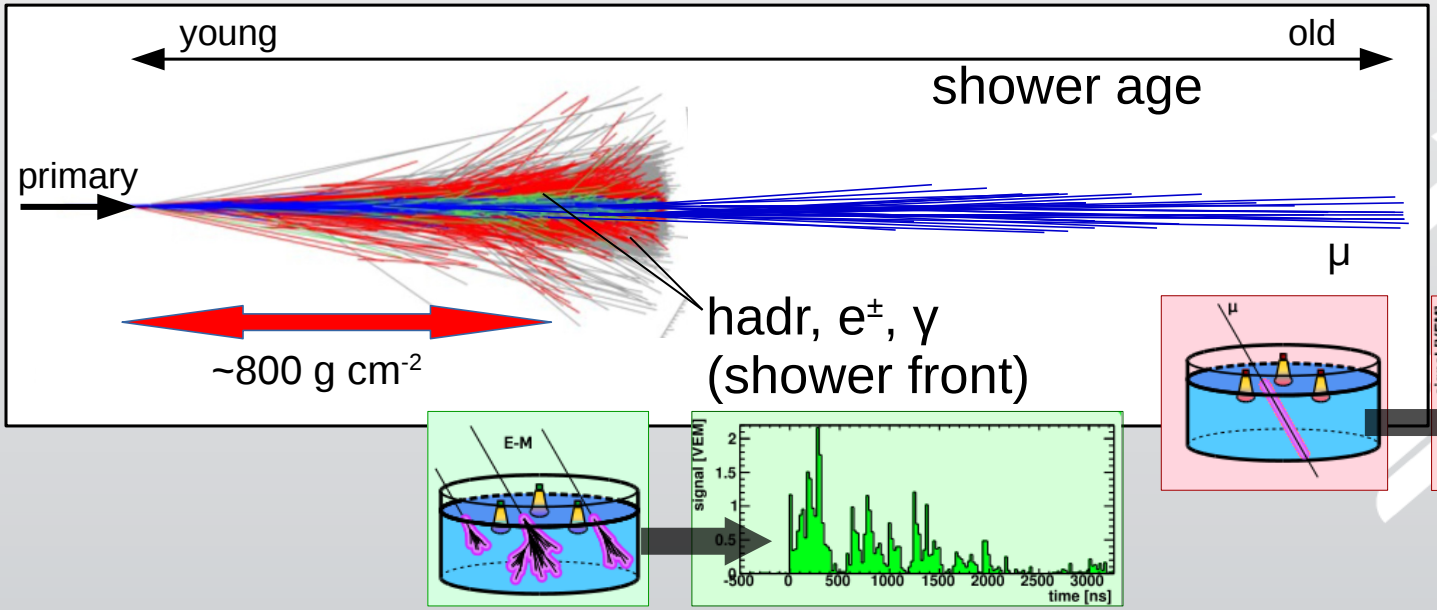

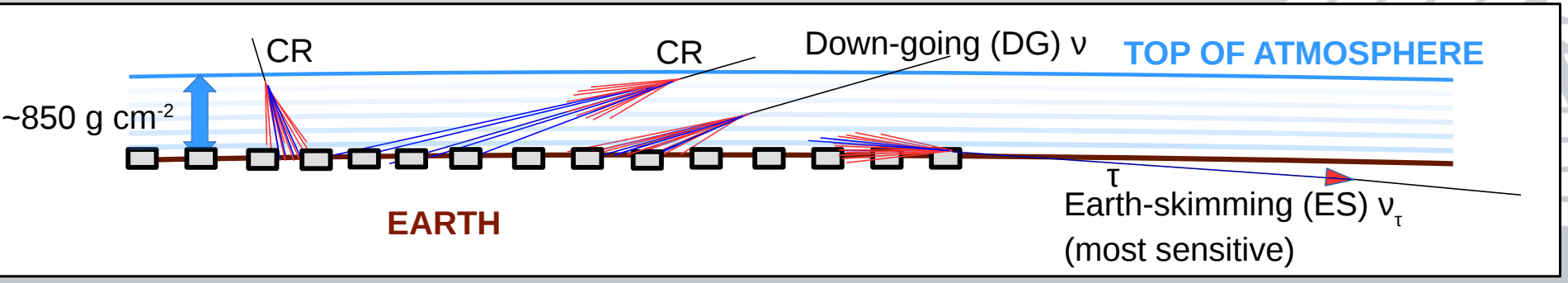

Neutrino detection with the Pierre Auger SD

Reasonable separation:
θ > 60 deg

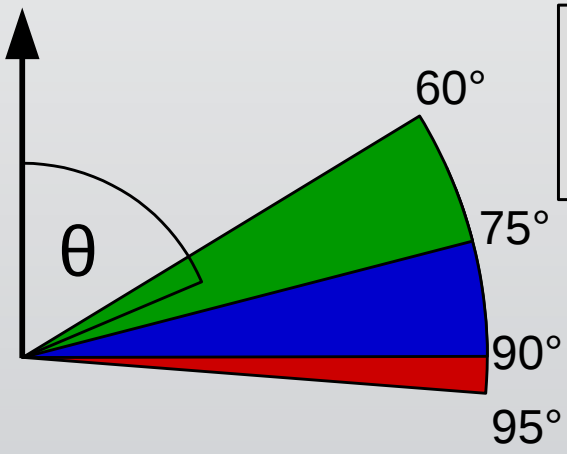

- Down-going low
- Down-going high
- Earth-skimming

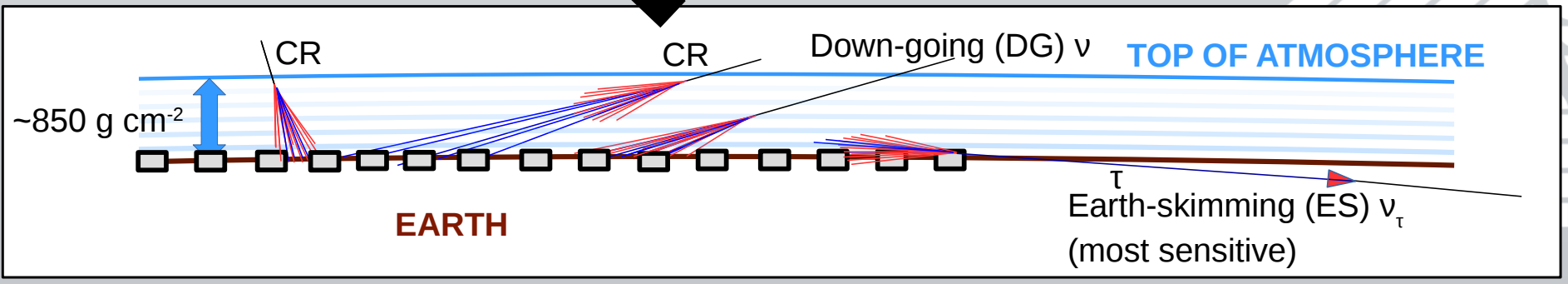

Flux limits

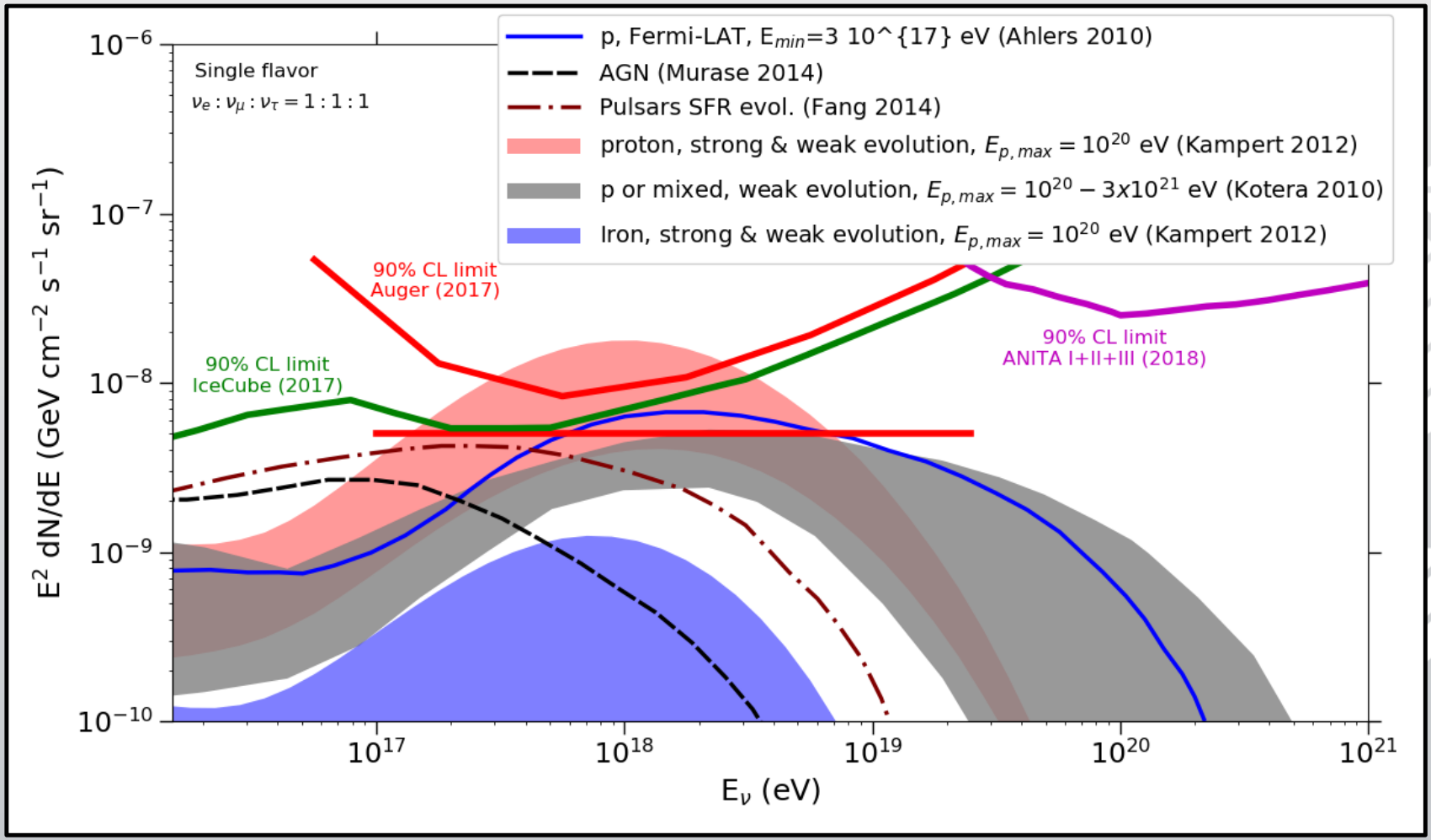
p, Fermi-LAT, E_min=3 10^{17} eV (Ahlers 2010)
AGN (Murase 2014)
Pulsars SFR evol. (Fang 2014)
proton, strong & weak evolution, E_p,max = 10^20 eV (Kampert 2012)
p or mixed, weak evolution, E_p,max = 10^20 − 3x10^21 eV (Kotera 2010)
Iron, strong & weak evolution, E_p,max = 10^20 eV (Kampert 2012)
Single flavor
ν_e : ν_μ : ν_τ = 1 : 1 : 1
90% CL limit
Auger (2017)
90% CL limit
IceCube (2017)
90% CL limit
ANITA I+II+III (2018)
E² dN/dE (GeV cm⁻² s⁻¹ sr⁻¹)
E_ν (eV)

Follow-up of GW170817 with PAO (neutrinos)

Fermi

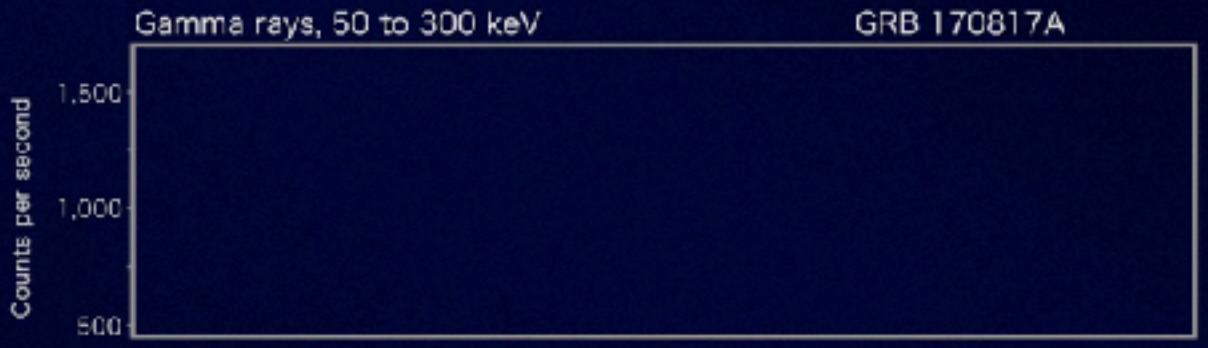

LIGO

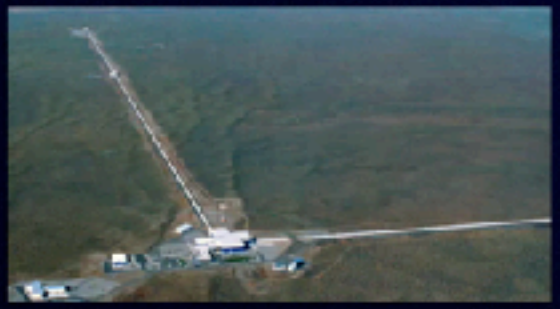

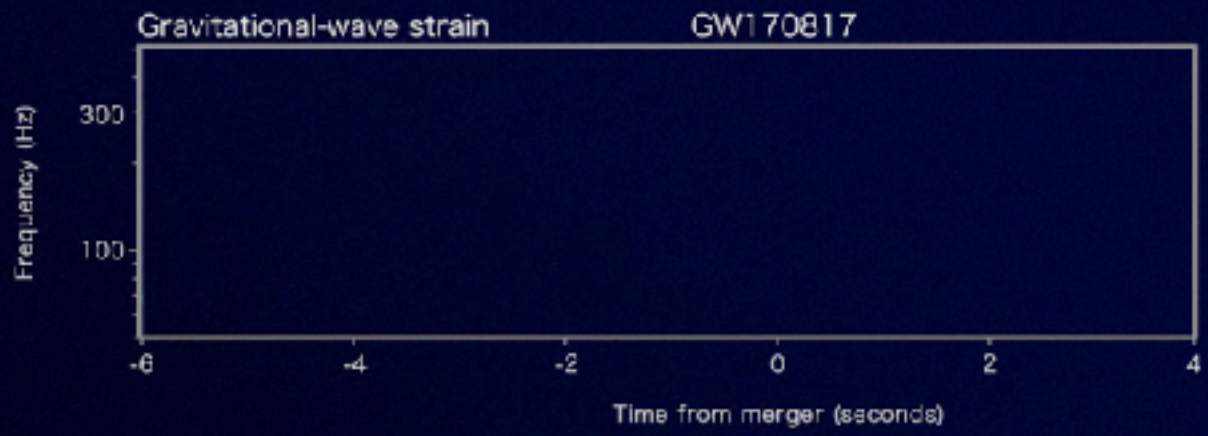

Follow-up of GW170817 with PAO (neutrinos)

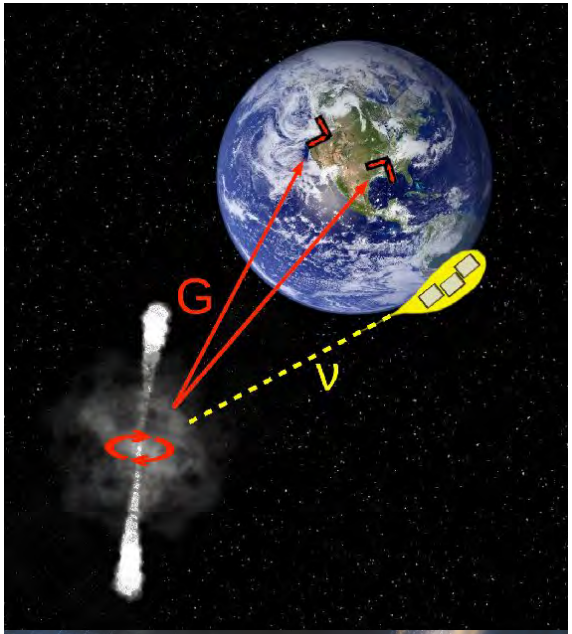

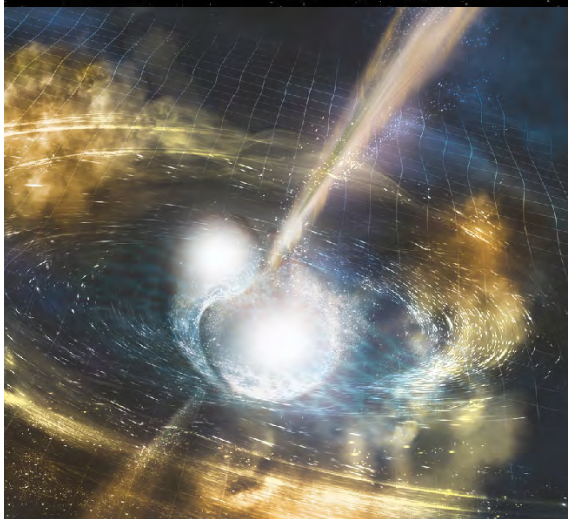

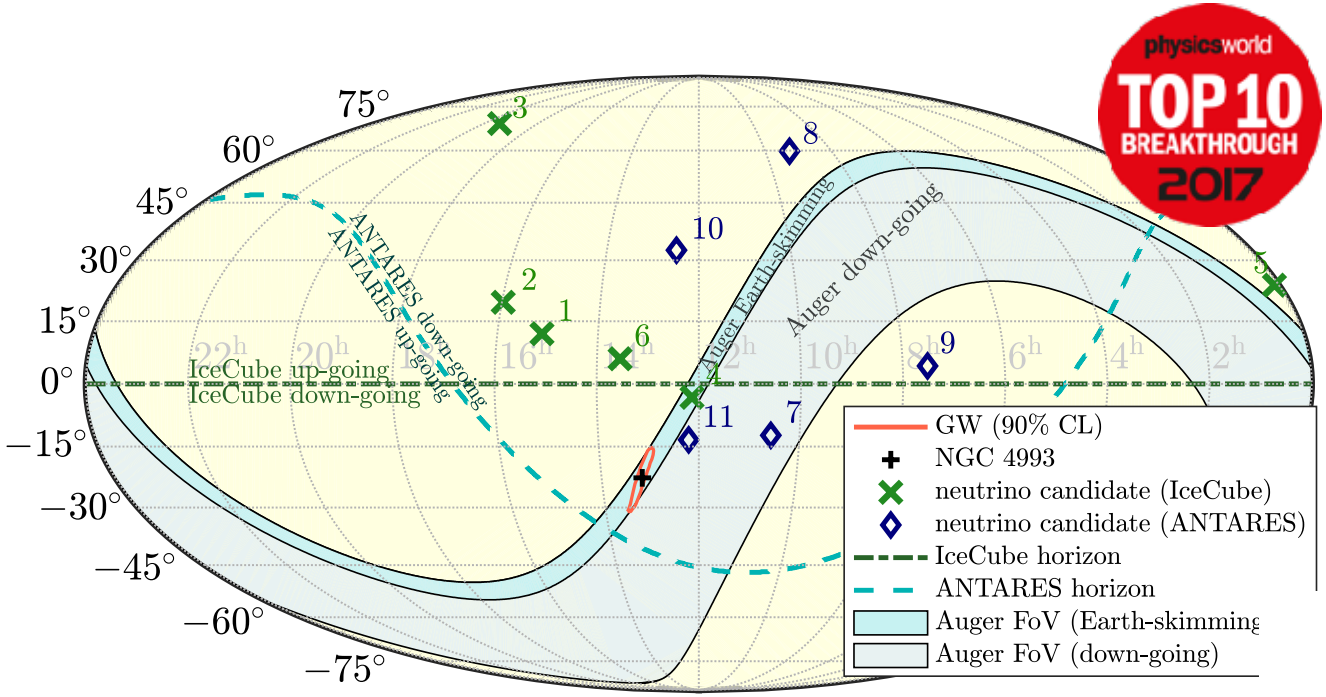

The Astrophysical Journal Letters, 848:L12 (59pp), 2017 October 20
https://doi.org/10.3847/2041-8213/aa91c9

Multi-messenger Observations of a Binary Neutron Star Merger

LIGO Scientific Collaboration and Virgo Collaboration, Fermi GBM, INTEGRAL, IceCube Collaboration, AstroSat Cadmium Zinc Telluride Imager Team, IPN Collaboration, The Insight-Hxmt Collaboration, ANTARES Collaboration, The Swift Collaboration, AGILE Team, The 1M2H Team, The Dark Energy Camera GW-EM Collaboration and the DES Collaboration, The DLT40 Collaboration, GRAWITA: GRAvitational Wave Inaf TeAm, The Fermi Large Area Telescope Collaboration, ATCA: Australia Telescope Compact Array, ASKAP: Australian SKA Pathfinder, Las Cumbres Observatory Group, OzGrav, DWF (Deeper, Wider, Faster Program), AST3, and CAASTRO Collaborations, The VINROUGE Collaboration, MASTER Collaboration, J-GEM, GROWTH, JAGWAR, Caltech-NRAO, TTU-NRAO, and NuSTAR Collaborations, Pan-STARRS, The MAXI Team, TZAC Consortium, KU Collaboration, Nordic Optical Telescope, ePESSTO, GROND, Texas Tech University, SALT Group, TOROS: Transient Robotic Observatory of the South Collaboration, The BOOTES Collaboration, MWA: Murchison Widefield Array, The CALET Collaboration, IKI-GW Follow-up Collaboration, H.E.S.S. Collaboration, LOFAR Collaboration, LWA: Long Wavelength Array, HAWC Collaboration, The Pierre Auger Collaboration, ALMA Collaboration, Euro VLBI Team, Pi of the Sky Collaboration, The Chandra Team at McGill University, DFN: Desert Fireball Network, ATLAS, High Time Resolution Universe Survey, RIMAS and RATIR, and SKA South Africa/MeerKAT
(See the end matter for the full list of authors.)

Received 2017 October 3; revised 2017 October 6; accepted 2017 October 6; published 2017 October 16

Malargüe, N

Follow-up of GW170817 with PAO (neutrinos)

The Astrophysical Journal Letters, 850:L35 (18pp), 2017 December 1 https://doi.org/10.3847/2041-8213/aa9aed

Search for High-energy Neutrinos from Binary Neutron Star Merger GW170817 with ANTARES, IceCube, and the Pierre Auger Observatory

ANTARES Collaboration, IceCube Collaboration, The Pierre Auger Collaboration, and LIGO Scientific Collaboration and Virgo Collaboration

PAO in pre-defined +/- 500 s window as sensitive as IceCube

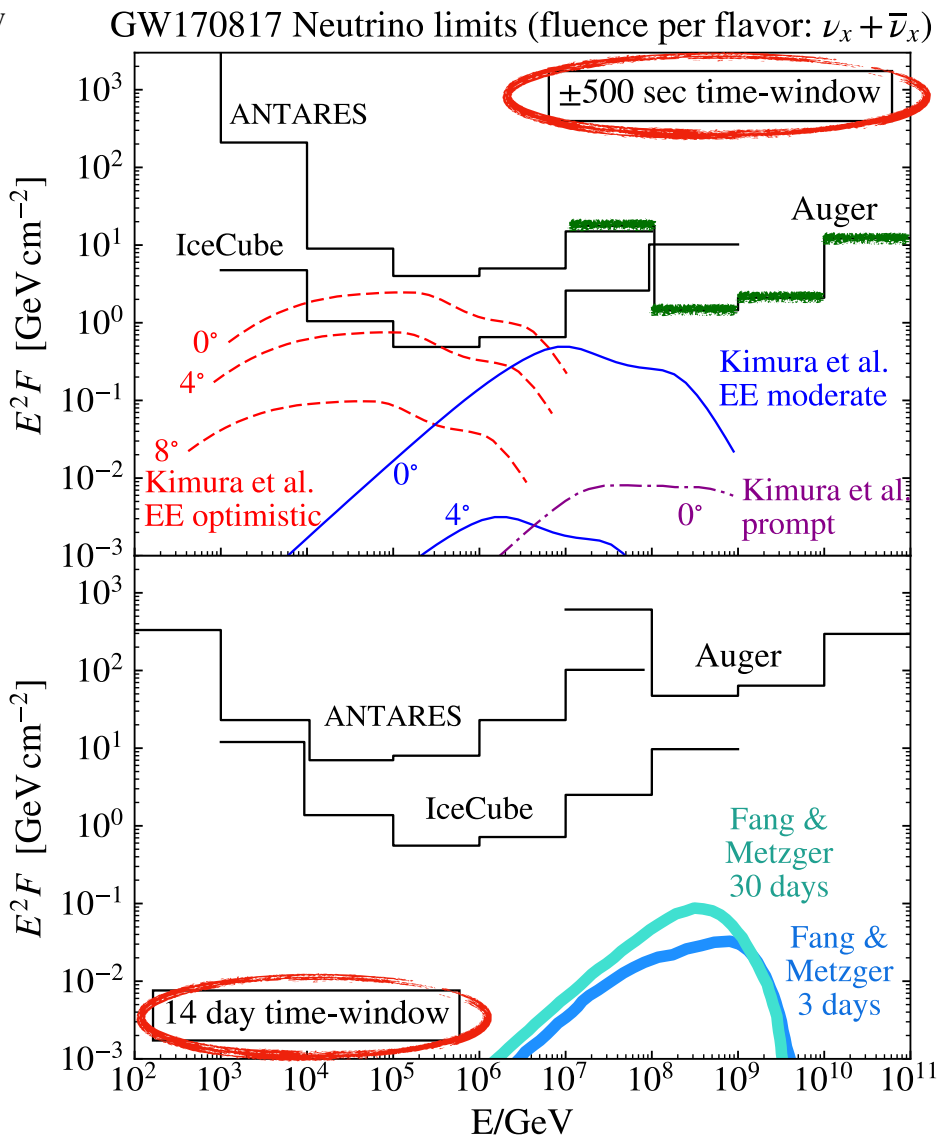

UPGRADE

Energy spectrum and mass composition

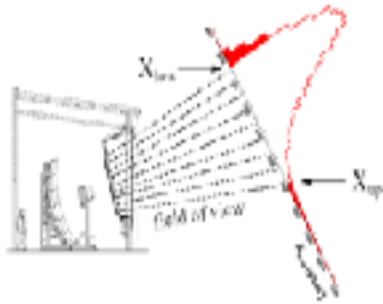

energy spectrum of cosmic rays

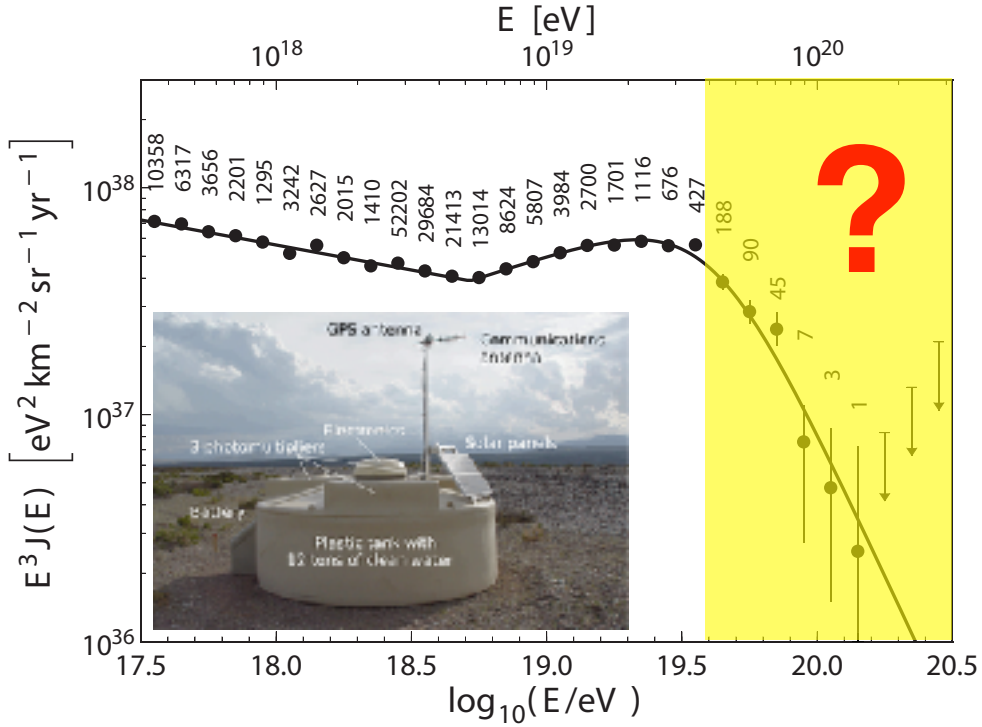

mass composition of cosmic rays

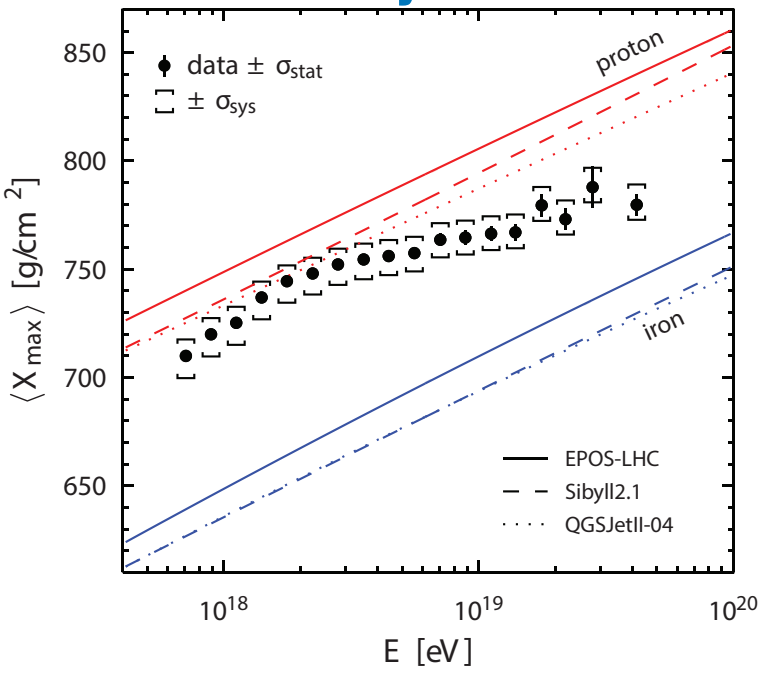

Upgrade of the Pierre Auger Observatory
(astro-)physics of the highest-energy particles in nature

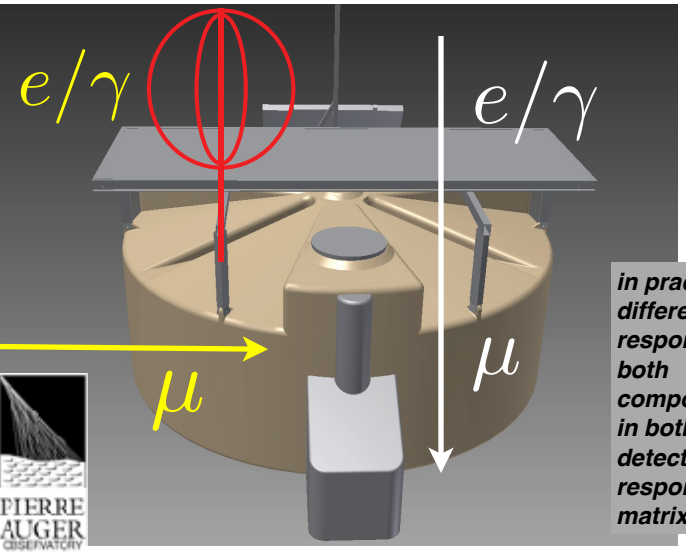

in practice: different response to both components in both detectors: response matrix

upgrade PAO
- electronics
- scintillator layer
- radio detector

Key science questions

- What are the sources and acceleration mechanisms of ultra-high-energy cosmic rays (UHECRs)?
- Do we understand particle acceleration and physics at energies well beyond the LHC (Large Hadron Collider) scale?
- What is the fraction of protons, photons, and neutrinos in cosmic rays at the highest energies?

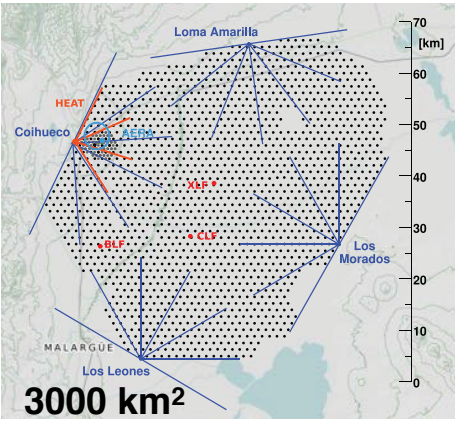

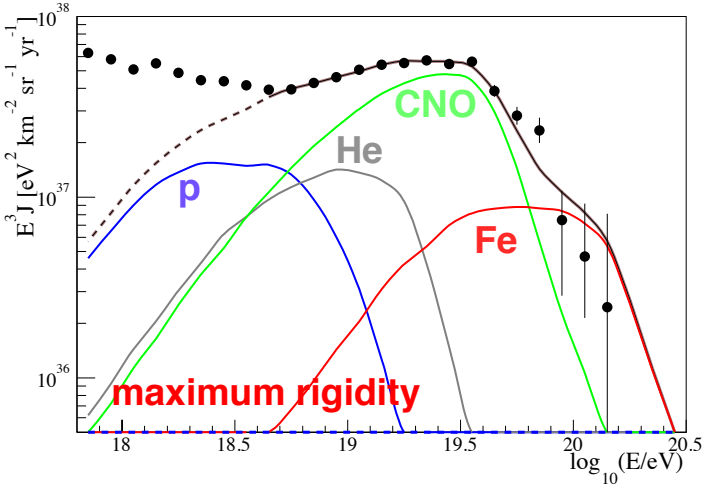

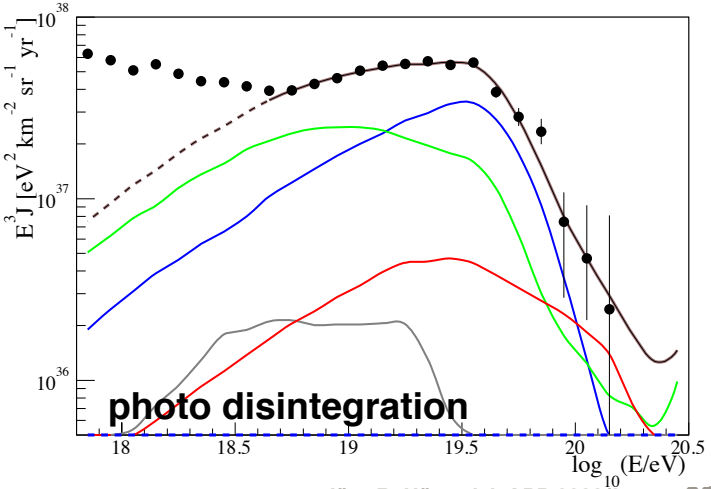

Upgrade of the Pierre Auger Observatory
(astro-)physics of the highest-energy particles in nature

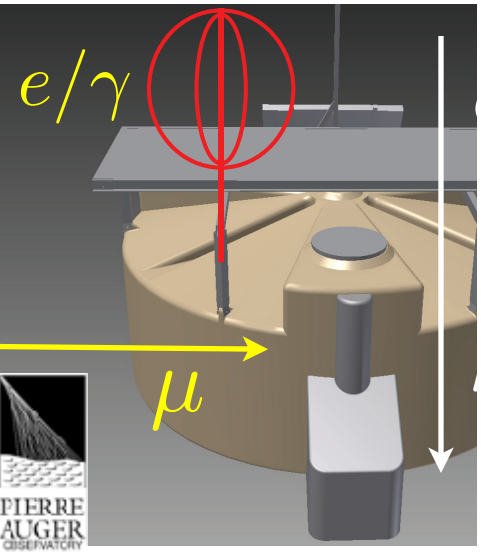

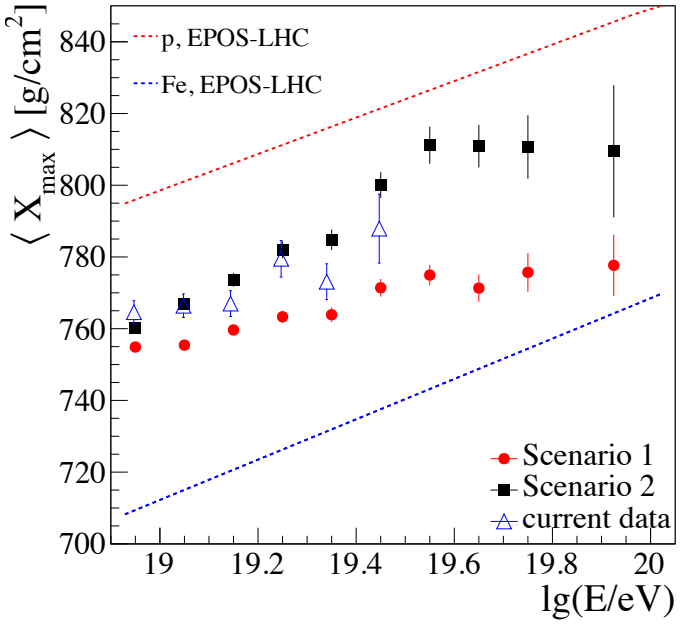

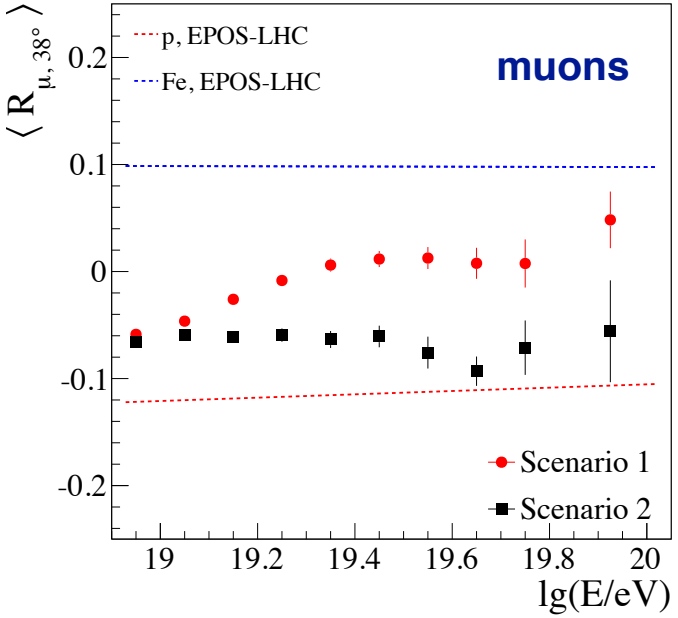

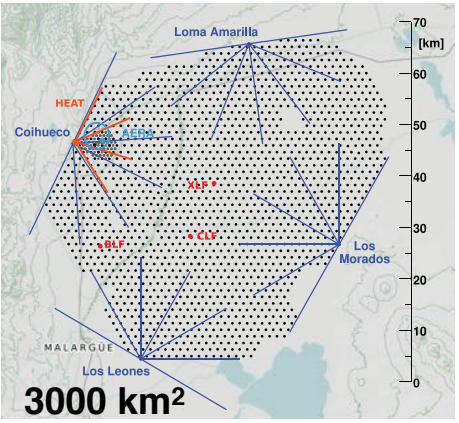

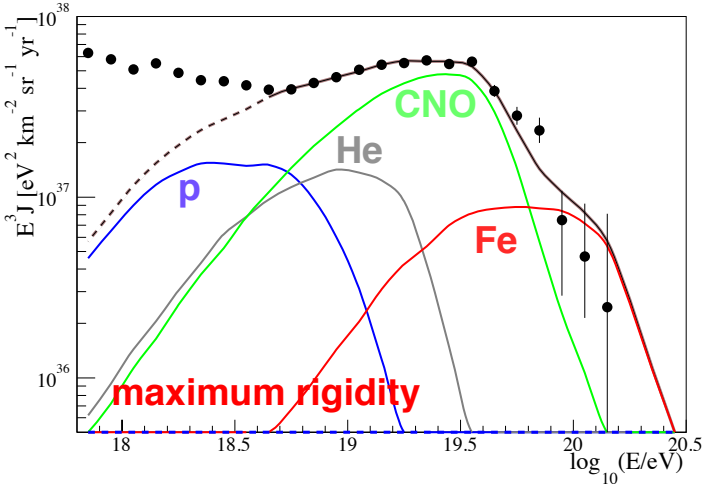

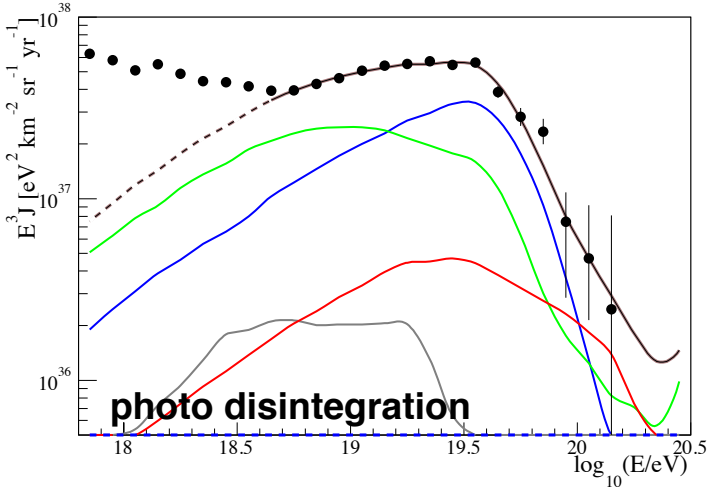

Key Elements of Upgrade

PIERRE AUGER OBSERVATORY

1) New Electronics for Surface Detector

→ faster sampling, better triggers, larger dynamic range, more channels

2) Enhanced Muon-Counting in Surface Detector

add scintillator on top of each tank

3) Extended operation of fluorescence telescopes

may double observation time

4) High Precision Array with shielded muon detectors

AMIGA

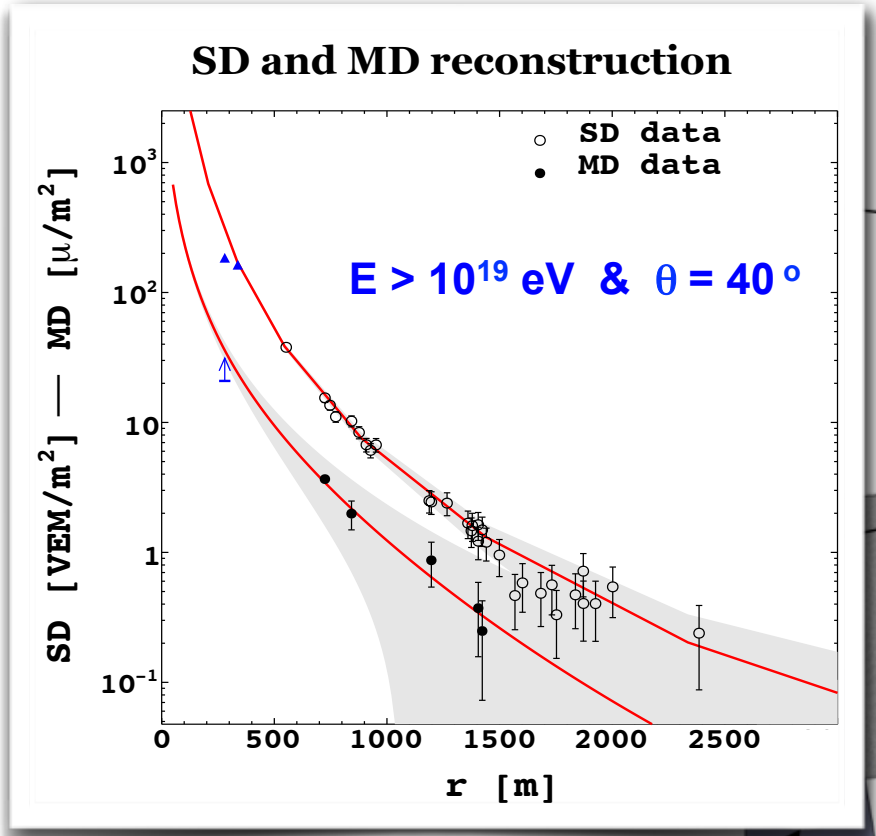

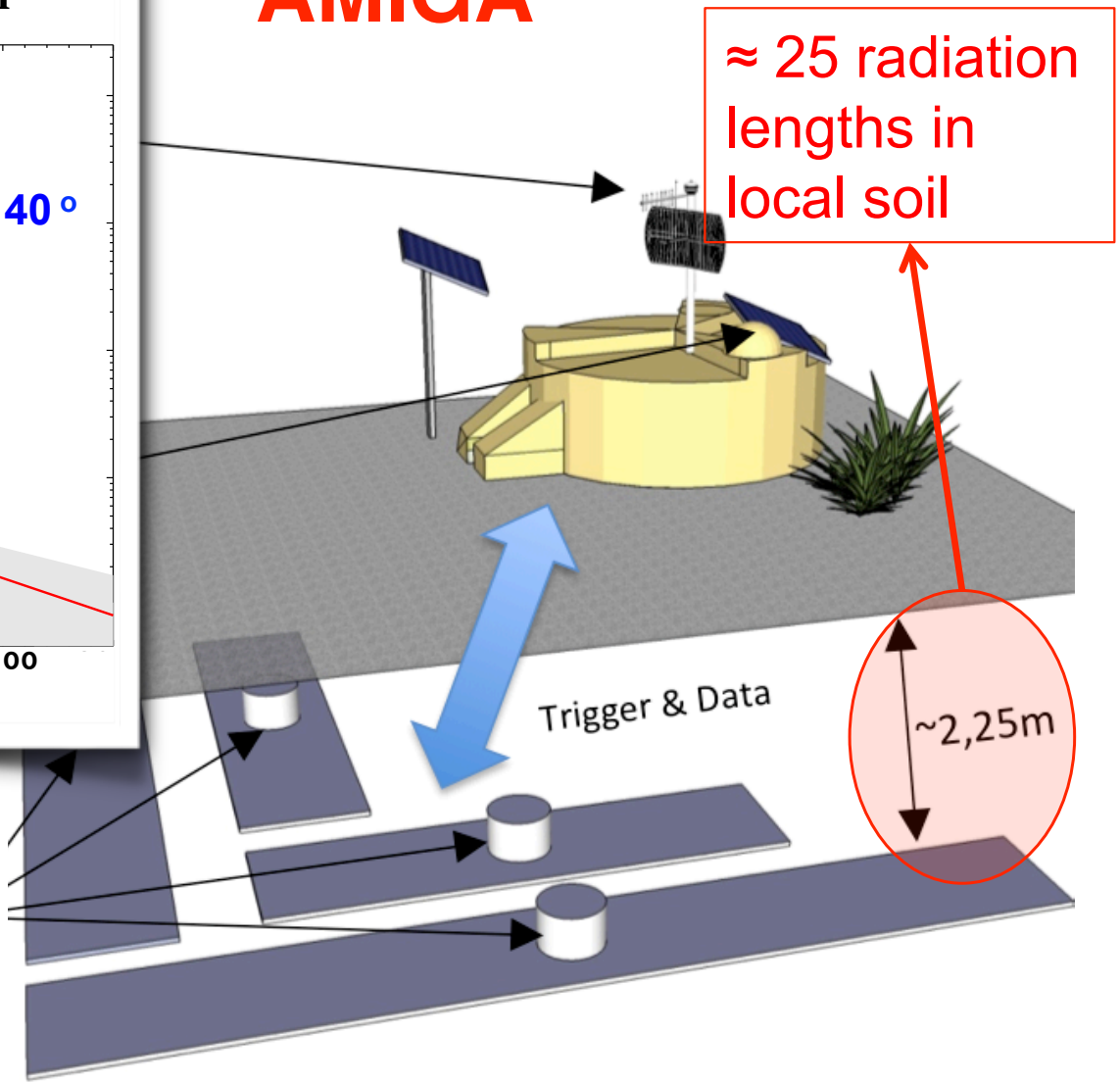

- No electromagetic contamination
- $E_{threshold}$ for muons of 1 GeV

PIERRE AUGER OBSERVATORY

Performance of scintillator upgrade

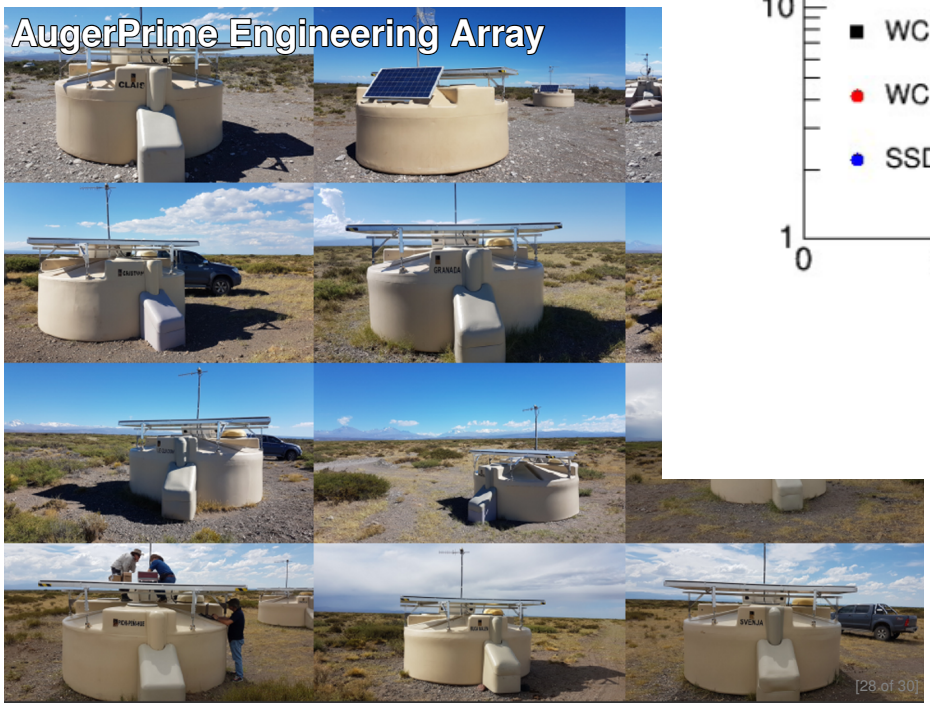

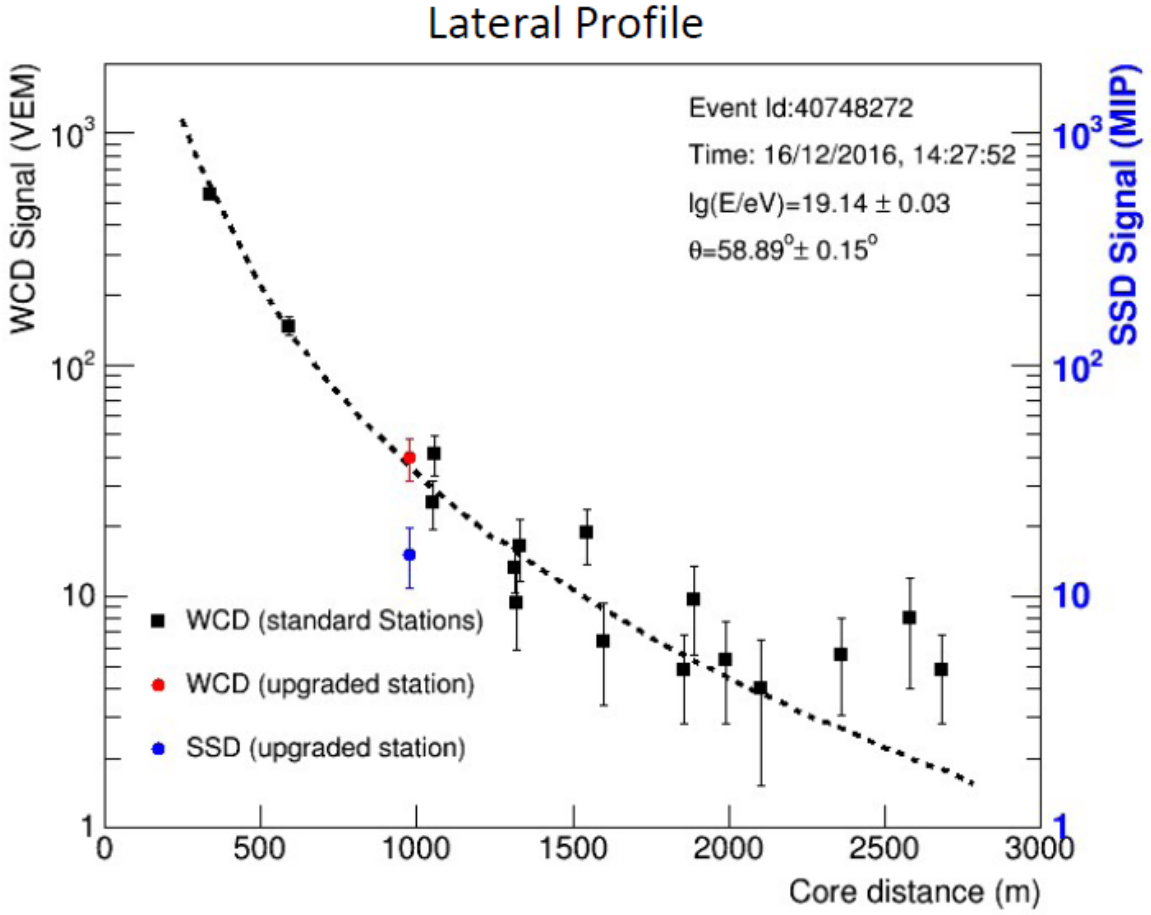

M. Unger, ICRC 2017

Performance of scintillator upgrade

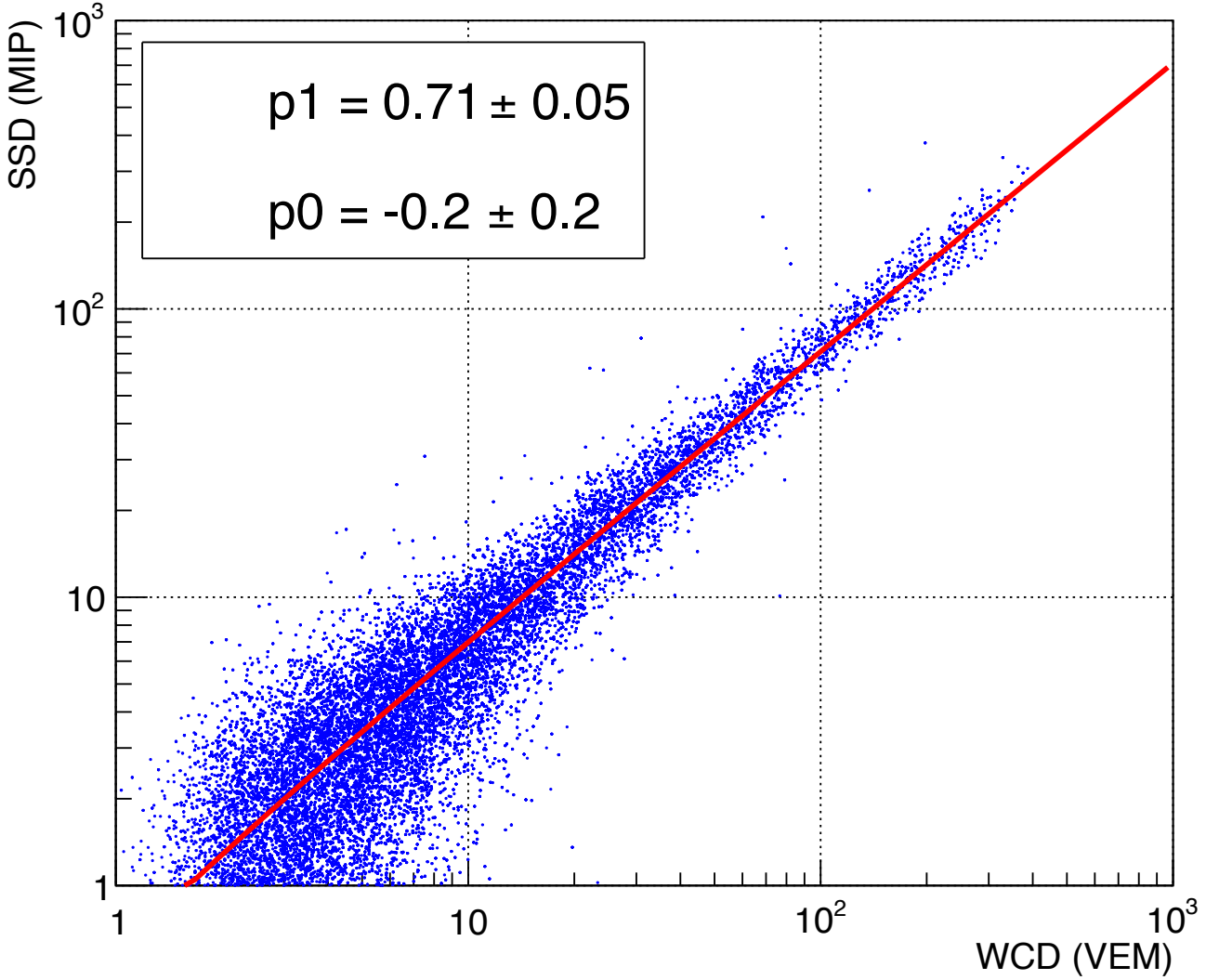

M. Unger, ICRC 2017